Thinning Instabilities in Biological and Electroactive Membranes

A thesis submitted
by

Paul Greaney

to the
School of Mathematics, Statistics and Applied Mathematics,
National University of Ireland, Galway
in partial fulfillment of the requirements
for the degree of Doctor of Philosophy

Supervisors: Dr Giuseppe Zurlo, Dr Martin Meere

Head of School: Dr Rachel Quinlan

Head of Discipline: Dr Martin Meere

October 2018

Contents

List of Figures **3**

Declaration **5**

Abstract **6**

Acknowledgements **7**

1 Introduction **8**

1.1 Biological membranes 8

1.1.1 Pore formation in membranes 12

1.2 Electroactive membranes and instabilities 13

1.3 Overview of thesis 15

2 Mathematical Preliminaries **17**

2.1 Differential geometry of surfaces 17

2.1.1 Some important results 20

2.2 Nonlinear elasticity 26

3 Euler-Lagrange Equations for Lipid Bilayers **30**

3.1 The membrane energy density 31

3.2 Energy variation and minimisation 32

3.2.1 Modelling area and volume preservation 34

3.2.2 The constrained variational problem 35

3.3 Calculation of equilibrium configurations 37

3.4 Tangential variations 41

3.5 Normal variations 47

3.6 Boundary terms 54

3.7 Radial extension of a circular membrane 58
3.8 Conclusion 62

4 Instabilities in Dielectric Elastomers 64
4.1 Introduction 64
4.2 Variational formulation of electroelasticity 69
4.3 Power series expansion of the energy 70
4.4 Energy relaxation and voltage-induced wrinkles 77
4.4.1 Construction of the relaxed membranal energy 77
4.4.2 Comparison with experiments 81
4.5 Electroelastic stability 86
4.5.1 Convexity and existence of minimisers 88
4.6 Energy regularization and electroelastic stability 93
4.7 Conclusion 97

5 Pore Formation in Lipid Membranes 99
5.1 Introduction 99
5.2 Motivation 103

6 Conclusion 107
6.1 Biological membranes 107
6.2 Electroactive devices 108

Bibliography 109

List of Figures

1.1 Overview of the structure of a phospholipid 9
1.2 Structures formed by self assembly of lipids in solution 10
1.3 The 1935 Danielli-Davson model for the structure of cell membranes . . 10
1.4 Electron micrograph of a human red blood cell showing the lipid bilayer structure 11
1.5 Overview of the fluid mosaic model of the cell membrane 12
1.6 Pore formation in a lipid bilayer 13
1.7 Illustration of the working principle of a dielectric elastomer actuator . 14
1.8 Wrinkles in a planar dielectric membrane 15

2.1 Schematic of geometry for the deformation of a surface 18
2.2 Schematic for the deformation of an arbitrary body 26

3.1 Comparison of experimental and theoretical vesicle shapes 32
3.2 Cross-sections of a model red blood cell 33
3.3 Schematic of geometry on membrane midsurface and its boundary . . . 45
3.4 Overview of thickness gradients in a biomembrane 58
3.5 Cross-section of a circular membrane stretched in the radial direction . 62

4.1 Illustration of the pull-in phenomenon 65
4.2 Examples of wrinkled states of dielectric membranes 66
4.3 Plots of the original and relaxed energy densities 80
4.4 Electrically actuated VHB4905 membrane under equibiaxial dead loads 81
4.5 Wrinkling in an annular dielectric device 86
4.6 Theoretical profiles of the annular membrane under voltage control, showing wrinkled and non-wrinkled regions 87
4.7 Experimental setup for wrinkling and breakdown of an annular dielectric membrane 94

4.8 Plots of actuation vs. voltage for the breakdown of an annular dielectric device 96
4.9 Membrane cross-section profiles at various voltages 97

5.1 Schematic of pore formation in a lipid membrane interacting with peptides. 100
5.2 Plot of dimensionless molar fraction $\chi(h)$ vs. thickness h 105

Declaration

I declare that the work presented in this thesis is my own, and has not been previously submitted for award at another degree granting institution.

Paul Greaney.

Abstract

This thesis addresses several problems in the mathematical modelling of biological and electroactive membranes.

We begin with a review of the necessary scientific background of biological and electroactive membranes in Chapter 1. In Chapter 2, we introduce the mathematical framework required for modelling such membranes, consisting of an overview of differential geometry and nonlinear elasticity. Following this, in Chapter 3 we give a full derivation of the shape equations of a lipid membrane whose energy density depends on the mean and Gaussian curvatures, the stretch of the membrane midsurface, and the gradient of this stretch. While the first three of these quantities has received much attention previously in the literature, the inclusion of the stretch gradient dependence is a recent development in this area and allows for more sophisticated mathematical modelling of membranes. We also show how these equations can be specialised to a specific geometry to obtain a set of ordinary differential equations, and thus how they can be used to predict the behaviour of membranes, and possibly to calibrate experimental results with the theory.

In Chapter 4, we turn our focus to the modelling of dielectric membranes, and develop a new mathematical model describing wrinkling and dielectric breakdown in thin dielectric elastomer devices. We compare our theory with experimental results reported in the literature, and find a good match between theory and experiment.

Chapter 5 presents some suggestions on how the theory developed for dielectric membranes might be extended to the case of biological membranes, in particular, to the modelling of pore formation in lipid bilayers interacting with peptide proteins. We conclude the thesis with some suggestions for future work in Chapter 6.

Acknowledgements

Firstly, I thank my parents, brothers, and extended family for their unwavering encouragement and support over the past four years.

My supervisors, Dr Giuseppe Zurlo and Dr Martin Meere, have been excellent mentors, and I thank them for their good humour and constant availability to offer advice and support.

The School of Mathematics, Statistics and Applied Mathematics has provided a wonderful environment in which to study and work as a researcher, and I am grateful to the academic and administrative staff for fostering such a pleasant atmosphere. My fellow postgraduate students have been a constant source of encouragement and friendship, for which I am thankful. I am fortunate to have shared an office with many friends, and to have benefitted from such a positive and friendly work environment.

I am particularly grateful to the members of my graduate research committee, Prof. Michel Destrade, Dr Niall Madden and Dr Petri Piiroinen, for many helpful discussions, and for their constant encouragement throughout the PhD programme.

Finally, my thanks to the College of Science at NUI Galway for their financial support.

Chapter 1

Introduction

This thesis presents research on various problems concerning biological and electroactive membranes. While biological membranes and thin dielectric elastomers differ greatly in size, composition, and character, much of the same mathematical framework, using the theories of differential geometry and nonlinear elasticity, can be applied to modelling their mechanical behaviour.

This chapter gives a broad overview of previous experimental and theoretical research on biological and electroactive membranes, and provides the foundations for the problems considered in the following chapters.

1.1 Biological membranes

A *biological membrane* or *biomembrane* is a semi-permeable barrier which encloses the cell, separating its interior from the surrounding extracellular fluid [Alberts et al., 2015].

Following the first microscopy experiments in the seventeenth century, it was established by Robert Hooke that animal and plant tissues were composed of cells [Sharp, 1934]. By the nineteenth century, it was recognised that cells were enclosed by a semi-permeable barrier, and, in 1900, Charles Ernest Overton proposed that these barriers were made up of lipids [Harris, 2000]. He had earlier experimentally drawn a distinction between the cell wall and cell membrane in plant cells.

The bulk of the bilayer structure is composed of *amphiphilic phospholipid molecules*, which consist of a hydrophilic headgroup and a hydrophobic tailgroup. A typical phospohlipid molecule consists of a hydrophilic head group containing phosphate attached to a glycerol molecule, together with two hydrophobic tails, each containing a saturated or unsaturated fatty acid [Alberts et al., 2015]. The structure is typically

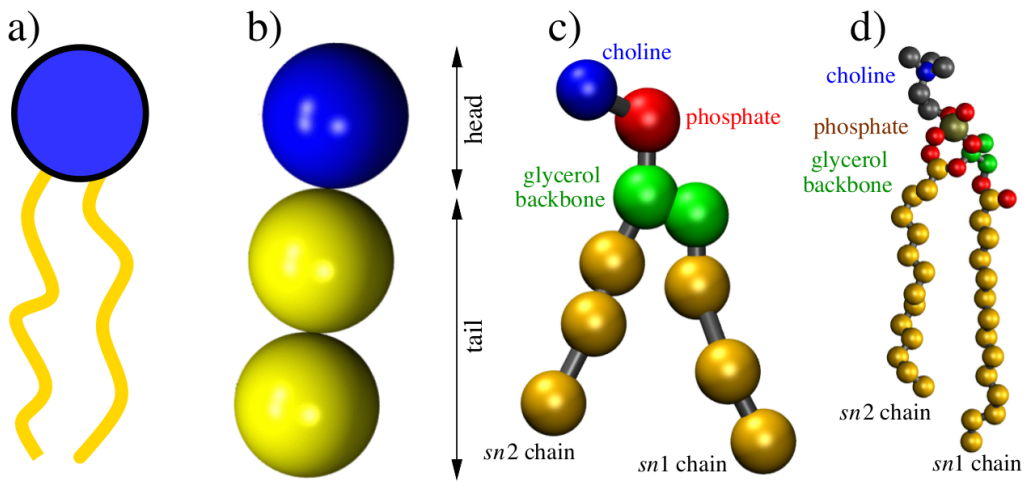

Figure 1.1: An overview of the structure of a phospholipid, the principal component of the cell membrane; extracted from [Terzi and Deserno, 2018]. Panel (a) gives the most simplistic view of a lipid, with the representations increasing in complexity up to (d), a full atomic schematic of a DMPC (dimyristoylphosphatidylcholine) lipid.

visualised as shown in Figure 1.1. The amphiphilic nature of lipids means that, in an aqueous solution, they will undergo a spontaneous process of self-assembly, forming a structure which uses the hydrophilic heads to shield the hydrophobic tails. Depending on the lipid shape and composition, the structure formed can be a bilayer sheet, a single-layered lipid sphere, or a lipid bilayer sphere; see Figure 1.2.

The lipid bilayer structure of cell membranes was first identified in the 1920s in a series of experiments by Dutch physiologists Ever Gorter and François Grendel, who compared the surface area of a cell to the area of a flattened monolayer obtained from a cell membrane. They found a ratio of two to one, and concluded that biomembranes consist of two opposing thin layers of molecules, constructed so as to orient the lipid head groups towards the aqueous environment [Gorter and Grendel, 1925]. Their experimental findings were made possible by an apparatus for spreading molecular layers of lipids, developed by Irving Langmuir in 1917 [Langmuir, 1917].

It was not until the mid 1930s that models for biomembrane structure began to take account of the presence of proteins, when James Danielli and Hugh Davson proposed that the cell membrane was composed of a lipid bilayer together with a protein layer associated with the lipid headgroups [Danielli and Davson, 1935], as shown in Figure 1.3.

The thickness of a typical biomembrane, approximately 5-10 nm, meant that the structure of the membrane could not be elucidated by light microscopy, which is limited

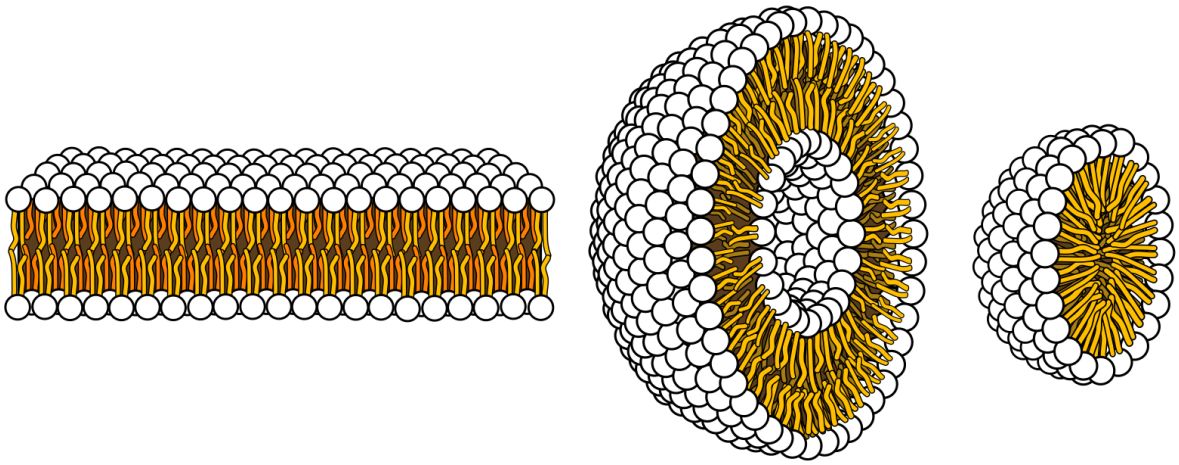

Figure 1.2: Lipids immmersed in an aqueous solution will undergo self-assembly, and the possible resulting structures include a bilayer sheet, a *micelle* formed by a single layer of lipids, and a closed bilayer sphere; adapted from https://commons.wikimedia.org/wiki/File:Phospholipids_aqueous_solution_structures.svg.

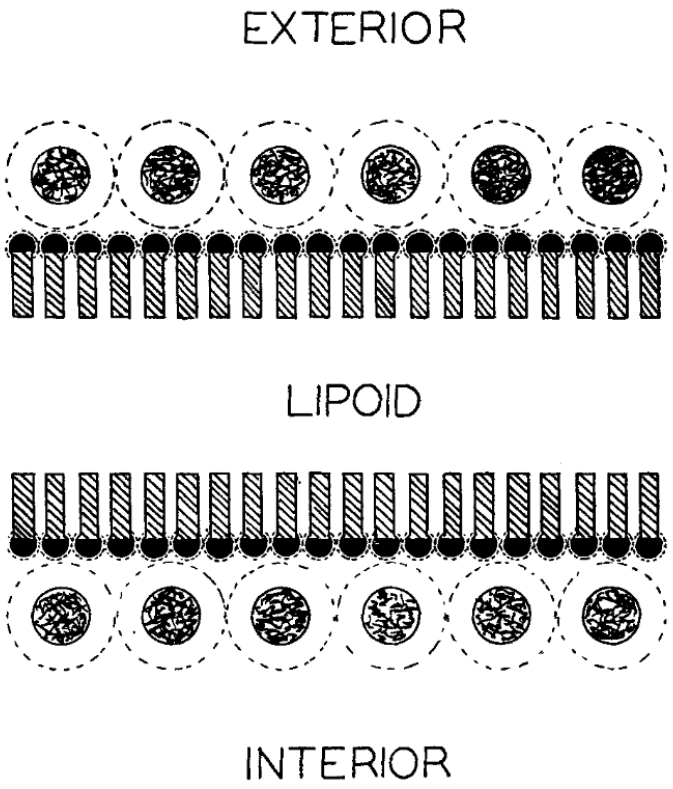

Figure 1.3: The 1935 model of Danielli and Davson, consisting of a lipid bilayer with associated protein layer; extracted from [Danielli and Davson, 1935].

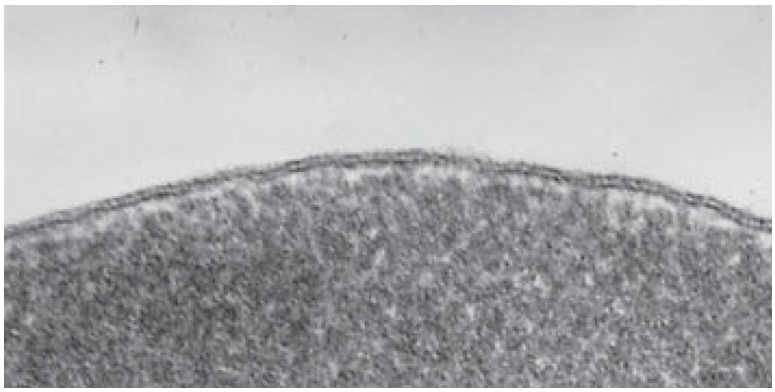

Figure 1.4: Electron micrograph of a human red blood cell showing the lipid bilayer structure; extracted from [Alberts et al., 2015].

to ranges above 200 nm. Developments in electron microscopy in the 1950s thus allowed direct experimental study of lipid membranes for the first time. In 1959, J. David Robertson reported direct observations of the lipid bilayer structure using electron microscopy [Robertson, 1959], confirming the earlier models of Gorter and Grendel, and Danielli and Davson. The bilayer structure can be easily seen in the electron micrograph of the cell membrane shown in Figure 1.4.

Research on the structures of soluble proteins during the 1960s culminated in the emergence of the *fluid mosaic model*, developed by Singer and Nicolson in 1972 [Singer and Nicolson, 1972]. Their theory proposed that the membrane could be described as a two-dimensional liquid, composed mainly of regular lipids together with embedded proteins, as shown in the schematic given in Figure 1.5. It was also recognised around this time that proteins were free to diffuse within the bilayer, as observed by Frye and Edidin [Frye and Edidin, 1970], who reported that, following the fusion of two cells containing differing proteins, the proteins are rapidly distributed over the surface of the aggregate. Whilst much research has been done to elucidate the structure and function of biomembranes in the past forty years, the fluid mosaic model of Singer and Nicolson remains the widely accepted model, albeit with much refinement [Nicolson, 2014].

Cell membranes interact mechanically with the cell interior via the *cytoskeleton*, a system of filaments which ensures that the cell retains the correct shape and internal structure, ultimately helping to maintain the usual functions of a cell [Alberts et al., 2015]. Most animal cells are equipped with three main types of filaments: *intermediate filaments*, which provide mechanical strength; *microtubules*, which regulate the position of membrane-enclosed organelles and direct intracellular transport; and *actin filaments*, which govern the overall shape of the cell membrane and are responsible for

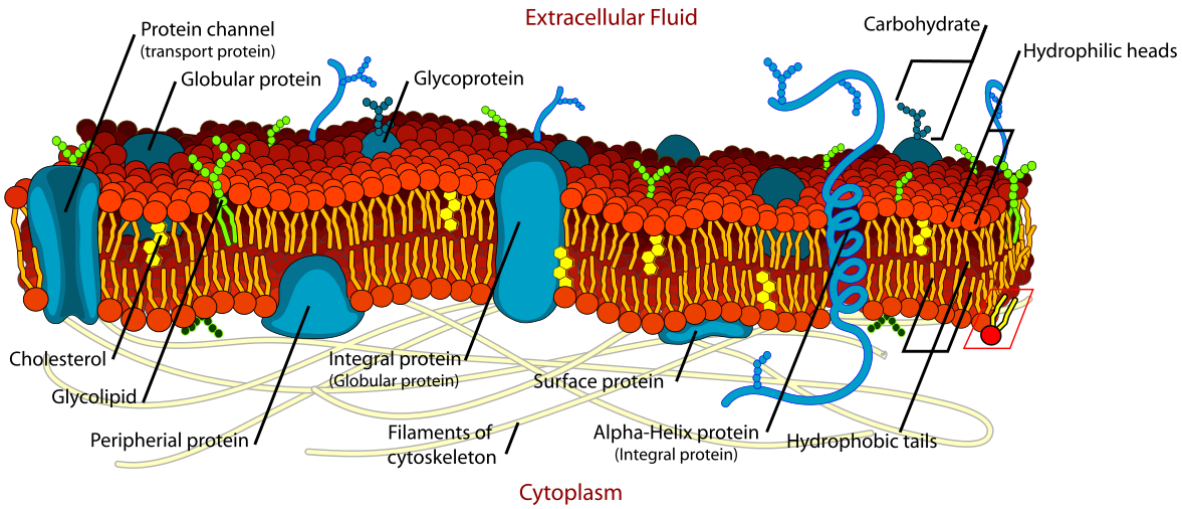

Figure 1.5: Overview of the fluid mosaic model of the cell membrane, taken from http://commons.wikimedia.org/wiki/File:Cell_membrane_detailed_diagram_en.svg.

motion at a whole-cell level; they are formed through polymerization of the actin protein [Dos Remedios et al., 2003]. These filaments are linked to each other and to other cell components by accessory proteins. In particular, motor proteins are responsible for the conversion of energy from ATP hydrolysis into mechanical forces which facilitate movement of filaments and of organelles within the cell [Alberts et al., 2015].

The mathematical modelling of biomembrane behaviour developed contemporaneously with the formulation of the fluid mosaic model in the early 1970s. The ideas proposed by Canham [Canham, 1970] and Helfrich [Helfrich, 1973] for membrane energy densities depending on the membrane curvature have formed the basis for much of the subsequent modelling work, in addition to inspiring much research in the areas of statistical physics and molecular dynamics simulations for cell membranes [Venable et al., 2015, Farago and Pincus, 2004]. Much of the early mathematical models idealise the membrane as a two-dimensional surface embedded in three dimensions, with the surface itself corresponding to the midsurface of the membrane, where the tail groups of the lipids meet. Subsequent developments in the mathematical modelling of membranes will be discussed in Chapter 3.

1.1.1 Pore formation in membranes

A mechanically-interesting function of proteins within the cell membrane is in the formation of membrane *pores*. A large proportion of the proteins found within the membrane

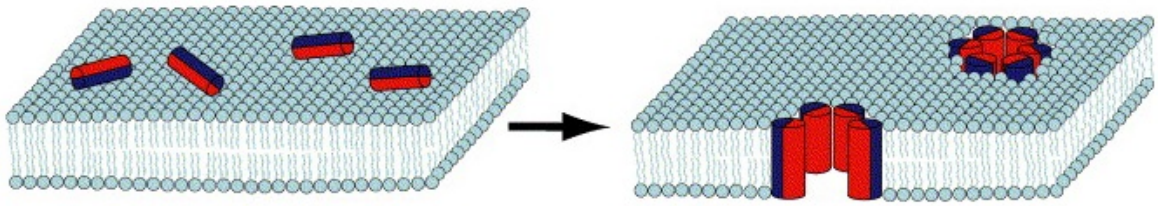

Figure 1.6: Illustration of the *barrel-stave model* of pore formation in lipid membranes, where peptides, present parallel to the membrane mid-surface at lower concentrations, flip to span the membrane in the thickness direction, forming pores; adapted from [Chan et al., 2006].

perform similar functions in regulating cell defence, and are known as *host-defense antimicrobial peptides* [Brown and Hancock, 2006]. Melittin, the peptide found in bee venom, is one of the most widely studied of these antimicrobial peptides. When present at low concentrations, melittin proteins binding to the membrane typically lie parallel to the membrane surface, in the region of the head group of lipids in the outer leaflet of the bilayer.

If present in higher concentrations, the proteins switch into a transmembrane orientation, lying perpendicular to the bilayer surface. When in this orientation, they can then aggregate to form pores in the membrane, creating a *membrane edge* lined with peptide proteins [Terwilliger et al., 1982], as shown in Figure 1.6. The presence of a sufficient number of these pores in the membrane can eventually cause the complete disintegration of the cell membrane, leading to cell lysis. The nature of this phenomenon makes it highly amenable to mathematical modelling; in Chapter 5, we present some results towards a model for the prediction of pores in a biomembrane, based on an averaged density of proteins distributed in the bilayer, and propose that the formation of pores depends on the reaching of a critical density of proteins.

1.2 Electroactive membranes and instabilities

Dielectric elastomers are devices formed by sandwiching a piece of dielectric material between two electrodes, which undergo large deformations when an electric field is applied to them [Pelrine et al., 1998]. These devices have potential uses in a wide array of technologies and applications, including in soft robotics and prosthetics, energy harvesting and microfluidics.

Dielectric elastomer actuator membranes are constructed by coating an elastomer

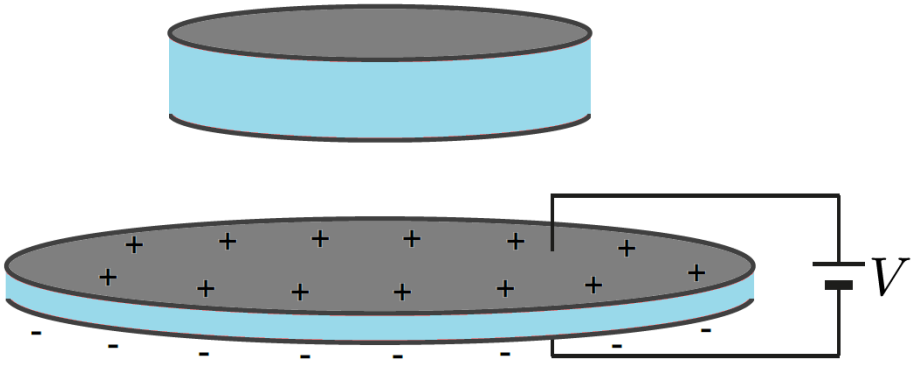

Figure 1.7: Illustration of the working principle of a dielectric elastomer actuator: a piece of dielectric elastomer is coated with a conductive electrode, typically made from carbon grease or hydrogel. The application of a voltage to the electrodes causes a compressive stress in the thickness direction, with a consequent increase in area.

film, such as VHB-4905 or VHB-4910 produced commercially by 3M [Mao et al., 2018a], with electrodes typically made from brushed carbon grease or hydrogel. The application of a voltage to the electrodes then results in a compressive pressure across the thickness direction, due to attractive Coulomb forces acting between the electrodes [Zurlo et al., 2017]; see Figure 1.7. Typical strains exhibited by these devices are in the range of 10-35%, while maximum values can reach as high as 500% [Huang et al., 2012a].

The performance of dielectric elastomer devices is affected by two main types of instability: the formation of wrinkles in the membrane, as shown in Figure 1.8, the occurrence of which is due to the presence of compressive stresses in the membrane; and *electric breakdown* or *dielectric breakdown*, where the voltage applied across the dielectric exceeds a critical *breakdown voltage*, and the insulator becomes conductive [Suo, 2010]. Since the realisation of large deformations requires the application of a large voltage, dielectric elastomer devices typically operate at a voltage which is close to the breakdown voltage, and thus an accurate prediction of the value of this breakdown voltage is of immense value in moving towards the implementation of devices using this technology. Much of the mathematical modelling techniques applied to biological membranes can also be applied to elastic membranes used in physical and industrial applications [Roxburgh, 1995], and by extension to electroactive membranes.

Figure 1.8: Wrinkles in a pre-stretched planar dielectric membrane under voltage control, extracted from [Suo, 2010].

1.3 Overview of thesis

The remainder of this thesis is structured as follows.

Chapter 2 outlines the necessary mathematical preliminaries for the remainder of the thesis. Cell membranes are typically described using the language of *differential geometry*, and thus we begin with a general introduction to this area, limited to a discussion of the theory and results required for the subsequent modelling work. The modelling of electroactive devices requires some of the tools of continuum mechanics, and so we conclude this chapter with a brief discussion of the required elements of *nonlinear elasticity*.

In Chapter 3 we use the calculus of variations, together with the background differential geometry material provided in Chapter 2, to give a complete derivation of the shape equations for equilibrium configurations of thin membranes. In particular, we focus on membrane energy densities which depend on the areal stretch and its gradient, as required to accurately capture thickness variations, in addition to the dependence on curvatures provided for by the usual Helfrich-type model. We then demonstrate the application of this theory by specialising to a simple radially symmetric geometry, illustrating the stretching behaviour of an initially flat membrane.

Our focus in Chapter 4 shifts to a non-biological application of membrane theory: the prediction of instabilities in dielectric elastomer membranes which undergo inhomogeneous thinning under the application of an electric field. We first examine the conditions which lead to wrinkling in thin dielectric elastomer devices, and formulate a straightforward method of predicting wrinkle occurrence, based on a classical approach called *tension field theory* [Steigmann, 1990]. Then, based on suitable conditions on the convexity of the energy density, we derive conditions on the value of the electric field for the avoidance of catastrophic thinning, which leads to breakdown.

In Chapter 5, we discuss how the breakdown criterion might be applied to the case of biological membranes, where instabilities occur via pore formation, due to the presence of certain proteins in the lipid bilayer. Taking an initially spherical membrane as an idealisation for the reference configuration, we consider the deformation resulting from peptide proteins binding to the outer leaflet of the bilayer.

Finally, Chapter 6 presents concluding remarks and discussion on the thesis, together with suggestions and possible avenues for further work.

Chapter 2

Mathematical Preliminaries

In this chapter, we introduce the mathematical framework required to formulate a model for the mechanical behaviour of a membrane in three dimensions. Biological membranes are typically modelled within the framework of differential geometry, where the membrane is idealised as a two-dimensional surface embedded in three dimensions [Jenkins, 1977]. More recently, this has been extended to account for the thickness of the membrane, using an asymptotic expansion of the energy justified by smallness of the membrane thickness relative to the lateral dimensions of the membrane [Deseri et al., 2008]. In modelling electroactive membranes, one typically employs the language of *nonlinear elasticity* to describe the membrane behaviour. Here, the same reasoning justifies the asymptotic expansion of the energy in powers of the membrane thickness.

We begin with an overview of the differential geometry required for biomembrane modelling, which will be used in Chapter 3 to derive the equilibrium shape equations for a lipid bilayer. We follow this with an outline of the theory of continuum mechanics used in modelling electroactive membranes, which will be used in Chapter 4 to formulate a model for the behaviour of thin dielectric elastomers, and from this to analyse wrinkling and breakdown instabilities which occur in such devices.

The material presented here is well-known, and good accounts may be found in, for example, [Do Carmo, 1976, Kreyszig, 1959] for the differential geometry of surfaces, and [Ogden, 1997, Atkin and Fox, 2005] for an introduction to nonlinear elasticity.

2.1 Differential geometry of surfaces

We consider the membrane as a surface in three dimensional space, having an associated flat or undeformed reference configuration in two dimensional space. Points on the

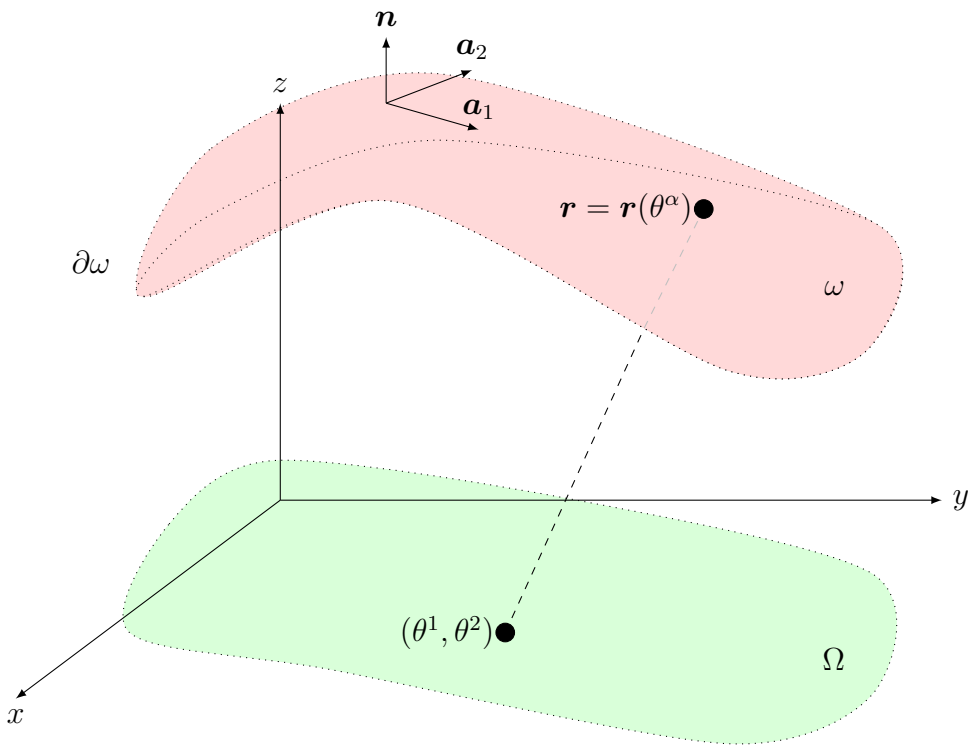

Figure 2.1: The reference configuration of the membrane midsurface, a flat domain $\Omega \subset \mathbb{R}^2$, is mapped by the deformation $\boldsymbol{r}$ to the current configuration, a curved two-dimensional surface $\omega \in \mathbb{R}^3$ embedded in three dimensions, with local tangent vectors $\boldsymbol{a}_1$ and $\boldsymbol{a}_2$, and normal vector $\boldsymbol{n} = (\boldsymbol{a}_1 \times \boldsymbol{a}_2)/|\boldsymbol{a}_1 \times \boldsymbol{a}_2|$.

reference surface are given by the coordinates $\{\theta^\alpha\}$, where Greek indices take values in $\{1, 2\}$. This surface is mapped to a smooth orientable surface ω in $\mathbb{R}^3$, with boundary $\partial\omega$, as shown in Figure 2.1. We denote by $\boldsymbol{r} = \boldsymbol{r}(\theta^\alpha)$, the position of a point on the surface ω. We may then define local tangent vectors to ω given by

$$\boldsymbol{a}_\alpha = \boldsymbol{r}_{,\alpha}, \tag{2.1}$$

where a comma denotes differentiation with respect to the coordinate which follows it. A unit normal field to ω is then given by

$$\boldsymbol{n} = \frac{\boldsymbol{a}_1 \times \boldsymbol{a}_2}{|\boldsymbol{a}_1 \times \boldsymbol{a}_2|}. \tag{2.2}$$

These quantities enable the definition of the first fundamental form, or *metric tensor*, and the second fundamental form, or *curvature tensor*, which have components given

by

$$a_{\alpha\beta} = \boldsymbol{a}_\alpha \cdot \boldsymbol{a}_\beta, \tag{2.3}$$

$$b_{\alpha\beta} = \boldsymbol{n} \cdot \boldsymbol{a}_{\alpha,\beta} = -\boldsymbol{n}_{,\alpha} \cdot \boldsymbol{a}_\beta, \tag{2.4}$$

respectively. It is typically more convenient to use the first expression given by (2.4) in calculating the components of $b_{\alpha\beta}$, since the second expression involves the derivative of the unit vector $\boldsymbol{n}$. The equivalence of the two expressions is easily seen by differentiating the identity $\boldsymbol{a}_\alpha \cdot \boldsymbol{n} = 0$ with respect to θ^β. The dual metric $a^{\alpha\beta}$ is obtained by simply taking the inverse of the metric tensor. It can also be written

$$a^{\alpha\beta} = \boldsymbol{a}^\alpha \cdot \boldsymbol{a}^\beta.$$

where

$$\boldsymbol{a}^\alpha = a^{\alpha\beta}\boldsymbol{a}_\beta, \tag{2.5}$$

are the tangent vectors in the dual basis, and where the summation convention, that is, repeated indices are summed over {1,2}, applies here and henceforth. We note for future use that the components of the metric tensor and its inverse satisfy

$$a_{\alpha\beta}a^{\beta\gamma} = \delta^\gamma_\alpha, \tag{2.6}$$

where

$$\delta^\gamma_\alpha = \begin{cases} 1 & \text{if } \alpha = \gamma \\ 0 & \text{if } \alpha \neq \gamma \end{cases}$$

is the Kronecker delta. Equation (2.5) is an example of a *contraction*: in general the metric tensor may be used to raise or lower indices in general tensor equations. Thus, for example, we can raise both indices of the curvature tensor by writing

$$a^{\alpha\gamma}a^{\beta\mu}b_{\gamma\mu} = a^{\alpha\gamma}b^\beta_\gamma = b^{\alpha\beta},$$

where we have used that the order of the indices does not matter due to the symmetry of both the metric and curvature tensors.

The determinant $g = \det(a_{\alpha\beta})$ of the metric tensor can be written

$$g = \frac{1}{2} e^{\alpha\mu} e^{\gamma\beta} a_{\alpha\gamma} a_{\mu\beta} = a_{11}a_{22} - a_{12}a_{21},$$

where $e^{11} = e^{22} = 0$, and $e^{12} = -e^{21} = 1$. This quantity is a measure of the local area on ω; to see this, we define θ to be the angle between $\boldsymbol{a}_1$ and $\boldsymbol{a}_2$, and rewrite the above equation as

$$\begin{aligned} g &= (\boldsymbol{a}_1 \cdot \boldsymbol{a}_1)(\boldsymbol{a}_2 \cdot \boldsymbol{a}_2) - (\boldsymbol{a}_1 \cdot \boldsymbol{a}_2)^2 \\ &= |\boldsymbol{a}_1|^2 |\boldsymbol{a}_2|^2 - |\boldsymbol{a}_1|^2 |\boldsymbol{a}_2|^2 \cos^2\theta, \\ &= |\boldsymbol{a}_1|^2 |\boldsymbol{a}_2|^2 \sin^2\theta \\ &= |\boldsymbol{a}_1 \times \boldsymbol{a}_2|^2. \end{aligned}$$

Now, since the tangent vectors $\boldsymbol{a}_1$ and $\boldsymbol{a}_2$ span the local area element on the surface ω, the local area element can be written as

$$da = |\boldsymbol{a}_1 d\theta^1 \times \boldsymbol{a}_2 d\theta^2| = |\boldsymbol{a}_1 \times \boldsymbol{a}_2| d\theta^1 d\theta^2 = \sqrt{g}\, d\theta^1 d\theta^2.$$

Equipped with this geometric description of the membrane, we define the mean and Gaussian curvatures of ω as

$$H = \tfrac{1}{2} a^{\alpha\beta} b_{\alpha\beta} = \tfrac{1}{2} b^{\alpha}_{\alpha} = \frac{1}{2}(b^1_1 + b^2_2), \tag{2.7}$$

$$K = \det(b_{\alpha\beta} a^{\beta\gamma}) = \frac{1}{2} \varepsilon^{\alpha\beta} \varepsilon^{\lambda\mu} b_{\alpha\lambda} b_{\beta\mu}, \tag{2.8}$$

where $\varepsilon^{\alpha\beta} = e^{\alpha\beta}/\sqrt{g}$. We note that H and K are the scalar invariants of the tensor $b^{\alpha}_{\gamma} = a^{\alpha\beta} b_{\beta\gamma}$, and hence if κ_1 and κ_2 are the two nontrivial eigenvalues of this tensor, usually called the *principal curvatures* of ω, then the mean and Gaussian curvatures can be written

$$H = \frac{1}{2}(\kappa_1 + \kappa_2) \quad \text{and} \quad K = \kappa_1 \kappa_2. \tag{2.9}$$

2.1.1 Some important results

In general, indexed quantities are required to be tensors with covariant (lower) or contravariant (upper) components, or a mixture of both (a *mixed* tensor). This means that they are required to obey particular transformation laws (depending on their type),

which necessitates the introduction of some further rules for the differentiation of vectors and tensors on curved surfaces. This notion of transformations is at the heart of the difference between contravariant and covariant components: they are said to *transform differently*. For instance, if we define ϑ^β to be a set of coordinates given by a function of the original contravariant coordinates θ^α, using the chain rule, the differential $d\theta^\alpha$ transforms as

$$d\theta^\alpha = \frac{\partial \theta^\alpha}{\partial \vartheta^\beta} d\vartheta^\beta. \tag{2.10}$$

This transformation law is thus applicable for the contravariant case; for the covariant case, we consider the previously-defined tangent vectors as a representative example: they transform as

$$\boldsymbol{a}_\alpha = \frac{\partial \boldsymbol{r}}{\partial \theta^\alpha} = \frac{\partial \boldsymbol{r}}{\partial \vartheta^\beta}\frac{\partial \vartheta^\beta}{\partial \theta^\alpha} = \bar{\boldsymbol{a}}_\beta \frac{\partial \vartheta^\beta}{\partial \theta^\alpha}, \tag{2.11}$$

where the vectors $\bar{\boldsymbol{a}}_\beta$ are the tangent vectors in the transformed coordinate system. From this, we see that the Jacobian in the latter expression is the inverse of the Jacobian seen previously in (2.10).

We next consider the derivative of the tangent vectors under the same transformation as above. We have

$$\boldsymbol{a}_{\alpha,\beta} = \frac{\partial}{\partial \theta^\beta}\frac{\partial \boldsymbol{r}}{\partial \theta^\alpha} = \frac{\partial}{\partial \theta^\beta}\left(\frac{\partial \boldsymbol{r}}{\partial \vartheta^\lambda}\frac{\partial \vartheta^\lambda}{\partial \theta^\alpha}\right) = \bar{\boldsymbol{a}}_{\lambda,\mu}\left(\frac{\partial \vartheta^\mu}{\partial \theta^\beta}\right)\left(\frac{\partial \vartheta^\lambda}{\partial \theta^\alpha}\right) + \bar{\boldsymbol{a}}_\lambda \frac{\partial^2 \vartheta^\lambda}{\partial \theta^\alpha \partial \theta^\beta},$$

where the $\bar{\boldsymbol{a}}_{\lambda,\mu}$ are the derivatives of the tangent vectors in the transformed coordinate system, with respect to coordinates ϑ^μ in that system. Then $\boldsymbol{a}_{\alpha,\beta}$ is *not* a tensor; if it were, it should simply transform analogously to the first order transformations (2.10)–(2.11), with a second Jacobian appearing due to the increased order of the tensor. Thus, the second term on the right-hand side prevents it from transforming correctly as a tensor [Deserno, 2015]. It is necessary therefore to introduce a further notion of differentation, called *covariant differentiation*, to obtain objects which transform as tensors. This essentially involves a definition which subtracts out the problematic term appearing as a result of the transformation. For a first order contravariant tensor with components f^α, the covariant derivative is given by

$$f^\alpha_{;\beta} = f^\alpha_{,\beta} - \Gamma^\alpha_{\beta\mu} f^\mu, \tag{2.12}$$

where $\Gamma^{\gamma}_{\alpha\beta} = a^{\mu\gamma}\Gamma_{\alpha\beta\mu}$ are the Christoffel symbols of the second kind, defined by

$$\Gamma_{\alpha\beta\gamma} = \tfrac{1}{2}\left(a_{\gamma\beta,\alpha} + a_{\alpha\gamma,\beta} - a_{\alpha\beta,\gamma}\right). \tag{2.13}$$

This derivative is also called the *surface divergence*, and can equivalently be written

$$f^{\alpha}_{;\beta} = \frac{1}{\sqrt{g}}\left(\sqrt{g}f^{\alpha}\right)_{,\beta}, \tag{2.14}$$

using that $g_{,\alpha} = 2g\Gamma^{\mu}_{\mu\alpha}$ [Deserno, 2015]. The corresponding derivative for a vector with covariant components f_α is given by

$$f_{\alpha;\beta} = f_{\alpha,\beta} - \Gamma^{\mu}_{\alpha\beta}f_{\mu}. \tag{2.15}$$

Higher-order tensors require an extra Christoffel term for each extra index; thus the covariant derivative of a second order covariant tensor $A_{\alpha\beta}$ is given by [Deserno, 2015]

$$A_{\alpha\beta;\gamma} = A_{\alpha\beta,\gamma} - \Gamma^{\mu}_{\alpha\gamma}A_{\mu\beta} - \Gamma^{\mu}_{\gamma\beta}A_{\alpha\mu}. \tag{2.16}$$

In the case of a scalar field ϕ, we have

$$\phi_{;\alpha} = \phi_{,\alpha},$$

that is, partial differentiation and covariant differentiation conincide and no correction term is required.

Gauss & Weingarten Formulas

Beginning with the trivial identity $\boldsymbol{n}\cdot\boldsymbol{n} = 1$ and differentiating with respect to θ^α, we obtain $\boldsymbol{n}\cdot\boldsymbol{n}_{,\alpha} = 0$, which geometrically means that an infinitesimal displacement along the surface results in a change in the normal vector which is tangential to the surface. This change can thus be written as a combination of the tangent vectors, so we write $\boldsymbol{n}_{,\alpha} = A^{\beta}_{\alpha}\boldsymbol{a}_{\beta}$, where $A_{\alpha\beta}$ is a second order tensor. Taking the scalar product on both sides with $\boldsymbol{a}_\mu$ and using (2.4) gives $A_{\alpha\mu} = -b_{\alpha\mu}$, where $b_{\alpha\mu}$ is the curvature tensor. Raising an index, we obtain

$$\boldsymbol{n}_{,\alpha} = -b^{\beta}_{\alpha}\boldsymbol{a}_{\beta}, \tag{2.17}$$

which is Weingarten's formula.

For the partial derivative of the tangent vectors, assuming that the change in $\boldsymbol{a}_\alpha$ can occur in all three directions within the basis $\{\boldsymbol{a}_1, \boldsymbol{a}_2, \boldsymbol{n}\}$, we write

$$\boldsymbol{a}_{\alpha,\beta} = A^\mu_{\alpha\beta}\boldsymbol{a}_\mu + B_{\alpha\beta}\boldsymbol{n}, \tag{2.18}$$

and seek expressions for the third and second order tensors $A^\mu_{\alpha\beta}$ and $B_{\alpha\beta}$. Upon taking the scalar product of (2.18) with $\boldsymbol{n}$ and comparing with (2.4), we immediately have that

$$B_{\alpha\beta} = b_{\alpha\beta}. \tag{2.19}$$

Calculating the derivative $a_{\alpha\beta,\gamma} = \boldsymbol{a}_{\alpha,\gamma} \cdot \boldsymbol{a}_\beta + \boldsymbol{a}_\alpha \cdot \boldsymbol{a}_{\beta,\gamma}$ using the assumption (2.18), we have

$$\begin{aligned} a_{\alpha\beta,\gamma} &= A^\mu_{\alpha\gamma} a_{\mu\beta} + A^\mu_{\beta\gamma} a_{\alpha\mu} \\ &= A_{\alpha\gamma\beta} + A_{\beta\gamma\alpha}, \end{aligned} \tag{2.20}$$

so that, by symmetry,

$$a_{\alpha\gamma,\beta} = A_{\alpha\beta\gamma} + A_{\gamma\beta\alpha}, \tag{2.21}$$

$$a_{\beta\gamma,\alpha} = A_{\beta\alpha\gamma} + A_{\gamma\alpha\beta}. \tag{2.22}$$

Using the symmetry of $A_{\alpha\beta\gamma}$ in its first two indexes, adding (2.20) and (2.21) and subtracting (2.22) then gives

$$A_{\beta\gamma\alpha} = \frac{1}{2}[a_{\alpha\beta,\gamma} + a_{\alpha\gamma,\beta} - a_{\beta\gamma,\alpha}] = \Gamma_{\beta\gamma\alpha}. \tag{2.23}$$

Raising one index gives $A^\mu_{\beta\alpha} = \Gamma^\mu_{\beta\alpha}$, and substituting this together with (2.19) in (2.18) then gives Gauss's formula,

$$\boldsymbol{a}_{\alpha,\beta} = \Gamma^\gamma_{\alpha\beta}\boldsymbol{a}_\gamma + b_{\alpha\beta}\boldsymbol{n}. \tag{2.24}$$

As mentioned above, such a partial derivative, involving the Christoffel symbols, is called the *covariant* derivative, denoted by a semi-colon in place of the usual comma for partial differentiation. Thus the covariant derivative of the tangent vector $\boldsymbol{a}_\alpha$ is

written

$$\boldsymbol{a}_{\alpha;\beta} = \boldsymbol{a}_{\alpha,\beta} - \Gamma^{\gamma}_{\alpha\beta}\boldsymbol{a}_{\gamma} \tag{2.25}$$

so that Gauss's formula (2.24) can be written more compactly as

$$\boldsymbol{a}_{\alpha;\beta} = b_{\alpha\beta}\boldsymbol{n}. \tag{2.26}$$

The Mainardi-Codazzi Equations

We begin by considering the identity

$$\boldsymbol{a}_{\alpha,\beta\gamma} = \boldsymbol{a}_{\alpha,\gamma\beta}. \tag{2.27}$$

Whilst this may seem trivial, since partial derivatives typically commute, it turns out that calculating the derivatives explicitly leads to important *compatibility conditions* for the existence of solutions which prove useful in later calculations. Substituting for the first derivatives on the left and right-hand sides using (2.24), we have

$$(\Gamma^{\mu}_{\alpha\beta}\boldsymbol{a}_{\mu} + b_{\alpha\beta}\boldsymbol{n})_{,\gamma} = (\Gamma^{\mu}_{\alpha\gamma}\boldsymbol{a}_{\mu} + b_{\alpha\gamma}\boldsymbol{n})_{,\beta}.$$

Applying (2.24) again, and using Weingarten's formula (2.17), expanding on both sides leads to

$$\begin{aligned}\Gamma^{\mu}_{\alpha\beta,\gamma}\boldsymbol{a}_{\mu} + \Gamma^{\mu}_{\alpha\beta}(\Gamma^{\lambda}_{\mu\gamma}\boldsymbol{a}_{\lambda} + b_{\mu\gamma}\boldsymbol{n}) + b_{\alpha\beta,\gamma}\boldsymbol{n} - b_{\alpha\beta}b^{\mu}_{\gamma}\boldsymbol{a}_{\mu} \\ = \Gamma^{\mu}_{\alpha\gamma,\beta}\boldsymbol{a}_{\mu} + \Gamma^{\mu}_{\alpha\gamma}(\Gamma^{\lambda}_{\mu\beta}\boldsymbol{a}_{\lambda} + b_{\mu\beta}\boldsymbol{n}) + b_{\alpha\gamma,\beta}\boldsymbol{n} - b_{\alpha\gamma}b^{\lambda}_{\beta}\boldsymbol{a}_{\lambda}.\end{aligned}$$

Since $\boldsymbol{a}_{\alpha}$ and $\boldsymbol{n}$ are linearly independent vectors, the terms multiplying them in the above equation must be separately equal to each other. The condition arising from the equality of the tangential components, which we refrain from stating explicitly, leads to a condition involving the mixed Riemann curvature tensor. From the equality of the normal components we obtain the *Mainardi-Codazzi equations*

$$b_{\alpha\beta;\gamma} = b_{\alpha\gamma;\beta}, \tag{2.28}$$

which can be equivalently be written

$$b^{\alpha}_{\beta;\gamma} = b^{\alpha}_{\gamma;\beta}, \tag{2.29}$$

by raising an index using the metric tensor. These will prove useful in the calculations considered in Chapter 3.

The Gauss-Bonnet Theorem and Ricci's Lemma

The Gauss-Bonnet theorem [Do Carmo, 1976], relating the Gaussian curvature K of a surface ω to its topology, reads

$$\int_{\omega} K\, da = 2\pi\chi_p - \int_{\partial\omega} k_g\, ds, \tag{2.30}$$

where χ_p is the Euler characteristic of ω, $\partial\omega$ is the boundary of ω, and k_g is the geodesic curvature, which is a measure of how far a curve on the surface is from being a geodesic, the shortest arc between two points on the surface. A particularly significant consequence of the theorem, and our main concern here, is that for closed membranes the contour integral over $\partial\omega$ on the right-hand side is zero, so that the integral of K yields a constant, and thus the inclusion of the Gaussian curvature in the areal energy density for the membrane makes no contribution to the membrane shape.

We conclude this section with another important result, Ricci's lemma, which states that the covariant derivative of the metric tensor, and its inverse, are both zero. Substituting the metric tensor into the general covariant derivative for a second order tensor (2.16), we have

$$a_{\alpha\beta;\gamma} = a_{\alpha\beta,\gamma} - \Gamma^{\mu}_{\alpha\gamma} a_{\mu\beta} - \Gamma^{\mu}_{\gamma\beta} a_{\alpha\mu}. \tag{2.31}$$

For the first term on the right-hand side, (2.23) gives

$$a_{\alpha\beta,\gamma} = \Gamma_{\alpha\gamma\beta} + \Gamma_{\beta\gamma\alpha},$$

so that

$$a_{\alpha\beta;\gamma} = 0. \tag{2.32}$$

Taking the covariant derivative of (2.6) gives

$$(a^{\alpha\beta}a_{\beta\gamma})_{;\mu} = a^{\alpha\beta}_{;\mu}a_{\beta\gamma} + a^{\alpha\beta}a_{\beta\gamma;\mu} = 0,$$

so that $a^{\alpha\beta}_{;\mu} = 0$, that is, the dual metric tensor is also constant under covariant differentiation. We also note that the identity

$$(\sqrt{g})_{;\alpha} = 0$$

follows from Ricci's lemma, since $g = \frac{1}{2}e^{\alpha\mu}e^{\gamma\beta}a_{\alpha\gamma}a_{\mu\beta}$ is entirely determined by the components of the metric tensor.

2.2 Nonlinear elasticity

Cell membranes are typically modelled as fluid in their plane, and as such are not capable of supporting shear stresses. By contrast, the electroactive membrane devices considered in Chapter 4 are soft solids, and a general three-dimensional description of their behaviour requires the language of *nonlinear elasticity*, which describes the response of systems which undergo large deformations. The basic mathematical object describing the deformation is the deformation map $\boldsymbol{f} : \boldsymbol{X} \to \boldsymbol{x}$, which maps points $\boldsymbol{X} \in \mathcal{B}_0$ in some *reference configuration* $\mathcal{B}_0$ to points $\boldsymbol{x} \in \mathcal{B}$ in the *current configuration* $\mathcal{B}$, as shown in Figure 2.2.

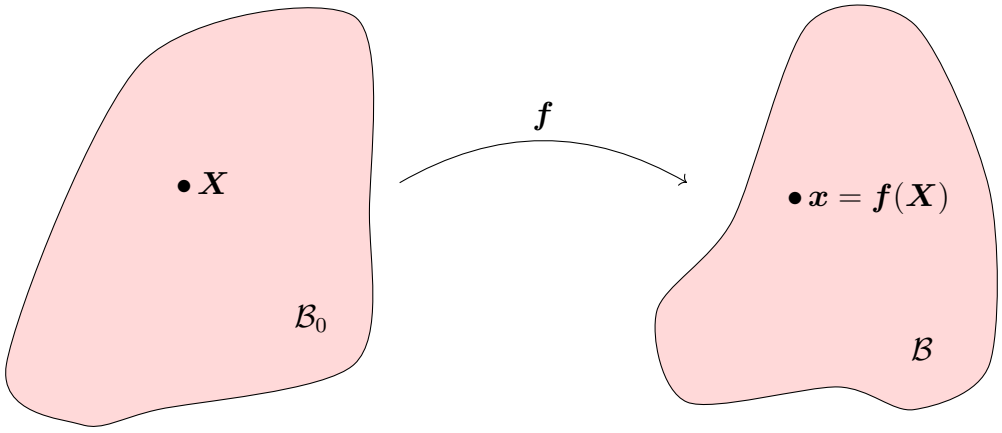

Figure 2.2: Points $\boldsymbol{X}$ in the reference configuration $\mathcal{B}_0$ are mapped by the deformation $\boldsymbol{f}$ to points $\boldsymbol{x}$ in the current configuration $\mathcal{B}$.

The nonlinear behaviour of a material is captured via a strain energy density function W which depends constitutively on the *gradient of deformation* $\mathbf{F}$, defined as the gradient of $\boldsymbol{f}$ with respect to coordinates in the reference configuration.

$$\mathbf{F} = \nabla \boldsymbol{f} = \operatorname{Grad} \boldsymbol{x} = \frac{\partial \boldsymbol{f}(\boldsymbol{X})}{\partial \boldsymbol{X}} = \frac{\partial x_i}{\partial X_j} \boldsymbol{e}_i \otimes \boldsymbol{E}_j.$$

Here, $\boldsymbol{E}_i$ and $\boldsymbol{e}_i$ are the basis unit vectors in the reference and current configurations, respectively. Note that $\mathbf{F}$ need not be square, as evidenced later in the thesis when considering the deformation of an initially flat membrane. The strain energy density function $W(\mathbf{F})$ is chosen constitutively, so as to accurately capture the experimentally-observed behaviour of the material under consideration [Ogden, 1997]. It is equivalent, and often more convenient, to define the right Cauchy-Green deformation tensor

$$\mathbf{C} = \mathbf{F}^{\mathsf{T}}\mathbf{F},$$

and to then consider W as a function of $\mathbf{C}$ instead of $\mathbf{F}$. The quantity

$$J = \det \mathbf{F} = (\det \mathbf{C})^{1/2}$$

measures the change in volume between the reference and current configurations; to see this, consider the volume of a parallelepiped in the reference configuration, formed by the line elements $d\boldsymbol{X}_1$, $d\boldsymbol{X}_2$, and $d\boldsymbol{X}_3$. Its volume is given by

$$dV = d\boldsymbol{X}_1 \cdot (d\boldsymbol{X}_2 \times d\boldsymbol{X}_3) = \det(d\boldsymbol{X}_1 | d\boldsymbol{X}_2 | d\boldsymbol{X}_3),$$

where the columns in the latter determinant are the components of the line elements. The three line elements are mapped under the deformation to $d\boldsymbol{x}_i = \mathbf{F} d\boldsymbol{X}_i$ in the current configuration, so that the corresponding volume is

$$dv = \mathbf{F}d\boldsymbol{X}_1 \cdot (\mathbf{F}d\boldsymbol{X}_2 \times \mathbf{F}d\boldsymbol{X}_3) = \det(\mathbf{F}) \det(d\boldsymbol{X}_1 | d\boldsymbol{X}_2 | d\boldsymbol{X}_3),$$

that is,

$$dv = J\, dV.$$

For *incompressible* materials, we have $J = 1$ since the volume remains fixed everywhere during the deformation.

The principal invariants of $\mathbf{C}$ are

$$I_1 = \mathrm{tr}(\boldsymbol{C}), \quad I_2 = \frac{1}{2}\left(\mathrm{tr}(\boldsymbol{C}^2) - \mathrm{tr}(\boldsymbol{C})^2\right), \quad I_3 = \det(\boldsymbol{C}) = J^2. \tag{2.33}$$

and thus we can equivalently take W to be a function of I_1, I_2, and I_3. For incompressible materials, we have $I_3 = 1$, and so $W = W(I_1, I_2)$. The Cayley-Hamilton theorem [Atkin and Fox, 2005] states that

$$\mathbf{C}^3 - I_1\mathbf{C}^2 + I_2\mathbf{C} - I_3\boldsymbol{I} = \mathbf{0},$$

where $\boldsymbol{I}$ is the identity tensor and $\mathbf{0}$ is the zero tensor.

The Cauchy stress tensor $\boldsymbol{\sigma}$ measures the stress at any point in the current configuration. It relates the unit normal $\boldsymbol{n}$ to the stress vector $\boldsymbol{T}^{(\boldsymbol{n})}$ across a surface perpendicular to $\boldsymbol{n}$, via the relation

$$\boldsymbol{T}^{(\boldsymbol{n})} = \boldsymbol{\sigma}\boldsymbol{n}. \tag{2.34}$$

For large deformations, the Piola-Kirchoff stress tensor

$$\boldsymbol{S} = J\boldsymbol{\sigma}\mathbf{F}^{-\mathsf{T}} \tag{2.35}$$

is often used; it measures the stress relative to areas in the reference configuration, rather than relative to areas in the current configuration as is the case for the Cauchy stress tensor.

For later reference, we record the following relations for the transformation of line, surface, and volume elements, which follow from the definition of the deformation gradient:

$$d\boldsymbol{x} = \mathbf{F}d\boldsymbol{X}, \tag{2.36}$$

$$\boldsymbol{n}da = J\mathbf{F}^{-\mathsf{T}}\boldsymbol{N}dA, \tag{2.37}$$

$$dv = J\,dV. \tag{2.38}$$

Here, $d\boldsymbol{x}, da$, and dv are line, area, and volume elements in the current configuration; $d\boldsymbol{X}, dA$, and dV are the corresponding quantities in the reference configuration; and $\boldsymbol{N}$ and $\boldsymbol{n}$ are unit normal vectors to the area elements dA and da, respectively. Equation (2.37) is known as Nanson's formula and is used frequently in calculations.

The foregoing theory forms the basis for mathematically modelling the elastic behaviour of thin dielectric elastomer devices, considered in Chapter 4.

Chapter 3

Euler-Lagrange Equations for Lipid Bilayers

In this chapter, we present a complete analysis and derivation of the shape equations for a lipid bilayer, for a wide class of membrane energy densities depending on the mean and Gaussian curvatures, on the stretching of the membrane mid-surface, and on the gradient of this stretch. We begin by giving a historical overview of the modelling of lipid bilayers, beginning with the seminal works of Canham and Helfrich in the early 1970s [Canham, 1970, Helfrich, 1973]. After outlining the variational theory from which the shape equations for equilibrium configurations are obtained, we then proceed to given a full derivation of the shape equations for a lipid bilayer depending on curvatures, areal stretch and stretch-gradient, both by gathering together previous derivations for more specialised energy densities by several other authors, and by adding further analysis. All of this rests on the theory of differential geometry of surfaces outlined in Chapter 2.

Finally we consider an example demonstrating how the theory can be applied to model a membrane subject to deformations which result in non-uniform thickness profiles, an idea which is also central to the modelling of dielectric elastomers subject to out of plane deformations, discussed in Chapter 4, and which we return to in Chapter 5 in the modelling of pore formation in biological membranes.

3.1 The membrane energy density

The functional form of the energy density for lipid membranes has been the subject of much research over the past fifty years. Beginning in the early 1970s with the works of Canham [Canham, 1970] and Helfrich [Helfrich, 1973], many authors have expanded on the proposition that the membrane energy density W admits the expression

$$W = \frac{k}{2}\left(H - H_0\right)^2 + \bar{k}K, \tag{3.1}$$

where $H = \frac{1}{2}\left(\kappa_1 + \kappa_2\right)$ and $K = \kappa_1\kappa_2$ are the mean and Gaussian curvatures, respectively, κ_1, κ_2 are the local principal curvatures of the surface, and $k, \bar{k}$ are bending rigidities. The H_0 term allows for the presence of *spontaneous* curvature, whereby the membrane has a preferred natural curved configuration, such as the case when the internal and external leaves of the bilayer have differing chemical properties. The case $H_0 = 0$ thus corresponds to the preferred configuration being flat. In the case of a smooth, closed vesicle, the term involving Gaussian curvature may be neglected in the variational problem, since the Gaussian curvature is constant in such cases by the Gauss-Bonnet theorem (see equation (2.30)).

Within an elasticity framework, Helfrich's pioneering study viewed lipid bilayer elasticity as *a special case of the well-established theory of thin elastic shells*, treated comprehensively by Naghdi in [Naghdi, 1973]; the notation and concepts introduced in Naghdi's work have informed studies in the theory of lipid bilayer mechanics up to the present day [Agrawal and Steigmann, 2011, Kim and Steigmann, 2015, Agrawal and Steigmann, 2009]. Both the Canham and Helfrich studies have inspired hundreds of researchers as evidenced by thousands of citations to both papers; their ideas have been used for various purposes in diverse studies within the fields of statistical mechanics, biophysics and molecular dynamics [Deserno, 2004, Venable et al., 2015, Farago and Pincus, 2004].

While the model proposed by Helfrich's original study [Helfrich, 1973] adequately captures the bending behaviour of membranes, the study assumes that the stretching behaviour can be neglected relative to the bending elasticity. A later study by Deuling and Helfrich [Deuling and Helfrich, 1976] considered the membrane area as incompressible, with the membrane tension viewed as a Lagrange multiplier coupled to the membrane area. This notion has proved fruitful in developing a theoretical explanation for the range of configurations exhibited by lipid vesicles [Berndl et al., 1990], and for

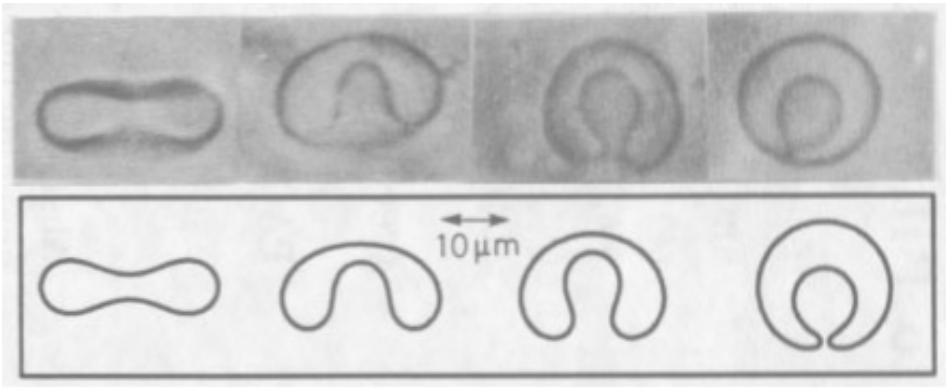

Figure 3.1: Comparison of experimental and theoretical results obtained by Berndl *et al.* [Berndl et al., 1990] for dipalmitoyl phosphatidyl choline (DMPC) vesicles, showing the transition from discocyte to stomatocyte shapes under temperature variation.

the biconcave shape of red blood cells [Jenkins, 1977], as shown in Figures 3.1 and 3.2. A major development in the prevailing theory came with the explicit inclusion of stretch dependence in the energy density. To account for the case where the membrane area is not required to be preserved, the membrane energy density is taken to depend explicitly on the surface stretch $J = da/dA$, the ratio of area elements in the current and reference configurations, respectively, in addition to the previous dependence on H and K. This was proposed by Baesu *et al.* [Baesu et al., 2004] in their study of some specific boundary problems.

3.2 Energy variation and minimisation

Following our discussion of the energy dependencies in Section 3.1, we consider membrane energy densities of the form

$$W = W(H, K, J, Q; \theta^\alpha), \tag{3.2}$$

where H and K are the mean and Gaussian curvatures, respectively; $J = da/dA$ is the local area change; and $Q = |\nabla J|$, the magnitude of ∇J, which is the gradient of J with respect to coordinates in the current configuration. Henceforth we assume no explicit dependence on the surface coordinates θ^α as is the case for uniform membranes; the energy then depends on the coordinates only implicitly through the various other quantities.

The calculation of equilibrium configurations based on the principle of virtual work

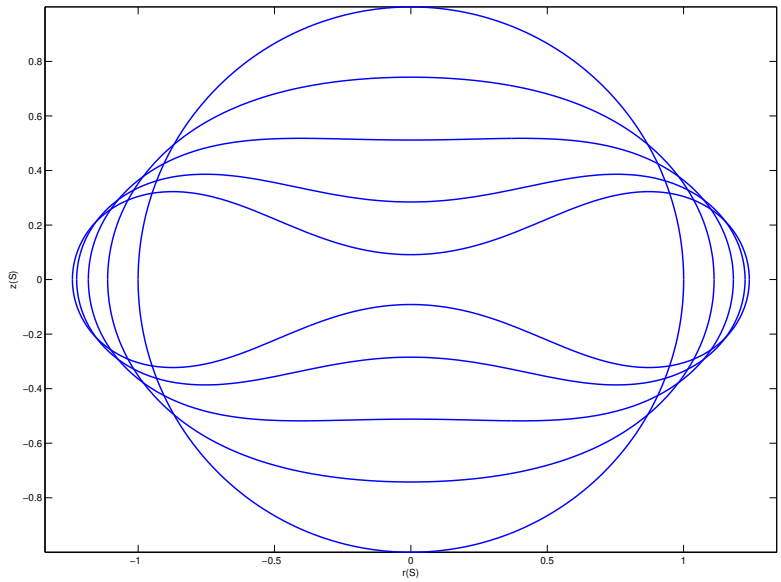

Figure 3.2: Cross-sections of a model red blood cell as obtained by Jenkins [Jenkins, 1977], by taking an initially spherical membrane and varying the pressure, with the cross-sectional profile eventually reaching the well-known biconcave shape; reproduced here using the Matlab `bvp4c` solver.

is well developed, and relies on imposing stationarity of the first variation of the energy

$$E = \int_\omega W \, da, \tag{3.3}$$

where W is the energy density per unit area of the current configuration ω. Using the area change J this may be written in the reference configuration Ω as

$$E = \int_\Omega W J \, dA. \tag{3.4}$$

Equilibrium configurations are obtained by taking the first variation of this energy, defined formally as

$$\dot{E} = \lim_{\varepsilon \to 0} \frac{E(\boldsymbol{r} + \varepsilon \delta \boldsymbol{r}) - E(\boldsymbol{r})}{\varepsilon} \tag{3.5}$$

where $\delta \boldsymbol{r}$ is a perturbation of the configuration defined by $\boldsymbol{r}$, and equating this to zero for all admissible perturbations $\delta \boldsymbol{r}$. Applying this to (3.4), we have

$$\begin{aligned} \dot{E} &= \int_\Omega [\dot{W} J + W \dot{J}] \, dA, \\ &= \int_\omega [\dot{W} + W \dot{J}/J] \, da, \end{aligned} \tag{3.6}$$

with $\dot{W} = \sum_{i=0}^{n} W_{Y_i} \dot{Y}_i$, where the Y_i are the parameters on which W depends explicitly, typically including at least the mean and Gaussian curvatures. A full account of this approach can be found in, for example, Steigmann [Steigmann, 2018]. Studies in this category prescribe the existence of a fixed reference surface Ω together with a map from Ω to ω with an associated local areal stretch J; however a precise description of the reference surface is typically absent, since the aim is to derive the shape of the deformed configuration.

3.2.1 Modelling area and volume preservation

Here and henceforth, the deformation $\boldsymbol{f}$ is taken to be a mapping from $\mathbb{R}^2$ to $\mathbb{R}^3$. The gradient of $\boldsymbol{f}$ with respect to points $\boldsymbol{X} \in \mathbb{R}^2$ in the current configuration is the 3×2 matrix denoted $\nabla_{\boldsymbol{X}} \boldsymbol{f}$.

Area Preservation

There are two main approaches to modelling preservation of midsurface area which appear in the literature. The first approach models the preservation locally: for a deformation specified by a deformation mapping $\boldsymbol{f}$, the constraint

$$J \equiv 1, \quad J = \sqrt{\det\left((\nabla_{\boldsymbol{X}} \boldsymbol{f})^T \nabla_{\boldsymbol{X}} \boldsymbol{f}\right)}, \tag{3.7}$$

is imposed via a Lagrange multiplier, so that the contribution to the energy reads

$$\int_\Omega \gamma(\boldsymbol{X})(J-1)dA, \tag{3.8}$$

where the multiplier γ is allowed to depend on $\boldsymbol{X} \in \Omega$. The second approach fixes the total surface area during the deformation, so that the constraint is written

$$\int_\omega da = \text{const.} \tag{3.9}$$

and is similarly imposed via a Lagrange multiplier, which, by contrast to the local constraint, does not depend on the surface coordinates [Steigmann et al., 2003]; the introduction of a local constraint in general results in an extra differential equation appearing in the system, so that the dependence on the multiplier on the surface coordinates is required in order for the system not to be overdetermined. Regardless of the choice of area-preservation condition, the approach taken is quite similar in the majority of studies, and so it seems natural to expect that the two approaches might be equivalent under certain conditions. This equivalence of the local and global approaches has been shown by Dharmavaram and Healey [Dharmavaram and Healey, 2015] for a smooth, closed surface of genus zero, and has also been discussed extensively by Steigmann et al. [Steigmann et al., 2003]. In our analysis, however, identification of tangential variations of the current configuration with a suitable reparameterisation of the surface is not possible due to the presence of the gradient of area dilation in the expression for the energy density, and thus this equivalence does not hold here, necessitating a suitable choice between the two formulations.

3.2.2 The constrained variational problem

In addition to a Lagrange multiplier associated with the membrane surface area, it is typical to also impose a global constraint on the volume enclosed by the membrane,

assuming the membrane bounds a volume of incompressible fluid, and associating a Lagrange multiplier p with the pressure in this fluid. The full minimisation problem may then be stated as seeking minimisers of

$$E = \int_\omega W\, da - \gamma \left(\int_\omega da - C \right) - p\,(V(\omega) - D)\,, \tag{3.10}$$

where C and D are constants. Since we seek to derive shape equations for membranes which admit stretching, we omit the constraint on the area. Now, writing the volume associated with a configuration ω as a volumetric integral, the incompressibility of the fluid bounded by the membrane is imposed by considering the augmented energy

$$E = \int_\omega W\, da - \int_B p\,[\det(\nabla \boldsymbol{f}) - 1] dV, \tag{3.11}$$

where $p = p(\boldsymbol{X})$ is interpreted as a Lagrange multiplier field associated with the volume incompressibility constraint, and B is a fixed reference configuration. Using (3.6), the variation $\dot{E}$ of E then reads

$$\dot{E} = \int_\omega \left(\dot{W} + W \dot{J}/J \right) da - \int_B p\, \dot{\overline{\det(\nabla \boldsymbol{f})}}\, dV, \tag{3.12}$$

since p, depending on the reference coordinates, is fixed under variations of the current configuration. Applying the identities

$$\begin{aligned} p \operatorname{div} \boldsymbol{u} &= \operatorname{div}(p\boldsymbol{u}) - \boldsymbol{u} \cdot \operatorname{grad} p, \\ \dot{\overline{\det(\nabla \boldsymbol{f})}} &= \det(\nabla \boldsymbol{f}) \operatorname{div} \boldsymbol{u}, \end{aligned}$$

with $\boldsymbol{u} = \dot{\boldsymbol{r}}$, to the second term gives

$$\begin{aligned} \int_B p\,(\det(\nabla \boldsymbol{f}) \operatorname{div} \boldsymbol{u}) dV &= \int_R p \operatorname{div} \boldsymbol{u}\, dv \\ &= \int_R \operatorname{div}(p\boldsymbol{u})\, dv - \int_R \boldsymbol{u} \cdot \operatorname{grad}\, p\, dv \\ &= \int_\omega p\, \boldsymbol{u} \cdot \boldsymbol{n}\, da - \int_R \boldsymbol{u} \cdot \operatorname{grad} p\, dv, \end{aligned}$$

where R is the current configuration of the bulk fluid corresponding to the reference configuration B, and the divergence theorem has been used to obtain the integral over ω. Thus, the area integral can be associated with the first term in (3.12), and so p may

be interpreted as a pressure exerted on the membrane in the normal direction. From the remaining volume integral, we must have $\operatorname{grad} p = \mathbf{0}$, so that p is constant in R. Imposing stationarity of the variation then gives

$$\dot{E} = \int_\omega \left(\dot{W} + W \dot{J}/J \right) \, da - \int_\omega p \, \boldsymbol{u} \cdot \boldsymbol{n} \, da = 0, \tag{3.13}$$

a statement of the principle of virtual work. In the following sections, we specialise this equation to perturbations $\boldsymbol{u}$ in directions normal and tangential to ω, deriving equilibrium shape equations in the normal and tangential directions.

Membrane Volume Preservation

More recent studies have considered the membrane as a thin, but three-dimensional object, by defining a thickness field on the membrane mid-surface, eventually adopting a constraint usually referred to as *quasi-incompressibility* [Deseri et al., 2008]. This involves imposing incompressibility only on the membrane midsurface, so that

$$\lambda_3 J = 1, \tag{3.14}$$

where λ_3 is the thickness stretch. This is satisfied exactly on ω and approximately at other points in the membrane, so that adopting this condition gives access to a measure of the thickness of the membrane. If h_0 is the reference thickness, then the *current* thickness h_c is given by $h_c = \lambda_3 h_0$, so that obtaining the scalar field J as part of the solution completely determines the current membrane thickness as $h_c = h_0/J$. This condition will be further discussed in greater depth in Chapter 4 where a similar constraint is imposed.

3.3 Calculation of equilibrium configurations

Although some the results derived below have been stated with varying degrees of detail by many authors (for example, [Deserno, 2015, Kim and Steigmann, 2015, Steigmann et al., 2003, Agrawal and Steigmann, 2009]), a complete description of their derivation does not seem to be available, and so a detailed derivation for each of the quantities is given here. In particular, we allow for the dependence of the energy on the stretch-gradient magnitude $Q = |\nabla J|$, as well as allowing for explicit dependence on J itself.

The inclusion of the stretch-gradient term here in deriving the shape equations is novel with respect to the aforementioned studies, many of which consider energies depending explicitly on the mean and Gaussian curvatures only. The dependence on $|\nabla J|$ has been briefly considered by Steigmann [Steigmann, 2018]. It is shown later that the expressions obtained here specialise to those obtained previously in the absence of dependence on J and Q.

We consider virtual displacements $\boldsymbol{u}$ of a point $\boldsymbol{r}$ on the membrane mid-surface ω, given by $\boldsymbol{r} \to \boldsymbol{r} + \varepsilon \boldsymbol{u}$, where

$$\boldsymbol{u} = u^\alpha \boldsymbol{a}_\alpha + w\boldsymbol{n}, \tag{3.15}$$

and where u^α, w are the displacements in the tangential and normal directions $\boldsymbol{a}_\alpha$ and $\boldsymbol{n}$, respectively. In deriving the shape equations for the membrane, we seek to obtain expressions for the variation in the various quantities associated with the energy. The mean and Gaussian curvatures are defined in equations (2.7) and (2.8), respectively, as

$$H = \frac{1}{2} a^{\alpha\beta} b_{\alpha\beta}, \quad K = \frac{1}{2} \varepsilon^{\alpha\beta} \varepsilon^{\lambda\mu} b_{\alpha\lambda} b_{\beta\mu}, \tag{3.16}$$

where $\varepsilon^{\alpha\beta} = e^{\alpha\beta}/\sqrt{g}$, with $g = \det(a_{\alpha\beta})$ and $e^{12} = -e^{21} = 1$, $e^{11} = e^{22} = 0$. For later use, we record that the contravariant cofactor or adjugate $\tilde{b}^{\alpha\beta}$ of the curvature tensor $b_{\alpha\beta}$ is defined as [Steigmann, 1999]

$$\tilde{b}^{\alpha\beta} = \varepsilon^{\alpha\lambda} \varepsilon^{\beta\mu} b_{\lambda\mu}. \tag{3.17}$$

This simplifies the expression for the Gaussian curvature to

$$K = \frac{1}{2} b_{\alpha\beta} \tilde{b}^{\alpha\beta}. \tag{3.18}$$

Writing this as $K = \frac{1}{2} a_{\beta\alpha} b^\beta_\mu \tilde{b}^{\mu\alpha}$ and noting that $a_{\alpha\beta} a^{\alpha\beta} = \delta^\alpha_\alpha = 2$, we obtain the identity

$$b^\beta_\mu \, \tilde{b}^{\mu\alpha} = K a^{\beta\alpha}, \tag{3.19}$$

which will be useful in later calculations. We also note for later use that the adjugate can be equivalently expressed as [Steigmann, 1999]

$$\tilde{b}^{\alpha\beta} = 2H a^{\alpha\beta} - b^{\alpha\beta}. \tag{3.20}$$

We will also make use of the fact that the adjugate is constant under covariant differentiation; in particular, we note the identity

$$\tilde{b}^{\alpha\beta}_{;\alpha} = 0, \tag{3.21}$$

which can be shown by taking the derivative of (3.17) and noting that $g_{;\alpha} = 0$ follows from Ricci's lemma (2.32). This gives

$$\tilde{b}^{\alpha\beta}_{;\alpha} = \varepsilon^{\alpha\lambda}\varepsilon^{\beta\mu}b_{\alpha\lambda;\mu} = \varepsilon^{\beta\mu}(\varepsilon^{\alpha\lambda}b_{\alpha\lambda})_{;\mu},$$

where we have used the Mainardi-Codazzi equations (2.28). Expanding, we have $\varepsilon^{\alpha\lambda}b_{\alpha\lambda} = \varepsilon^{12}b_{12} + \varepsilon^{21}b_{21} = 0$, using the symmetry of $b_{\alpha\beta}$ and that $\varepsilon^{12} = -\varepsilon^{21}$.

We calculate variations in the various quantities introduced above, denoting variations with respect to a parameter ε by a superposed dot (see (3.5)), so that the variation in $\boldsymbol{a}_\alpha$ is written $\dot{\boldsymbol{a}}_\alpha = \boldsymbol{u}_{,\alpha}$. We may then write the variation in the metric tensor as

$$\begin{aligned} \dot{a_{\alpha\beta}} &= \dot{\boldsymbol{a}}_\alpha \cdot \boldsymbol{a}_\beta + \boldsymbol{a}_\alpha \cdot \dot{\boldsymbol{a}}_\beta \\ &= \boldsymbol{a}_\alpha \cdot \boldsymbol{u}_{,\beta} + \boldsymbol{u}_{,\alpha} \cdot \boldsymbol{a}_\beta. \end{aligned} \tag{3.22}$$

We have from (3.5) and (3.15) that

$$\begin{aligned} \dot{\boldsymbol{a}}_\alpha = \dot{\overline{\boldsymbol{r}_{,\alpha}}} &= \lim_{\varepsilon\to 0} \frac{(\boldsymbol{r} + \varepsilon\boldsymbol{u})_{,\alpha} - \boldsymbol{r}_{,\alpha}}{\varepsilon} = \boldsymbol{u}_{,\alpha} \\ &= (u^\lambda \boldsymbol{a}_\lambda + w\boldsymbol{n})_{,\alpha} \\ &= u^\lambda_{;\alpha}\boldsymbol{a}_\lambda + u^\lambda \boldsymbol{a}_{\lambda;\alpha} + w_{,\alpha}\boldsymbol{n} + w\boldsymbol{n}_{,\alpha}, \end{aligned}$$

which can be written

$$\dot{\boldsymbol{a}}_\alpha = u^\lambda_{;\alpha}\boldsymbol{a}_\lambda + u^\lambda \boldsymbol{a}_{\lambda;\alpha} + w_{,\alpha}\boldsymbol{n} - wb^\beta_\alpha \boldsymbol{a}_\beta \tag{3.23}$$

using Weingarten's formula (2.17).

The variation in the inverse metric tensor follows from taking the variation of the identity

$$a^{\alpha\beta}a_{\beta\gamma} = \delta^\alpha_\gamma,$$

to give

$$a_{\beta\gamma}\dot{a}^{\alpha\beta} = -a^{\alpha\mu}\dot{a}_{\mu\gamma},$$

which yields

$$\dot{a}^{\alpha\beta} = -a^{\beta\gamma}a^{\alpha\mu}\dot{a}_{\mu\gamma}. \tag{3.24}$$

The variation in the metric determinant $g = \det(a_{\alpha\beta})$ may be calculated using Jacobi's formula [Magnus and Neudecker, 1988], which gives the derivative of the determinant of a matrix $\boldsymbol{A}$ with entries depending on a parameter ε as

$$\frac{d}{d\varepsilon}\det \boldsymbol{A} = \operatorname{tr}\left(\operatorname{adj}(\boldsymbol{A})\frac{d\boldsymbol{A}}{d\varepsilon}\right), \tag{3.25}$$

where $\operatorname{adj}(\boldsymbol{A}) = \det(\boldsymbol{A})\boldsymbol{A}^{-1}$ is the adjugate of $\boldsymbol{A}$, and $\operatorname{tr}(\boldsymbol{A})$ denotes the trace of $\boldsymbol{A}$. Here, the adjugate of the metric tensor is $ga^{\alpha\beta}$, so the formula (3.25) becomes

$$\dot{g} = \operatorname{tr}\left(ga^{\alpha\beta}\dot{a_{\beta\mu}}\right). \tag{3.26}$$

We also have that $\operatorname{tr}(a^{\alpha\beta}\dot{a}_{\beta\mu}) = a^{\alpha\beta}\dot{a}_{\alpha\beta}$, which gives

$$\dot{g} = ga^{\alpha\beta}\dot{a}_{\alpha\beta}. \tag{3.27}$$

The variation in the curvature tensor (2.4) is

$$\dot{b}_{\alpha\beta} = \dot{\boldsymbol{n}}\cdot\boldsymbol{a}_{\alpha;\beta} + \boldsymbol{n}\cdot\dot{\boldsymbol{a}}_{\alpha;\beta}.$$

Gauss's formula (2.26) gives $\dot{\boldsymbol{n}}\cdot\boldsymbol{a}_{\alpha;\beta} = b_{\alpha\beta}\dot{\boldsymbol{n}}\cdot\boldsymbol{n}$, and since $\boldsymbol{n}\cdot\boldsymbol{n} = 1$ we have $\dot{\boldsymbol{n}}\cdot\boldsymbol{n} = 0$, so that the variation in the curvature tensor simplifies to

$$\dot{b}_{\alpha\beta} = \boldsymbol{n}\cdot\boldsymbol{u}_{;\alpha\beta} \tag{3.28}$$

For the mean and Gaussian curvatures, taking the variations of H and K in (3.16) gives

$$\dot{H} = \frac{1}{2}(\dot{a^{\alpha\beta}}b_{\alpha\beta} + a^{\alpha\beta}\dot{b_{\alpha\beta}}), \tag{3.29}$$

$$\dot{K} = \frac{1}{2}e^{\alpha\beta}e^{\lambda\mu}\left[\frac{1}{g}(\dot{b}_{\alpha\lambda}b_{\beta\mu} + b_{\alpha\lambda}\dot{b}_{\beta\mu}) - \frac{\dot{g}}{g^2}b_{\alpha\lambda}b_{\beta\mu}\right]. \tag{3.30}$$

The latter of these may be simplified by using (3.17), (3.19) and (3.27) to obtain

$$\begin{aligned}\dot{K} &= \frac{1}{2}(\tilde{b}^{\alpha\lambda}\dot{b}_{\alpha\lambda} + \tilde{b}^{\beta\mu}\dot{b}_{\beta\mu}) - a^{\alpha\beta}\dot{a}_{\alpha\beta}K \\ &= \tilde{b}^{\alpha\beta}\dot{b}_{\alpha\beta} - a^{\alpha\beta}\dot{a}_{\alpha\beta}K. \end{aligned} \tag{3.31}$$

For the variation in $J = \sqrt{g}$, using (3.27), we have

$$\begin{aligned}\dot{J} &= \frac{1}{2}\dot{g}/\sqrt{g} \\ &= \frac{1}{2}Ja^{\alpha\beta}\dot{a_{\alpha\beta}}. \end{aligned} \tag{3.32}$$

We now specialise these expressions to variations in directions tangential and normal to the membrane surface.

3.4 Tangential variations

For *tangential* variations we set $w = 0$ in (3.15) so that $\boldsymbol{u} = u^\alpha \boldsymbol{a}_\alpha$. Then (3.23) and (2.26) give the variation in the tangent vectors as

$$\begin{aligned}\dot{\boldsymbol{a}}_\alpha &= u^\beta_{;\alpha}\boldsymbol{a}_\beta + u^\beta \boldsymbol{a}_{\beta;\alpha} \\ &= u^\beta_{;\alpha}\boldsymbol{a}_\beta + u^\beta b_{\alpha\beta}\boldsymbol{n}. \end{aligned} \tag{3.33}$$

Substituting (3.33) in (3.22) we have

$$\begin{aligned}\dot{a}_{\alpha\beta} &= \boldsymbol{a}_\alpha \cdot (u^\lambda_{;\beta}\boldsymbol{a}_\lambda) + (u^\lambda_{;\alpha}\boldsymbol{a}_\lambda)\cdot \boldsymbol{a}_\beta \\ &= u^\lambda_{;\beta}a_{\alpha\lambda} + u^\lambda_{;\alpha}a_{\lambda\beta} \\ &= (a_{\alpha\lambda}u^\lambda)_{;\beta} + (a_{\lambda\beta}u^\lambda)_{;\alpha} \\ &= u_{\alpha;\beta} + u_{\beta;\alpha}, \end{aligned} \tag{3.34}$$

since $a_{\alpha\lambda;\beta} = a_{\lambda\beta;\alpha} = 0$, according to Ricci's lemma (2.32). Substituting (3.34) in (3.24) then gives

$$\dot{a}^{\alpha\beta} = -a^{\beta\gamma}a^{\alpha\mu}(u_{\gamma;\mu} + u_{\mu;\gamma}). \tag{3.35}$$

The tangential variation in $b_{\alpha\beta}$ follows from substitution of $\boldsymbol{u} = u^\lambda \boldsymbol{a}_\lambda$ in equation (3.28), giving

$$\begin{aligned}\dot{b}_{\alpha\beta} &= \boldsymbol{n} \cdot (u^\lambda \boldsymbol{a}_\lambda)_{;\alpha\beta} \\ &= \boldsymbol{n} \cdot (u^\lambda_{\alpha;\beta}\boldsymbol{a}_\lambda + u^\lambda_{;\alpha}\boldsymbol{a}_{\lambda;\beta} + u^\lambda_{;\beta}\boldsymbol{a}_{\lambda;\alpha} + u^\lambda \boldsymbol{a}_{\lambda;\alpha\beta}) \\ &= u^\lambda_{;\alpha} b_{\lambda\beta} + u^\lambda_{;\beta} b_{\lambda\alpha} + u^\lambda b_{\lambda\alpha;\beta}, \end{aligned} \tag{3.36}$$

where we have used Gauss's formula (2.26).

We can now calculate the tangential variation in the mean curvature by substituting (3.35) and (3.36) in (3.29) to obtain

$$2\dot{H} = u^\alpha b^\beta_{\alpha;\beta}.$$

Using the Mainardi-Codazzi equations (2.29), we have $b^\beta_{\alpha;\beta} = b^\beta_{\beta;\alpha} = 2H_{,\alpha}$, which gives

$$\dot{H} = u^\alpha H_{,\alpha}. \tag{3.37}$$

The variation in the areal stretch J is obtained by substituting (3.34) in equation (3.32) to obtain

$$\dot{J} = J u^\alpha_{;\alpha}. \tag{3.38}$$

We now calculate the tangential variation of the Gaussian curvature K. We begin by multiplying on both sides of (3.19) by $a_{\beta\gamma}$ to obtain

$$a_{\beta\gamma} b^\beta_\mu \tilde{b}^{\mu\alpha} = K a^{\beta\alpha} a_{\beta\gamma} = K \delta^\alpha_\gamma,$$

so that, relabelling indexes, we have

$$b_{\lambda\alpha}\tilde{b}^{\alpha\beta} = \delta^\beta_\lambda K. \tag{3.39}$$

Using this identity and equations (3.21) and (3.36), we have that the first term of (3.31) specialises to

$$\begin{aligned}\tilde{b}^{\alpha\beta}\dot{b}_{\alpha\beta} &= (u^\lambda_{;\alpha} b_{\lambda\beta} + u^\lambda_{;\beta} b_{\lambda\alpha})\tilde{b}^{\alpha\beta} + u^\lambda (b_{\lambda\alpha}\tilde{b}^{\alpha\beta})_{;\beta} \\ &= 2u^\alpha_{;\alpha} K + u^\alpha K_{,\alpha} \end{aligned} \tag{3.40}$$

for tangential variations. Further noting that (3.34) gives

$$a^{\alpha\beta}\dot{a}_{\alpha\beta} = a^{\alpha\beta}(u_{\alpha;\beta} + u_{\beta;\alpha}) = 2u^{\alpha}_{;\alpha}, \tag{3.41}$$

we substitute (3.40) and (3.41) into (3.31) to obtain

$$\dot{K} = u^{\alpha}K_{,\alpha}. \tag{3.42}$$

We next calculate the tangential variation of the stretch-gradient magnitude $Q = |\nabla J|$ where

$$\nabla J = J_{,\alpha}\boldsymbol{a}^{\alpha} \tag{3.43}$$

so that

$$Q^2 = (\nabla J)\cdot(\nabla J) = J_{,\alpha}J_{,\beta}\boldsymbol{a}^{\alpha}\cdot\boldsymbol{a}^{\beta}. \tag{3.44}$$

Taking the variation of this expression gives

$$2Q\dot{Q} = 2J_{,\alpha}\boldsymbol{a}^{\alpha}\cdot(\dot{J}_{,\beta}\boldsymbol{a}^{\beta} + J_{,\beta}\dot{\boldsymbol{a}}^{\beta}),$$

so that

$$\dot{Q} = Q^{-1}(J_{,\alpha}\dot{J}_{,\beta}a^{\alpha\beta} + J_{,\alpha}J_{,\beta}\boldsymbol{a}^{\alpha}\cdot\dot{\boldsymbol{a}}^{\beta}). \tag{3.45}$$

Simplifying this expression requires the calculation of $\dot{\boldsymbol{a}}^{\beta} = (a^{\alpha\beta}\boldsymbol{a}_{\alpha})^{\cdot}$, which we obtain using (3.35) and Weingarten's formula (2.17) to be

$$\begin{aligned}
\dot{\boldsymbol{a}}^{\beta} &= \dot{a}^{\alpha\beta}\boldsymbol{a}_{\alpha} + a^{\alpha\beta}\boldsymbol{u}_{,\alpha} \\
&= \dot{a}^{\alpha\beta}\boldsymbol{a}_{\alpha} + a^{\alpha\beta}(u^{\lambda}\boldsymbol{a}_{\lambda})_{,\alpha} \\
&= -a^{\beta\gamma}a^{\alpha\mu}(u_{\gamma;\mu} + u_{\mu;\gamma})\boldsymbol{a}_{\alpha} + a^{\alpha\beta}(u^{\lambda}_{;\alpha}\boldsymbol{a}_{\lambda} + u^{\lambda}\boldsymbol{a}_{\lambda;\alpha}) \\
&= -u^{\beta}_{;\mu}\boldsymbol{a}^{\mu} - u^{\alpha}_{;\gamma}a^{\beta\gamma}\boldsymbol{a}_{\alpha} + a^{\alpha\beta}u^{\lambda}_{;\alpha}\boldsymbol{a}_{\lambda} + a^{\alpha\beta}u^{\lambda}b_{\lambda\alpha}\boldsymbol{n} \\
&= u^{\lambda}b^{\beta}_{\lambda}\boldsymbol{n} - u^{\beta}_{;\mu}\boldsymbol{a}^{\mu}.
\end{aligned} \tag{3.46}$$

Differentiating (3.38) with respect to θ^{β} gives

$$\dot{J}_{,\beta} = (Ju^{\alpha}_{;\alpha})_{,\beta}. \tag{3.47}$$

and substituting this together with (3.46) into (3.45) then yields

$$\begin{aligned}\dot{Q} &= Q^{-1}\left(J_{,\mu}(Ju^{\alpha}_{;\alpha})_{,\beta}a^{\mu\beta} + J_{,\alpha}J_{,\beta}\boldsymbol{a}^{\alpha}\cdot(u^{\lambda}b^{\beta}_{\lambda}\boldsymbol{n} - u^{\beta}_{;\mu}\boldsymbol{a}^{\mu})\right)\\ &= Q^{-1}J_{,\mu}a^{\mu\beta}\left[(Ju^{\alpha}_{;\alpha})_{,\beta} - J_{,\alpha}u^{\alpha}_{;\beta}\right]\end{aligned} \tag{3.48}$$

Now, assuming that the membrane energy density W depends on H, K, J, and Q, we have

$$\dot{W} = W_H\dot{H} + W_K\dot{K} + W_J\dot{J} + W_Q\dot{Q}. \tag{3.49}$$

Substituting the tangential variations (3.37), (3.42), (3.38), and (3.48) into this expression gives

$$\dot{W} = W_H H_{,\alpha}u^{\alpha} + W_K K_{,\alpha}u^{\alpha} + JW_J u^{\alpha}_{;\alpha} + Q^{-1}W_Q J_{,\mu}a^{\mu\beta}\left[(Ju^{\alpha}_{;\alpha})_{,\beta} - J_{,\alpha}u^{\alpha}_{;\beta}\right]. \tag{3.50}$$

We also record for later use that, using (3.38), we have

$$\begin{aligned}W\dot{J}/J &= Wu^{\alpha}_{;\alpha}\\ &= (Wu^{\alpha})_{;\alpha} - u^{\alpha}W_{,\alpha}.\end{aligned} \tag{3.51}$$

At this point we note that divergence terms can be easily moved to the boundary using Stokes' theorem; for example, we have

$$\int_{\omega} u^{\alpha}_{;\alpha}\,da = \int_{\partial\omega} u^{\alpha}\nu_{\alpha}\,ds, \tag{3.52}$$

where $\partial\omega$ is the boundary of ω, i.e. the edge of the membrane, with corresponding arc-length element ds, and ν_{α} are the components of $\boldsymbol{\nu}$, the normal vector to the boundary $\partial\omega$, as illustrated in Figure 3.3. This eventually allows the factoring of the perturbation term from the remaining terms in the area integral; for example, we have

$$\int_{\omega} W\dot{J}/J\,da = \int_{\omega}\left[(Wu^{\alpha})_{;\alpha} - u^{\alpha}W_{,\alpha}\right]da = \int_{\partial\omega} Wu^{\alpha}\nu_{\alpha}\,ds - \int_{\omega} u^{\alpha}W_{,\alpha}\,da,$$

where the term in the bulk integral now factors the perturbation u^{α}, and the remaining term has been moved to the boundary.

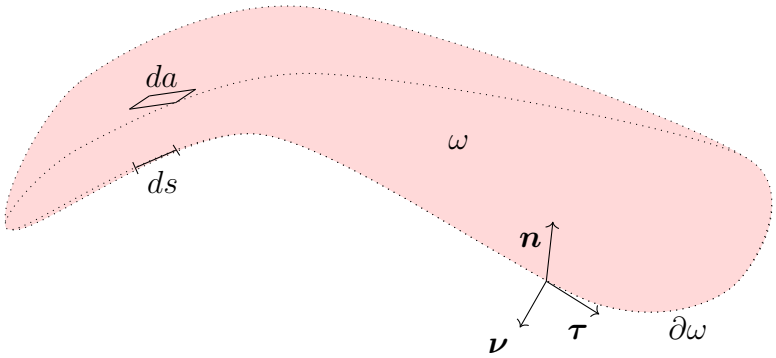

Figure 3.3: The membrane midsurface ω has area element da and is bounded by the closed curve $\partial\omega$, which has corresponding arc-length element ds. The vectors $\boldsymbol{\nu}$ and $\boldsymbol{\tau}$ are normal and tangential to the boundary $\partial\omega$, and $\boldsymbol{n} = \boldsymbol{\nu} \times \boldsymbol{\tau}$ is the normal to ω. In the analysis, Stokes' theorem is applied to write surface divergence terms on ω as terms involving the scalar product with $\boldsymbol{\nu}$ on the boundary $\partial\omega$.

Next, observing that

$$W_{,\alpha} = W_H H_{,\alpha} + W_K K_{,\alpha} + W_J J_{,\alpha} + W_Q Q_{,\alpha}, \tag{3.53}$$

and using (3.51), we have that

$$\dot{W} + W\dot{J}/J = \dot{W} + (Wu^\alpha)_{;\alpha} - u^\alpha W_{,\alpha}.$$

Substituting in this expression for $\dot{W}$ and $W_{,\alpha}$ using (3.50) and (3.53), we arrive at

$$\begin{aligned}\dot{W} + W\dot{J}/J = {} & (JW_J u^\alpha)_{;\alpha} - (JW_J)_{,\alpha} u^\alpha + Q^{-1} W_Q J_{,\mu} a^{\mu\beta} \left[(Ju^\alpha_{;\alpha})_{,\beta} - J_{,\alpha} u^\alpha_{;\beta}\right] \\ & + (Wu^\alpha)_{;\alpha} - u^\alpha (W_J J_{,\alpha} + W_Q Q_{,\alpha}).\end{aligned} \tag{3.54}$$

For the third term on the right-hand side, we rearrange to obtain terms which either involve a single divergence or from which the perturbation u^α can be explicitly factored. This gives

$$\begin{aligned}Q^{-1} W_Q J_{,\mu} a^{\mu\beta} \left[(Ju^\alpha_{;\alpha})_{,\beta} - J_{,\alpha} u^\alpha_{;\beta}\right] = {} & (Q^{-1} W_Q J J_{,\mu} a^{\mu\beta} u^\alpha_{;\alpha})_{;\beta} - [Ju^\alpha (Q^{-1} W_Q J_{,\mu} a^{\mu\beta})_{;\beta}]_{;\alpha} \\ & + Ju^\alpha (Q^{-1} W_Q J_{,\mu} a^{\mu\beta})_{;\beta\alpha} + J_{,\alpha} u^\alpha (Q^{-1} W_Q J_{,\mu} a^{\mu\beta})_{;\beta} \\ & - (Q^{-1} W_Q J_{,\mu} J_{,\alpha} a^{\mu\beta} u^\alpha)_{;\beta} + u^\alpha (Q^{-1} W_Q J_{,\mu} J_{,\alpha} a^{\mu\beta})_{;\beta}.\end{aligned} \tag{3.55}$$

Differentiating $Q^2 = J_{,\mu}J_{,\beta}a^{\mu\beta}$ with respect to θ^α gives

$$\begin{aligned} 2QQ_{,\alpha} &= (J_{,\mu}J_{,\beta}a^{\mu\beta})_{;\alpha} \\ &= 2J_{;\mu\alpha}J_{,\beta}a^{\mu\beta}, \end{aligned}$$

where we have used that $(a^{\mu\beta})_{;\alpha} = 0$ by Ricci's lemma (2.32). Then we can write

$$\begin{aligned} W_Q Q_{,\alpha} &= Q^{-1}W_Q J_{,\beta}J_{;\mu\alpha}a^{\mu\beta} \\ &= (Q^{-1}W_Q J_{,\alpha}J_{,\beta}a^{\mu\beta})_{;\mu} - J_{,\alpha}(Q^{-1}W_Q J_{,\beta}a^{\mu\beta})_{;\mu}. \end{aligned} \tag{3.56}$$

Substituting (3.55) and (3.56) into (3.54) then yields

$$\begin{aligned} \int_\omega (\dot{W} + W\dot{J}/J)\,da = \int_\omega u^\alpha [&-(JW_J)_{,\alpha} - W_J J_{,\alpha} - (Q^{-1}W_Q J_{,\alpha}J_{,\beta}a^{\mu\beta})_{;\mu} \\ &+ J_{,\alpha}(Q^{-1}W_Q J_{,\beta}a^{\mu\beta})_{;\mu} + J(Q^{-1}W_Q J_{,\mu}a^{\mu\beta})_{;\beta\alpha} \\ &+ J_{,\alpha}(Q^{-1}W_Q J_{,\mu}a^{\mu\beta})_{;\beta} + (Q^{-1}W_Q J_{,\mu}J_{,\alpha}a^{\mu\beta})_{;\beta}]\,da \\ &+ \int_{\partial\omega} [JW_J u^\alpha \nu_\alpha + W u^\alpha \nu_\alpha + Q^{-1}W_Q J J_{,\mu}a^{\mu\beta}u^\alpha_{;\alpha}\nu_\beta \\ &- J u^\alpha (Q^{-1}W_Q J_{,\mu}a^{\mu\beta})_{;\beta}\nu_\alpha - Q^{-1}W_Q J_{,\mu}J_{,\alpha}a^{\mu\beta}u^\alpha \nu_\beta]\,ds. \end{aligned}$$

Thus, comparing with (3.13), we see that the Euler-Lagrange equations arising from the bulk term are

$$(JW_J)_{,\alpha} + W_J J_{,\alpha} - 2J_{,\alpha}(Q^{-1}W_Q J_{,\mu}a^{\mu\beta})_{;\beta} - J(Q^{-1}W_Q J_{,\mu}a^{\mu\beta})_{;\beta\alpha} = 0. \tag{3.57}$$

The terms on the boundary $\partial\omega$ correspond to forces and bending moments on the edge of the membrane, together with a higher-order hydrostatic hyperstress (see, for example, [Podio-Guidugli and Vianello, 2010]) acting on the membrane edge, involving $u^\alpha_{;\alpha}$, the divergence of the perturbation. We denote by B_t the work done by a tangential perturbation, and by T_t the hyperwork arising from the imposition of tangential variations. From the boundary terms above, we see that these terms have expressions

$$B_t = \int_{\partial\omega} u^\alpha [JW_J\nu_\alpha + W\nu_\alpha - J(Q^{-1}W_Q J_{,\mu}a^{\mu\beta})_{;\beta}\nu_\alpha - Q^{-1}W_Q J_{,\mu}J_{,\alpha}\nu^\mu]\,ds, \tag{3.58}$$

$$T_t = \int_{\partial\omega} Q^{-1}W_Q J J_{,\mu}u^\alpha_{;\alpha}\nu^\mu\,ds. \tag{3.59}$$

Next, writing the vectors normal and tangential to the membrane boundary as

$$\boldsymbol{\nu} = \nu^\alpha \boldsymbol{a}_\alpha, \quad \boldsymbol{\tau} = \tau^\alpha \boldsymbol{a}_\alpha, \tag{3.60}$$

respectively, we have

$$\begin{aligned} u^\alpha &= \boldsymbol{u} \cdot \boldsymbol{a}^\alpha \\ &= \boldsymbol{u} \cdot ((\boldsymbol{a}^\alpha \cdot \boldsymbol{\tau})\boldsymbol{\tau} + (\boldsymbol{a}^\alpha \cdot \boldsymbol{\nu})\boldsymbol{\nu}) \\ &= \boldsymbol{u} \cdot (\tau^\alpha \boldsymbol{\tau} + \nu^\alpha \boldsymbol{\nu}). \end{aligned} \tag{3.61}$$

Using this decomposition, and defining $J_\nu = \nu^\alpha J_{,\alpha}$ and $J' = \tau^\alpha J_{,\alpha}$, the *normal* and *tangential derivatives* of J respectively, B_t may be resolved into components normal and tangential to the boundary,

$$B_t = \int_{\partial\omega} \boldsymbol{u} \cdot \left\{ \left[W + W_J J - J(Q^{-1} W_Q J_{,\mu} a^{\mu\beta})_{;\beta} - Q^{-1} W_Q J_\nu^2 \right] \boldsymbol{\nu} - Q^{-1} W_Q J_\nu J' \boldsymbol{\tau} \right\} ds, \tag{3.62}$$

while the hyperwork T_t may be written

$$T_t = \int_{\partial\omega} Q^{-1} W_Q J J_\nu \operatorname{div} \boldsymbol{u} \, ds. \tag{3.63}$$

We will return to these expressions in Section 3.6, where they will be combined with the corresponding terms obtained by taking normal variations.

3.5 Normal variations

For *normal* variations we have $u^\alpha = 0$ in (3.15), so that $\boldsymbol{u} = w\boldsymbol{n}$. Using (3.23) and (3.22), we have that

$$\begin{aligned} \dot{a}_{\alpha\beta} &= \boldsymbol{a}_\alpha \cdot \boldsymbol{u}_{,\beta} + \boldsymbol{u}_{,\alpha} \cdot \boldsymbol{a}_\beta \\ &= \boldsymbol{a}_\alpha \cdot (w_{,\beta}\boldsymbol{n} - w b^\mu_\beta \boldsymbol{a}_\mu) + \boldsymbol{a}_\beta \cdot (w_{,\alpha}\boldsymbol{n} - w b^\mu_\alpha \boldsymbol{a}_\mu) \\ &= -2w b_{\alpha\beta} \end{aligned} \tag{3.64}$$

Substituting this in (3.32) and recalling (3.16) gives that the normal variation in J is

$$\dot{J} = -Ja^{\alpha\beta}wb_{\alpha\beta} = -2HJw, \tag{3.65}$$

so that

$$W_J\dot{J} = -2HJW_Jw. \tag{3.66}$$

For the inverse metric variation, substituting (3.64) in (3.24) gives

$$\dot{a}^{\alpha\beta} = -a^{\beta\gamma}a^{\alpha\mu}\dot{a}_{\mu\gamma} = 2wa^{\beta\gamma}a^{\alpha\mu}b_{\mu\gamma} = 2wb^{\alpha\beta}. \tag{3.67}$$

For the variation in the curvature tensor components, we first note that

$$\begin{aligned}
\boldsymbol{u}_{,\alpha\beta} &= (w\boldsymbol{n})_{,\alpha\beta} \\
&= (w_{,\alpha}\boldsymbol{n} + w\boldsymbol{n}_{,\alpha})_{,\beta} \\
&= w_{,\alpha\beta}\boldsymbol{n} + w_{,\alpha}\boldsymbol{n}_{,\beta} + w_{,\beta}\boldsymbol{n}_{,\alpha} + w(\boldsymbol{n}_{,\alpha})_{,\beta} \\
&= w_{,\alpha\beta}\boldsymbol{n} - w_{,\alpha}b^{\mu}_{\beta}\boldsymbol{a}_{\mu} - w_{,\beta}b^{\mu}_{\alpha}\boldsymbol{a}_{\mu} - w(b^{\mu}_{\alpha;\beta}\boldsymbol{a}_{\mu} + b^{\mu}_{\alpha}\boldsymbol{a}_{\mu;\beta}),
\end{aligned}$$

where we have applied Weingarten's formula (2.17) in the final step. Substituting this in (3.28), we obtain

$$\begin{aligned}
\dot{b}_{\alpha\beta} &= \boldsymbol{n}\cdot(w_{,\alpha\beta}\boldsymbol{n} - w_{,\alpha}b^{\mu}_{\beta}\boldsymbol{a}_{\mu} - w_{,\beta}b^{\mu}_{\alpha}\boldsymbol{a}_{\mu} - wb^{\mu}_{\alpha;\beta}\boldsymbol{a}_{\mu} - wb^{\mu}_{\alpha}b_{\mu\beta}\boldsymbol{n}) \\
&= w_{,\alpha\beta} - b^{\mu}_{\alpha}b_{\mu\beta}w.
\end{aligned} \tag{3.68}$$

Substitution of (3.67) and (3.68) in (3.29) then gives

$$\begin{aligned}
2\dot{H} &= \dot{a}^{\alpha\beta}b_{\alpha\beta} + a^{\alpha\beta}\dot{b}_{\alpha\beta} \\
&= 2wb^{\alpha\beta}b_{\alpha\beta} + a^{\alpha\beta}w_{,\alpha\beta} - a^{\alpha\beta}b^{\mu}_{\alpha}b_{\mu\beta}w \\
&= wb^{\alpha\beta}b_{\alpha\beta} + a^{\alpha\beta}w_{,\alpha\beta}.
\end{aligned} \tag{3.69}$$

Writing

$$\begin{aligned} b^{\alpha\beta}b_{\alpha\beta} = a^{\alpha\gamma}a^{\beta\mu}b_{\gamma\mu}b_{\alpha\beta} &= b^{\beta}_{\alpha}b^{\alpha}_{\beta} \\ &= b_1^{1\,2} + 2b_1^2 b_2^1 + b_2^{2\,2} \\ &= (b_1^1 + b_2^2)^2 - 2b_1^1 b_2^2 + 2b_1^2 b_2^1 \\ &= b_\alpha^{\alpha\,2} - 2(b_1^1 b_2^2 - b_1^2 b_2^1) \\ &= (2H)^2 - 2\det(b^{\beta}_{\alpha}) \\ &= (2H)^2 - 2K, \end{aligned} \tag{3.70}$$

and substituting in (3.69), we obtain that the normal variation in the mean curvature is

$$\dot{H} = \frac{1}{2}\Delta w + (2H^2 - K)w, \tag{3.71}$$

where $\Delta(\cdot) = a^{\alpha\beta}(\cdot)_{;\alpha\beta}$ is the surface Laplacian. We now have

$$W_H\dot{H} = \frac{1}{2}W_H\Delta w + W_H w(2H^2 - K).$$

Keeping in mind our aim to arrange terms so that they either factor the perturbation or are written as a single divergence term, we write the first term on the right-hand side as

$$\begin{aligned} \frac{1}{2}W_H\Delta w &= \frac{1}{2}W_H a^{\alpha\beta}w_{,\alpha\beta} \\ &= (\tfrac{1}{2}W_H a^{\alpha\beta}w_{,\alpha})_{;\beta} - \tfrac{1}{2}w_{,\alpha}(W_H a^{\alpha\beta})_{;\beta} \\ &= (\tfrac{1}{2}W_H a^{\alpha\beta}w_{,\alpha})_{;\beta} - [\tfrac{1}{2}w(W_H a^{\alpha\beta})_{;\beta}]_{;\alpha} + \tfrac{1}{2}w(W_H a^{\alpha\beta})_{;\alpha\beta} \\ &= (\tfrac{1}{2}W_H a^{\alpha\beta}w_{,\alpha})_{;\beta} - [\tfrac{1}{2}w(W_H a^{\alpha\beta})_{;\beta}]_{;\alpha} + \tfrac{1}{2}w\Delta W_H, \end{aligned} \tag{3.72}$$

so that

$$W_H\dot{H} = \left(\tfrac{1}{2}W_H a^{\alpha\beta}w_{,\alpha}\right)_{;\beta} - \tfrac{1}{2}[w(W_H a^{\alpha\beta})_{;\beta}]_{;\alpha} + \tfrac{1}{2}w\Delta W_H + W_H w(2H^2 - K). \tag{3.73}$$

For the variation in the Gaussian curvature, we first note that (3.68) together with the definition $(3.16)_1$ and the identities (3.19) and (3.21) gives

$$\begin{aligned}\tilde{b}^{\alpha\beta}\dot{b}_{\alpha\beta} &= \tilde{b}^{\alpha\beta}(w_{,\alpha\beta}) - w\tilde{b}^{\alpha\beta}b^{\lambda}_{\alpha}b_{\beta\lambda} \\ &= (\tilde{b}^{\alpha\beta}w_{,\alpha})_{;\beta} - 2wHK\end{aligned}$$

while (3.64) gives

$$a^{\alpha\beta}\dot{a}_{\alpha\beta} = -2a^{\alpha\beta}wb_{\alpha\beta} = -4Hw.$$

Substituting these two expressions in (3.31) and using the identity (3.20) then gives

$$\begin{aligned}\dot{K} &= \tilde{b}^{\alpha\beta}\dot{b}_{\alpha\beta} - a^{\alpha\beta}\dot{a}_{\alpha\beta}K \\ &= (\tilde{b}^{\alpha\beta}w_{,\alpha})_{;\beta} - 2wHK + 4wHK \\ &= 2KHw + (\tilde{b}^{\alpha\beta}w_{,\alpha})_{;\beta},\end{aligned}$$

so that, by reasoning analogously to (3.72), we obtain

$$W_K\dot{K} = 2HKW_Kw + (W_K\tilde{b}^{\alpha\beta}w_{,\alpha})_{;\beta} - ((W_K)_{;\beta}\tilde{b}^{\alpha\beta}w)_{;\alpha} + w(W_K)_{;\beta\alpha}\tilde{b}^{\beta\alpha}. \tag{3.74}$$

Next, for the normal variation of Q, taking the variation of equation (3.44) we have

$$2Q\dot{Q} = 2\dot{J}_{,\alpha}J_{,\beta}a^{\alpha\beta} + J_{,\alpha}J_{,\beta}\dot{a}^{\alpha\beta}. \tag{3.75}$$

Differentiating (3.65) with respect to θ^{α} gives

$$\dot{J}_{,\alpha} = -2(HJw)_{,\alpha},$$

and substitution of this and (3.67) into (3.75) gives

$$\dot{Q} = Q^{-1}\left[J_{,\alpha}J_{,\beta}b^{\alpha\beta}w - 2a^{\alpha\beta}(HJw)_{,\alpha}J_{,\beta}\right]. \tag{3.76}$$

Then with

$$Q^{-1}a^{\alpha\beta}(HJw)_{,\alpha}J_{,\beta} = (Q^{-1}a^{\alpha\beta}HJwJ_{,\beta})_{;\alpha} - HJw(Q^{-1}a^{\alpha\beta}J_{,\beta})_{;\alpha},$$

we have from (3.76) that

$$W_Q\dot{Q} = Q^{-1}W_Q J_{,\alpha}J_{,\beta}b^{\alpha\beta}w - (2Q^{-1}W_Q a^{\alpha\beta}J_{,\beta}JHw)_{;\alpha} + 2HJw(Q^{-1}W_Q a^{\alpha\beta}J_{,\beta})_{;\alpha} \tag{3.77}$$

Substituting (3.73), (3.74), (3.66) and (3.77) into

$$\dot{W} = W_H\dot{H} + W_K\dot{K} + W_J\dot{J} + W_Q\dot{Q}$$

together with (3.65) gives

$$\begin{aligned}\dot{W} + W\dot{J}/J =& w\,[\tfrac{1}{2}\Delta W_H + W_H(2H^2 - K) + 2HKW_K + (W_K)_{;\beta\alpha}\tilde{b}^{\beta\alpha} - 2HJW_J \\ &+ Q^{-1}W_Q J_{,\alpha}J_{,\beta}b^{\alpha\beta} + 2HJ(Q^{-1}W_Q a^{\alpha\beta}J_{,\beta})_{;\alpha} - 2HW] \\ &+ \left(\tfrac{1}{2}W_H a^{\alpha\beta}w_{,\alpha}\right)_{;\beta} - \tfrac{1}{2}[w(W_H a^{\alpha\beta})_{;\beta}]_{;\alpha} + (W_K\tilde{b}^{\alpha\beta}w_{,\alpha})_{;\beta} - ((W_K)_{;\beta}\tilde{b}^{\alpha\beta}w)_{;\alpha} \\ &- (2Q^{-1}W_Q a^{\alpha\beta}J_{,\beta}JHw)_{;\alpha}\end{aligned}$$

With this, the variation in the total energy (3.6) can be written

$$\begin{aligned}\dot{E} =& \int_\omega (\dot{W} + W\dot{J}/J)\,da \\ =& \int_\omega w\,[\tfrac{1}{2}\Delta W_H + W_H(2H^2 - K) + 2HKW_K + (W_K)_{;\beta\alpha}\tilde{b}^{\beta\alpha} - 2HJW_J \\ &+ Q^{-1}W_Q J_{,\alpha}J_{,\beta}b^{\alpha\beta} + 2HJ(Q^{-1}W_Q a^{\alpha\beta}J_{,\beta})_{;\alpha} - 2HW]\,da \\ &+ \int_{\partial\omega}\Big[\tfrac{1}{2}W_H w_{,\alpha}\nu^\alpha - \tfrac{1}{2}w(W_H)_{;\alpha}\nu^\alpha + W_K\tilde{b}^{\alpha\beta}w_{,\alpha}\nu_\beta \\ &\qquad -(W_K)_{;\beta}\tilde{b}^{\alpha\beta}w\nu_\alpha - 2Q^{-1}W_Q J_{,\beta}JHw\nu^\beta\Big]\,ds.\end{aligned} \tag{3.78}$$

Now recalling (3.13), we see that the pressure p exerted on the membrane in the normal direction may identified with the appropriate corresponding expression in the bulk integral, which gives the Euler-Lagrange equation

$$\begin{aligned}&\frac{1}{2}\Delta W_H + W_H(2H^2 - K) + 2HKW_K + (W_K)_{;\beta\alpha}\tilde{b}^{\beta\alpha} - 2HJW_J \\ &\quad + Q^{-1}W_Q J_{,\alpha}J_{,\beta}b^{\alpha\beta} + 2HJ(Q^{-1}W_Q a^{\alpha\beta}J_{,\beta})_{;\alpha} - 2HW = p.\end{aligned} \tag{3.79}$$

This equation may be readily compared with the shape equations obtained by other authors for more specialised forms of the energy density; for example, if $W = W(H, K)$,

the shape equation reduces to

$$\frac{1}{2}\Delta W_H + W_H(2H^2 - K) + 2HKW_K + (W_K)_{;\beta\alpha}\tilde{b}^{\beta\alpha} - 2HW = p,$$

as obtained by [Steigmann et al., 2003]. If the dependence of W on K is suppressed, the shape equation reads

$$\frac{1}{2}\Delta W_H + W_H(2H^2 - K) - 2HW = p,$$

which has been used, for example, in [Jenkins, 1977] to obtain equilibrium shapes for red blood cells, with the suppression of dependence on K justified by the Gauss-Bonnet theorem (2.30). For the classical Canham-Helfrich membrane energy density

$$W = kH^2 + \bar{k}K,$$

where k and $\bar{k}$ are bending rigidities, the corresponding shape equation is

$$k\left(\Delta H + 2H(H^2 - K)\right) + 2H(\bar{k}K - W) = p.$$

We note that for each of the foregoing cases, the corresponding tangential equations (3.57) are trivial.

The work done on the boundary arising from normal variations is given by (3.78) as

$$\begin{aligned} B_n = \int_{\partial\omega} \Big[&\tfrac{1}{2}W_H\nu^\alpha w_{,\alpha} - \tfrac{1}{2}(W_H)_{,\alpha}\nu^\alpha w + W_K\tilde{b}^{\alpha\beta}w_{,\alpha}\nu_\beta \\ &-(W_K)_{,\alpha}\tilde{b}^{\alpha\beta}w\nu_\beta - 2Q^{-1}W_Q J_{,\alpha}JHw\nu^\alpha \Big]\, ds. \end{aligned} \tag{3.80}$$

This may be expressed more usefully by recalling the definition of the vectors $\boldsymbol{\tau}$ and $\boldsymbol{\nu}$, the unit vectors tangent and normal to the boundary $\partial\omega$, given in (3.60), and by noting the decomposition

$$\begin{aligned} w_{,\alpha} = (\nabla w)\cdot\boldsymbol{a}_\alpha &= (\nabla w)\cdot((\boldsymbol{a}_\alpha\cdot\boldsymbol{\tau})\boldsymbol{\tau} + (\boldsymbol{a}_\alpha\cdot\boldsymbol{\nu})\boldsymbol{\nu}) \\ &= (\nabla w)\cdot(\tau_\alpha\boldsymbol{\tau} + \nu_\alpha\boldsymbol{\nu}) \\ &= \tau_\alpha w' + \nu_\alpha w_{,\nu}, \end{aligned} \tag{3.81}$$

where w' and $w_{,\nu}$ are the tangential and normal derivatives of w. This then gives

$$a^{\alpha\beta}w_{,\alpha} = \tau^{\beta}w' + \nu^{\beta}w_{,\nu}. \tag{3.82}$$

With this, and using (3.20), we write the third term in the integral (3.80) as

$$\begin{aligned} W_K\tilde{b}^{\alpha\beta}\nu_\beta w_{,\alpha} &= 2HW_K a^{\alpha\beta}\nu_\beta w_{,\alpha} - W_K b^{\alpha\beta}\nu_\beta w_{,\alpha} \\ &= 2HW_K w_{,\nu} - W_K b^{\alpha\beta}\nu_\beta w_{,\alpha}, \end{aligned} \tag{3.83}$$

recalling that $\nu^{\alpha}w_{,\alpha} = w_{,\nu}$. To simplify the second term on the right-hand side, we define

$$\tau = b^{\alpha\beta}\tau_\alpha\nu_\beta, \tag{3.84}$$

the twist of the surface on the $\boldsymbol{\nu}$-$\boldsymbol{\tau}$ axes, and

$$\kappa_\nu = \nu^\alpha\nu^\beta b_{\alpha\beta},$$

the normal curvature of ω in the direction of $\boldsymbol{\nu}$. Using these definitions, together with the decomposition (3.81) we obtain that

$$\begin{aligned} W_K b^{\alpha\beta}\nu_\beta w_{,\alpha} &= W_K(b^{\alpha\beta}\tau_\alpha\nu_\beta w' + b^{\alpha\beta}\nu_\alpha\nu_\beta w_{,\nu}) \\ &= W_K\tau w' + W_K\kappa_\nu w_{,\nu} \\ &= (W_K\tau w)' - w(\tau W_K)' + \kappa_\nu W_K w_{,\nu}, \end{aligned}$$

so that

$$W_K\tilde{b}^{\alpha\beta}\nu_\beta w_{,\alpha} = w(\tau W_K)' - (\tau W_K w)' + (2H - \kappa_\nu)W_K w_{,\nu}. \tag{3.85}$$

We can also write the first term in (3.80) as

$$\frac{1}{2}W_H\nu^\alpha w_{,\alpha} = \frac{1}{2}W_H w_{,\nu}. \tag{3.86}$$

Thus using (3.86) and (3.85), the integral (3.80) for B_n may be expressed in the more

useful form

$$B_n = \int_{\partial\omega} \boldsymbol{u} \cdot \left[(\tau W_K)' - \tfrac{1}{2}(W_H)_{,\nu} - (W_K)_{,\beta}\tilde{b}^{\alpha\beta}\nu_\alpha - 2Q^{-1}W_Q H J J_\nu \right] \boldsymbol{n}\, ds + \int_{\partial\omega} (\tfrac{1}{2}W_H + \kappa_\tau W_K) w_{,\nu}\, ds + \sum w W_K[\tau], \tag{3.87}$$

where

$$\kappa_\tau = \tau^\alpha \tau^\beta b_{\alpha\beta} = 2H - \kappa_\nu$$

is the normal curvature of ω in the direction of $\boldsymbol{\tau}$, and the final term arises from the integral $\int_{\partial\omega}(\tau W_K w)' ds$, where $[\tau]$ denotes the forward jump of τ at a corner of the boundary $\partial\omega$, at which point τ is discontinuous.

3.6 Boundary terms

Before gathering together the boundary terms from tangential and normal perturbations, we first note that $w = \boldsymbol{u} \cdot \boldsymbol{n}$, so that

$$w_{,\nu} = \boldsymbol{u}_{,\nu} \cdot \boldsymbol{n} + \boldsymbol{u} \cdot \boldsymbol{n}_{,\nu}.$$

Using Gauss's formula (2.26), we have $\boldsymbol{n}_{,\nu} = \nu^\alpha \boldsymbol{n}_{,\alpha} = -\nu_\alpha b^{\alpha\beta}\boldsymbol{a}_\beta$, and this, together with $\boldsymbol{a}_\beta = \tau_\beta \boldsymbol{\tau} + \nu_\beta \boldsymbol{\nu}$, gives

$$w_{,\nu} = \boldsymbol{u}_{,\nu} \cdot \boldsymbol{n} - \boldsymbol{u} \cdot (\tau \boldsymbol{\tau} + \kappa_\nu \boldsymbol{\nu}). \tag{3.88}$$

Seeking to further simplify the first term on the right-hand side, we note that taking the variation of $\boldsymbol{n} \cdot \boldsymbol{a}_\alpha = 0$ gives

$$\begin{aligned} \dot{\boldsymbol{n}} \cdot \boldsymbol{a}_\alpha &= -\boldsymbol{n} \cdot \boldsymbol{u}_{,\alpha} \\ &= -(\boldsymbol{n} \cdot \boldsymbol{u}_{,\beta})\boldsymbol{a}^\beta \cdot \boldsymbol{a}_\alpha, \end{aligned}$$

since $\boldsymbol{a}_\alpha \cdot \boldsymbol{a}^\beta = \delta_\alpha^\beta$. Comparing both sides, and recalling that $\dot{\boldsymbol{n}} \cdot \boldsymbol{n} = 0$, we have that the variation in $\boldsymbol{n}$ can be written

$$\dot{\boldsymbol{n}} = -(\boldsymbol{n} \cdot \boldsymbol{u}_{,\alpha})\boldsymbol{a}^\alpha.$$

Writing $\boldsymbol{a}^\alpha = \tau^\alpha \boldsymbol{\tau} + \nu^\alpha \boldsymbol{\nu}$, this becomes

$$\begin{aligned}\dot{\boldsymbol{n}} &= -(\boldsymbol{n}\cdot\boldsymbol{u}_{,\alpha})(\tau^\alpha\boldsymbol{\tau}+\nu^\alpha\boldsymbol{\nu}) \\ &= -(\boldsymbol{n}\cdot\tau^\alpha\boldsymbol{u}_{,\alpha})\boldsymbol{\tau} - (\boldsymbol{n}\cdot\nu^\alpha\boldsymbol{u}_{,\alpha})\boldsymbol{\nu} \\ &= -(\boldsymbol{n}\cdot\boldsymbol{u}')\boldsymbol{\tau} - (\boldsymbol{n}\cdot\boldsymbol{u}_{,\nu})\boldsymbol{\nu}. \end{aligned} \tag{3.89}$$

We next use the identity

$$\boldsymbol{a}\times(\boldsymbol{b}\times\boldsymbol{c}) = (\boldsymbol{a}\cdot\boldsymbol{c})\boldsymbol{b} - (\boldsymbol{a}\cdot\boldsymbol{b})\boldsymbol{c} \tag{3.90}$$

and the orthogonality of $\boldsymbol{n}$ and $\boldsymbol{\tau}$, $\boldsymbol{\nu}$ to obtain

$$\begin{aligned}(\boldsymbol{n}\cdot\boldsymbol{u}')\boldsymbol{\tau} &= \boldsymbol{n}\times(\boldsymbol{\tau}\times\boldsymbol{u}'), \\ (\boldsymbol{n}\cdot\boldsymbol{u}_{,\nu})\boldsymbol{\nu} &= \boldsymbol{n}\times(\boldsymbol{\nu}\times\boldsymbol{u}_{,\nu}),\end{aligned}$$

and substituting these identities into (3.89) yields

$$\begin{aligned}\dot{\boldsymbol{n}} &= -\boldsymbol{n}\times(\boldsymbol{\tau}\times\boldsymbol{u}' + \boldsymbol{\nu}\times\boldsymbol{u}_{,\nu}) \\ &= \boldsymbol{\omega}\times\boldsymbol{n}, \end{aligned} \tag{3.91}$$

where we have set $\boldsymbol{\omega} = \boldsymbol{\tau}\times\boldsymbol{u}' + \boldsymbol{\nu}\times\boldsymbol{u}_{,\nu}$. Rearranging equation (3.89), substituting for $\dot{\boldsymbol{n}}$ using (3.91), using $\boldsymbol{n} = \boldsymbol{\nu}\times\boldsymbol{\tau}$, and again applying the identity (3.90), we have

$$\begin{aligned}(\boldsymbol{n}\cdot\boldsymbol{u}_{,\nu})\boldsymbol{\nu} &= -\boldsymbol{\omega}\times\boldsymbol{n} - (\boldsymbol{n}\cdot\boldsymbol{u}')\boldsymbol{\tau} \\ &= -\boldsymbol{\omega}\times(\boldsymbol{\nu}\times\boldsymbol{\tau}) - (\boldsymbol{n}\cdot\boldsymbol{u}')\boldsymbol{\tau} \\ &= -[(\boldsymbol{\omega}\cdot\boldsymbol{\tau})\boldsymbol{\nu} - (\boldsymbol{\omega}\cdot\boldsymbol{\nu})\boldsymbol{\tau}] - (\boldsymbol{n}\cdot\boldsymbol{u}')\boldsymbol{\tau} \\ &= -(\boldsymbol{\omega}\cdot\boldsymbol{\tau})\boldsymbol{\nu} + [\boldsymbol{\omega}\cdot\boldsymbol{\nu} - \boldsymbol{n}\cdot\boldsymbol{u}']\boldsymbol{\tau}. \end{aligned} \tag{3.92}$$

Comparing the left and right-hand sides of this equation, we obtain

$$\boldsymbol{n}\cdot\boldsymbol{u}_{,\nu} = -\boldsymbol{\tau}\cdot\boldsymbol{\omega}, \tag{3.93}$$

$$\boldsymbol{n}\cdot\boldsymbol{u}' = \boldsymbol{\nu}\cdot\boldsymbol{\omega}. \tag{3.94}$$

and substituting the first of these in (3.88) gives

$$w_{,\nu} = -\boldsymbol{\tau}\cdot\boldsymbol{\omega} - \boldsymbol{u}\cdot(\tau\boldsymbol{\tau} + \kappa_\nu\boldsymbol{\nu}). \tag{3.95}$$

To simplify the second integral in (3.87), we identify the bending moment

$$M = \frac{1}{2}W_H + \kappa_\tau W_K, \tag{3.96}$$

which can be interpreted as a moment which bends the unit normal in the direction of $\boldsymbol{\nu}$ at the boundary, and which can be obtained by calculating

$$M = M^{\alpha\beta}\nu_\alpha\nu_\beta$$

where $M^{\alpha\beta} = \frac{1}{2}W_H a^{\alpha\beta} + W_K\tilde{b}^{\alpha\beta}$ is the bending moment tensor [Sahu et al., 2017]. This, together with (3.95), allows us to write the second integral in (3.87) as

$$\int_{\partial\omega} M w_{,\nu}\, ds = -\int_{\partial\omega} M\boldsymbol{\tau}\cdot\boldsymbol{\omega}\, ds - \int_{\partial\omega} M\boldsymbol{u}\cdot(\tau\boldsymbol{\tau} + \kappa_\nu\boldsymbol{\nu})\, ds, \tag{3.97}$$

so that the terms in the second integral on the right-hand side contribute to the forces tangential and normal to the boundary, acting alongside those previously obtained in (3.62).

With the Euler-Lagrange equations in the normal and tangential directions satisfied, we can write the virtual work statement (3.13) as

$$\begin{aligned}\dot{E}^* &= P = B_t + T_t + B_n \\ &= \int_{\partial\omega_f} \boldsymbol{F}\cdot\boldsymbol{u}\, ds + \int_{\partial\omega_t} Q^{-1}W_Q J J_\nu \operatorname{div}\boldsymbol{u}\, ds - \int_{\partial\omega_m} M\boldsymbol{\tau}\cdot\boldsymbol{\omega}\, ds + \sum \boldsymbol{f}_i\cdot\boldsymbol{u}_i\end{aligned} \tag{3.98}$$

where P is the virtual work of the applied loads which induce the virtual displacement, $\partial\omega_f, \partial\omega_t$, and $\partial\omega_m$ are parts of the boundary on which force, hyperstress, and bending moment are imposed, respectively, $\boldsymbol{f}_i = W_K[\tau]_i\boldsymbol{n}$ is the force applied at the i^{th} corner, and where

$$\boldsymbol{F} = F_\nu\boldsymbol{\nu} + F_\tau\boldsymbol{\tau} + F_n\boldsymbol{n}, \tag{3.99}$$

where $\boldsymbol{\nu}$ and $\boldsymbol{\tau}$ are unit vectors normal and tangential to the boundary, respectively,

with

$$\begin{aligned} F_\nu &= W + W_J J - J(Q^{-1}W_Q J_{,\mu} a^{\mu\beta})_{;\beta} - Q^{-1}W_Q J_\nu^2 - \kappa_\nu M, \\ F_\tau &= -\tau M - Q^{-1}W_Q J_\nu J', \\ F_n &= (\tau W_K)' - \left(\tfrac{1}{2}W_H\right)_\nu - (W_K)_{,\beta}\tilde{b}^{\alpha\beta}\nu_\alpha - 2Q^{-1}W_Q H J J_\nu, \end{aligned} \tag{3.100}$$

where

$$J_\nu = \nu^\alpha J_{,\alpha} \quad \text{and} \quad J' = \tau^\alpha J_{,\alpha} = dJ/ds, \tag{3.101}$$

are the normal and tangential derivatives of J. In the foregoing boundary terms, only one of the terms in each integral may be prescribed; thus either force *or* displacement, and bending moment and hypertraction *or* surface orientation, may be prescribed on parts of the boundary $\partial\omega_f, \partial\omega_t$, and $\partial\omega_m$ which are complementary to each other.

Summary of field equations and boundary conditions

The results of the foregoing sections may be summarised as follows. Perturbations in the normal and tangential directions, respectively, yield the Euler-Lagrange equations (3.57) and (3.79), which read

$$(JW_J)_{,\alpha} + W_J J_{,\alpha} - 2J_{,\alpha}(Q^{-1}W_Q J_{,\mu} a^{\mu\beta})_{;\beta} - J(Q^{-1}W_Q J_{,\mu} a^{\mu\beta})_{;\beta\alpha} = 0, \tag{3.102}$$

$$\begin{aligned} &\frac{1}{2}\Delta W_H + W_H(2H^2 - K) + 2HKW_K + (W_K)_{;\beta\alpha}\tilde{b}^{\beta\alpha} - 2HJW_J \\ &+ Q^{-1}W_Q J_{,\alpha} J_{,\beta} b^{\alpha\beta} + 2HJ(Q^{-1}W_Q a^{\alpha\beta} J_{,\beta})_{;\alpha} - 2HW = p, \end{aligned} \tag{3.103}$$

where H and K are the mean and Gaussian curvatures, respectively, J is the surface stretch with gradient Q, W is the energy density per unit area, with derivatives $W_Y = \partial W/\partial Y$, and p is the pressure exerted on the membrane. The forces normal and tangential to the boundary, and normal to the surface, are

$$\begin{aligned} F_\nu &= W + W_J J - J(Q^{-1}W_Q J_{,\mu} a^{\mu\beta})_{;\beta} - Q^{-1}W_Q J_\nu^2 - \kappa_\nu M, \\ F_\tau &= -\tau M - Q^{-1}W_Q J_\nu J', \\ F_n &= (\tau W_K)' - \left(\tfrac{1}{2}W_H\right)_\nu - (W_K)_{,\beta}\tilde{b}^{\alpha\beta}\nu_\alpha - 2Q^{-1}W_Q H J J_\nu, \end{aligned} \tag{3.104}$$

respectively, and

$$Q^{-1}W_Q J J_\nu \tag{3.105}$$

is the hyperstress acting at the boundary.

3.7 Radial extension of a circular membrane

With the general theory developed, we now turn our focus to the application of the theory to some biologically-motivated problems. In order to obtain an explicit system of differential equations describing the shape of a membrane, it is necessary to first specify a geometric framework. For a simple example which serves as a good exposition of the theory, we consider the extension in the radial direction of a circular membrane, of uniform reference thickness, where the midsurface of the membrane remains flat.

This demonstrates more generally how the foregoing theory can be used to model situations where gradients in the membrane thickness arise; one example of this is the embedding of an inclusion, such as a protein, in a lipid bilayer, where the dimensions of the hydrophobic region of the inclusion differ from that of the bilayer. This results in the bilayer conforming to match the hydrophobic tail groups of the lipids with the hydrophobic region of the inclusion, with a consequent change in the stretch in the cross-section [Andersen and Koeppe, 2007].

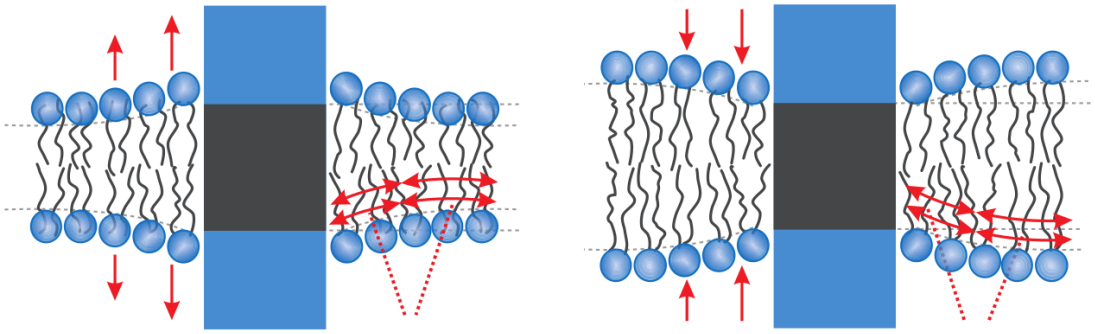

Figure 3.4: Thickness gradients in a biomembrane arise from a mismatch in the dimensions of the hydrophobic lipid tailgroups in the bilayer, and the hydrophobic region (shaded grey) of a protein embedded therein; adapted from [Andersen and Koeppe, 2007].

In order to proceed, we specialise the geometry to a circular portion of membrane

with reference midsurface given by

$$\Omega = \{\boldsymbol{X} = R\boldsymbol{e}_R(\theta) \,|\, 0 \leq R \leq R_0, 0 \leq \theta \leq 2\pi\}, \tag{3.106}$$

where R_0 is the reference radius. The corresponding current configuration can be described by

$$\omega = \{\boldsymbol{x} = r(R)\boldsymbol{e}_R(\theta) \,|\, 0 \leq R \leq R_0, 0 \leq \theta \leq 2\pi\} \tag{3.107}$$

with a corresponding deformation map $\boldsymbol{f} : \mathbb{R}^2 \to \mathbb{R}^2, (R, \theta) \to (r(R), \theta)$, so that $\boldsymbol{x} = \boldsymbol{f}(\boldsymbol{X})$. The associated deformation gradient is

$$\nabla \boldsymbol{f} = \begin{pmatrix} \frac{dr}{dR} & \frac{dr}{d\theta} \\ \frac{d\theta}{dR} & \frac{r}{R}\frac{d\theta}{d\theta} \end{pmatrix} = \begin{pmatrix} r'(R) & 0 \\ 0 & r(R)/R \end{pmatrix}.$$

The current midsurface ω has tangent vectors given by $\boldsymbol{a}_\alpha = \boldsymbol{x}_{,\alpha}$, $(\alpha = 1, 2)$, so that

$$\boldsymbol{a}_1 = r'(R)\boldsymbol{e}_R, \quad \text{and} \quad \boldsymbol{a}_2 = \tfrac{r(R)}{R}\boldsymbol{e}_\theta, \tag{3.108}$$

and the normal vector to ω is $\boldsymbol{n} = \hat{\boldsymbol{k}}$. The tangent vectors define the components $a_{\alpha\beta} = \boldsymbol{a}_\alpha \cdot \boldsymbol{a}_\beta$ of the metric tensor,

$$a_{\alpha\beta} = \begin{pmatrix} r'(R)^2 & 0 \\ 0 & r(R)^2/R^2 \end{pmatrix}. \tag{3.109}$$

so that the area element, the square root of the determinant of the metric, is $J = \sqrt{g} = \sqrt{\det(a_{\alpha\beta})} = rr'/R$. The principal stretches are the square roots of the eigenvalues of $\boldsymbol{C} = (\nabla \boldsymbol{f})^T(\nabla \boldsymbol{f})$, so that

$$\lambda_1 = r'(R), \quad \lambda_2 = \frac{r(R)}{R} \tag{3.110}$$

which similarly gives

$$J = \lambda_1\lambda_2 = \frac{r(R)r'(R)}{R}. \tag{3.111}$$

Adopting the quasi-incompressibility condition $\lambda_3 J = 1$, introduced in equation (3.14),

gives access to a measure of the current membrane thickness,

$$h = h_0 \lambda_3 = \frac{h_0}{J}, \tag{3.112}$$

where h_0 is the reference thickness. Thus the thickness field is completely determined by the midsurface stretch, and thus untimately by $r(R)$ in the current geometry.

At the membrane boundary, we identify the normal and tangent vectors, in line with the notation introduced in the previous sections, as

$$\boldsymbol{\nu} = \boldsymbol{e}_R, \quad \boldsymbol{\tau} = \boldsymbol{e}_\theta, \tag{3.113}$$

respectively. The corresponding *normal derivative* of J is

$$J_\nu = \nu^\alpha J_{,\alpha} = J'(R) = \frac{r(R)r''(R) + r'(R)^2}{R} - \frac{r(R)r'(R)}{R^2}. \tag{3.114}$$

Since the mean and Gaussian curvatures are both zero in the absence of bending, the membrane energy density dependence reduces to

$$W = W(J, Q),$$

where $Q = |\nabla J|$ as introduced previously. We adopt the quadratic expression

$$W = a_1(J-1)^2 + a_2 Q^2, \tag{3.115}$$

taking a_1 and a_2 to be constants for simplicity. In general, for a biological membrane, these coefficients are themselves suitable functions of J [Deseri et al., 2008], and the dependence of W on J is given by a Landau expansion $W = \Sigma_{k=0}^4 a_k J^k$ [Deseri and Zurlo, 2013]. In such cases, it is difficult to determine accurate parameter values due to the lack of available experimental evidence on the stretching behaviour of biological membranes. For this reason, we focus here on the qualitative behaviour demonstrated by the constitutive model (3.115), rather than calibrating to attain a possible quantitative agreement with experimental data.

Since the current configuration is flat, the shape equation (3.103) resulting from normal variations is trivial here. The bending moment (3.96) and force components F_τ and F_n given by (3.104) can also be shown to be zero. Recalling the tangential shape

equation (3.102), which reads

$$(JW_J)_{,\alpha} + W_J J_{,\alpha} - 2J_{,\alpha}(Q^{-1}W_Q J_{,\mu} a^{\mu\beta})_{;\beta} - J(Q^{-1}W_Q J_{,\mu} a^{\mu\beta})_{;\beta\alpha} = 0,$$

we substitute for J, W, and their respective derivatives using (3.111) and (3.115) to obtain

$$a_1\left[(JJ'(J-1)\right)' + J'(J-1)\right] - a_2\left[\frac{2J'}{J}\left(\frac{JJ'}{r'^2}\right)' + \left(\frac{JJ'}{r'^2}\right)''\right] = 0, \tag{3.116}$$

where $J = J(R)$ and its derivative $J' = J'(R)$ are given by the expression (3.111). Symmetry at $R = 0$ requires the boundary condition

$$r(0) = 0. \tag{3.117}$$

At the outer boundary, we may either specify the force F_ν or the amount of extension; opting for the latter, we have

$$r(R_0) = \lambda R_0, \tag{3.118}$$

where λ is the amount of stretch. Requiring zero hyperstress on $\partial\omega$ gives

$$T = Q^{-1}W_Q J J_\nu = 0 \text{ on } R = R_0,$$

and since Q, W_Q and J are non-zero, this reduces to the requirement that $J_\nu = 0$ on the boundary $R = R_0$. Substituting this in (3.114) then gives the boundary condition

$$r''(R_0) = \frac{r'(R_0)}{R_0} - \frac{r'(R_0)^2}{r(R_0)}. \tag{3.119}$$

For the final boundary condition, imposing that the thickness is fixed at the outer boundary, and taking a reference thickness of $h_0 = 1$ for simplicity, gives $\lambda_3|_{R=R_0} = 1$, so that

$$J(R_0) = \frac{r(R_0)r'(R_0)}{R_0} = 1.$$

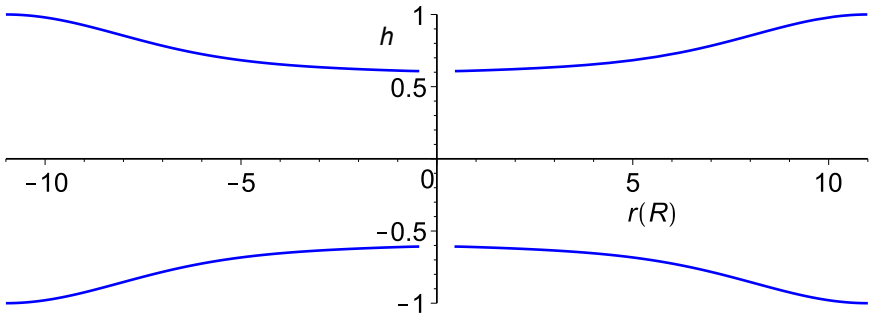

Figure 3.5: Cross-section of a circular membrane stretched in the radial direction, where for simplicity we have taken $R_0 = 10$, $a_1 = a_2 = 1$, $\lambda = 1.1$, and set the reference thickness to $h_0 = 1$, and fixed $h(R_0) = 1$ to illustrate the non-uniform thickness profile obtained from the theory; the region around $R = 0$ is removed to avoid the singularity which occurs at this point.

Substituting for $r(R_0)$ using (3.118) then gives

$$r'(R_0) = \lambda^{-1}. \tag{3.120}$$

Now, substituting this and (3.118) in (3.119) gives

$$r''(R_0) = \frac{1}{\lambda R_0}\left(1 - \lambda^{-2}\right). \tag{3.121}$$

We solve the fourth-order equation (3.116) numerically using Maple, subject to the boundary conditions (3.117), (3.118), (3.120) and (3.121). In Figure 3.5 we plot the deformed membrane thickness $h = h_0\lambda_3 = h_0/J$ as the primary quantity of interest.

3.8 Conclusion

In this chapter, we have presented a full derivation of the shape equations for a membrane whose energy density depends on its mean and Gaussian curvatures, the stretch of its midsurface, and the gradient of this stretch. The equations derived are fully general, making no reference to the geometry of a particular application, and thus can be specialised to a wide range of cases. We have shown their equivalence to equations derived in previous studies, where the membrane energy densities are more specialised than the general case considered here.

We have also shown how the equations derived can be specialised to a simple axially

symmetric geometry, and have demonstrated their utility in capturing deformations in which the membrane thickness varies. The system of equations considered in Section 3.7, could, therefore, be adapted and further developed to provide a realistic theoretical description of biological phenomena, such as describing the shape of a membrane in which there is a mismatch of the dimensions of hydrophobic regions of membranes and inclusions embedded therein.

We will return to some of the ideas developed here for biological membranes in Chapter 5, where we consider the application of the continuum mechanical theory to the specific problem of predicting pore formation as an instability in biomembranes.

Chapter 4

Instabilities in Dielectric Elastomers

The research presented in this chapter has been published in the Journal of the Mechanics and Physics of Solids [Greaney et al., 2019].

4.1 Introduction

In this chapter, we turn our focus to the behaviour of dielectric elastomer membranes. A dielectric elastomer is an electroresponsive device composed of a dielectric material sandwiched between two thin compliant electrodes [Pelrine et al., 1998]. The application of a voltage across the thickness direction results in an in-plane areal expansion, so that these *smart materials* find uses in a wide range of modern applications. We restrict our attention here to the case where the dielectric is sufficiently thin to justify the use of membrane theory in our modelling.

Dielectric elastomer devices in this category have shown strong potential in applications as diverse as sensing, actuation, robotics, energy harvesting, on-demand patterning and microfluidics [Pelrine et al., 2000, Mirvakili and Hunter, 2017, Bauer et al., 2014, Majidi, 2014, Yang et al., 2010, Cao and Hutchinson, 2012, Wang et al., 2014]. The simplicity of their working principle makes them particularly appealing: bulk incompressibility of the elastomer and attractive Coulomb forces between the electrodes cause expansion of the membrane upon application of a voltage, with areal strains as large as 500% [Huang et al., 2012a].

We outline the ideas of energy *relaxation* and *regularization*, and employ them to describe large, out-of-plane deformations of thin dielectric membranes under voltage control, together with their instabilities. This unifying perspective describes the nature and the hierarchy of pull-in and wrinkling instabilities. We explain why the occurrence

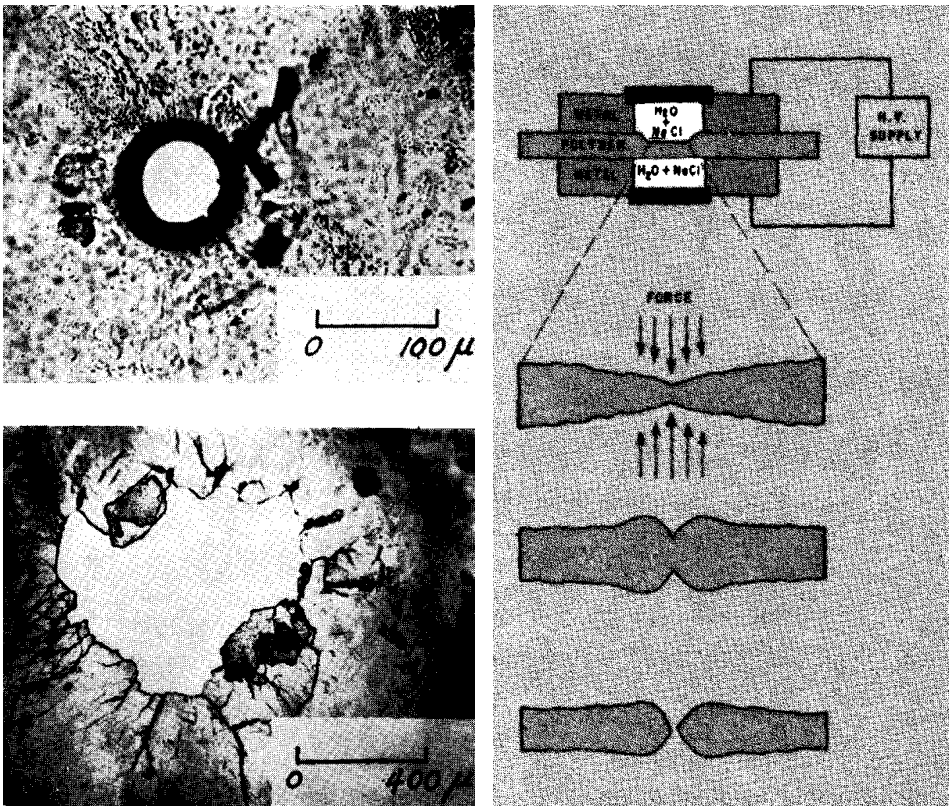

Figure 4.1: Illustration of the pull-in phenomenon from the 1969 paper of Blok & LeGrand [Blok and LeGrand, 1969]: (a) breakdown observed in polyethylene films; (b) qualitative sketch of the breakdown mechanism: the application of an electric field across the thickness direction causes an electrostrictive force which is greatest at the thinnest point of the film, where the electric strength is first reached and breakdown occurs.

of wrinkling does not necessarily lead to permanent device failure, as observed in experimental studies, and we show that a relaxed electroelastic energy can be effectively used to describe the onset and evolution of wrinkles for large out-of-plane deformations. By using the regularization approach, we provide a physical explanation of the *pull-in effect* for out-of-plane deformations, wherein the membrane undergoes irreversible damage and breakdown occurs; see Figures 4.1 and 4.2 (e) and (f) for a graphical representation and experimental evidence. We further show that for isotropic membranes the onset of wrinkles is never unstable before the occurence of pull-in. Finally, we compare the outcomes of our theory with recent experimental results on the out-of-plane behaviour of annular membranes under voltage control. Our theoretical predictions show good agreement both with the evolution of wrinkling and with the onset of pull-in; see Figure 4.2 (a)–(d) for examples of devices where this has been observed experimentally.

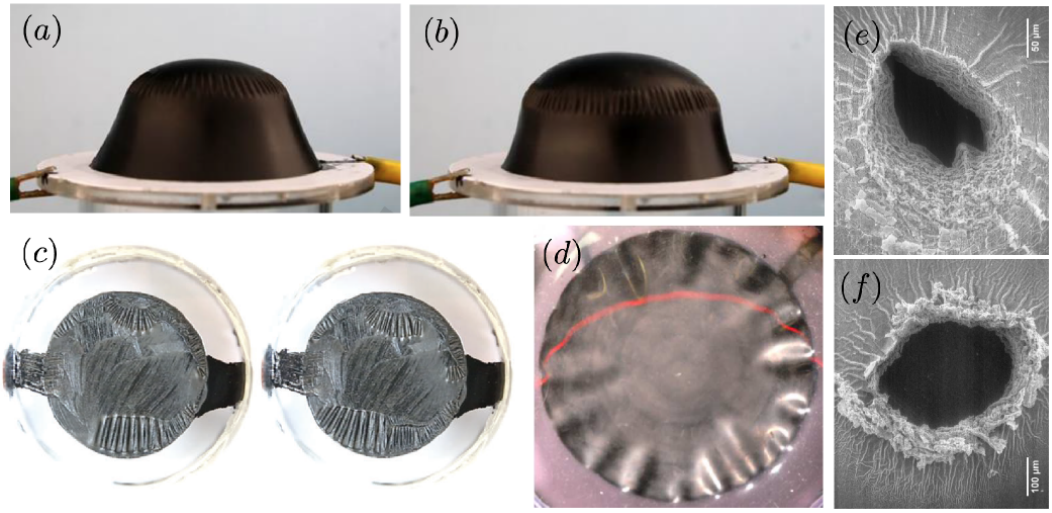

Figure 4.2: (a, b, c, d): examples of wrinkled states of dielectric membranes which do not lead the membrane to failure; (e, f): common brittle failures of silicone elastomers after electrical breakdown, showing that pull-in clearly leads to an unrestrainable process. Pictures $(a - b)$ are taken from [Mao et al., 2018b], (c) from [Godaba et al., 2017], (d) from [Bense et al., 2017], and (e, f) from [Mateiu et al., 2017].

Due to the interplay of constitutive and geometric nonlinearities, thin dielectric elastomers exhibit a very rich and complex behaviour. In particular, two types of instabilities drastically affect their performances: a *thinning instability*, often identified as 'pull-in' [Stark and Garton, 1955] or 'electromechanical instability' [Zhao and Suo, 2007], which precedes dielectric breakdown, and whereby the membrane undergoes highly localised thinning leading to the formation of cracks and holes; and a *wrinkling instability*, which is due to relaxation of in-plane compressive stresses through out-of-plane bending deformations. In contrast to pull-in, the occurrence of wrinkling is not immediately associated with failure; indeed, extensive experimental evidence demonstrates the possibility of controlling and maintaining wrinkled states without incurring permanent damage to the device [Liu et al., 2016, Mao et al., 2017, Kollosche et al., 2015].

The theoretical modelling of thin electroelastic membranes appears quite fragmented to date. The fundamental role played by bending stiffness in membrane theory has not received enough attention, despite its importance in securing the stability of wrinkled states. Furthermore, the powerful technique of *energy relaxation*, successfully introduced for purely elastic membranes, has not been exploited.

This chapter presents a unifying description of the stretching and bending behaviour

of dielectric membranes that encompasses both out-of-plane and inhomogeneous deformations. We discuss the nature of thinning and wrinkling instabilities by establishing quantitative hierarchies on their onset. After showing that wrinkled states can be stable without leading to failure, as extensively shown by experiments, we describe them by adopting the so-called *tension field theory* for electroelastic membranes [De Tommasi et al., 2011, De Tommasi et al., 2012]. To support our findings, we apply our theory to describe the out-of-plane behaviour of electrically-actuated annular membranes, and we show that our predictions satisfactorily describe both electrical breakdown and the onset and evolution of wrinkled domains.

We develop our theory based on the variational formulation of the electroelastostatic equilibrium of a plate-like body with uniform reference thickness $h > 0$, which we assume is small relative to the lateral dimensions of the plate mid-surface. By expressing the plate deformation as a power series in the coordinate along the thickness direction, we show that the electroelastic energy per unit initial area can be recast as

$$\psi = hM + h^3 (S + B), \tag{4.1}$$

where M is the *membranal stretching* energy term, B is the *bending* energy term and S is the *stretch-gradient* energy term [Hilgers and Pipkin, 1996]. The shape of the dielectric membrane for a given voltage is the solution to the Euler-Lagrange equations associated with the energy (4.1). For h small and away from the membrane edges, equilibrium configurations are essentially determined by the membranal energy M, since higher-order terms give negligible corrections of the membrane shapes in the bulk. However, while the terms S, B play a marginal role in the shape of the membrane, they are fundamental in assessing its stability [Hilgers and Pipkin, 1992, Hilgers and Pipkin, 1996].

Loss of convexity of the electroelastic energy density ψ and, more specifically, of the three counterparts M, S, B, is associated with the onset of instabilities of the wrinkling and thinning type. Loss of rank-one convexity (more precisely, of quasi-convexity, see [Pipkin, 1986] for details) corresponds to the onset of compressive stresses in the tangential plane of the membrane [Pipkin, 1986]. When this happens the membrane undergoes wrinkling, but this effect is stable as long as the regularisation term $Q = S+B$ satisfies suitable convexity requirements [Hilgers and Pipkin, 1996] with respect to higher order derivatives.

We will extensively discuss the physical relevance of the term S, the significance of

which is usually underplayed in the mechanics of electrically non-active membranes. It was recently shown, for planar dielectric membranes and for homogeneous deformations, that when S becomes non-convex in the stretch gradient, the onset of inhomogeneous deformations becomes energetically favoured and therefore stable minimisers of the electroelastic energy density $\mathcal{E}$ can not exist [Zurlo et al., 2017]. This is widely observed in experiments, showing that above the pull-in voltage an unrestrainable localisation process leads to the formation of holes and cracks [Wang et al., 2011, Mateiu et al., 2017], drastically affecting the insulating capacity of dielectric elastomers [Huang et al., 2012b, Plante and Dubowsky, 2006].

In this chapter we extend the modelling of pull-in, originally formulated for planar systems [Zurlo et al., 2017], to inhomogeneously deformed membranes undergoing out-of-plane deformations. We show that, for isotropic materials, convexity of S implies convexity of B, which explains why wrinkled states are always stable below the pull-in voltage [Liu et al., 2016, Mao et al., 2017]. Finally we use ideas from *tension field theory*, to show that wrinkled states of electroelastic membranes can be efficiently described by replacing the membranal energy M by its *relaxed* membranal energy M^*, which annihilates compressive stresses.

To assess the predictive power of our findings, we study the behaviour of annular dielectric membranes, undergoing out-of-plane, inhomogeneous deformations. Devices based on this layout have shown promising technological potential [Bortot and Gei, 2015, Berselli et al., 2011, Zhu et al., 2011, He et al., 2009]. The comparison with a first set of experiments [Zhang et al., 2016] shows that our theory predicts the experimental electric breakdown value with an error that ranges from 4% at low prestretches to 7% at higher prestretches. Our findings are also critically discussed in light of the *Hessian criterion* proposed in [Zhao and Suo, 2007], and of the empirical expression for dielectric breakdown obtained in [Huang et al., 2012b], by showing a very good overlap with the latter.

We then use a second set of experiments [Mao et al., 2017] to assess the predictive power of the theory in terms of wrinkling. In particular, we show that wrinkled states can be described by replacing the original membranal energy M by a relaxed energy M^*. Consistent with experiments, we show that wrinkles gradually appear in the whole membrane as voltage is increased. A final achievement of our work is to prove that wrinkling does not necessarily determine failure of an electrically actuated membrane. This finding is consistent with ubiquitous experimental evidence, showing that wrinkling can be maintained as long as the thinning instability does not take place.

Inspired by [Lancioni and Tomassetti, 2002, Podio-Guidugli and Tomassetti, 2001], we believe that our approach could be fruitful in studying the dynamical behaviour of electroelastic membranes under time-varying voltage. Here, experimental observations have shown that the coexistence of *phases* with multiple patterns of wrinkles can be tuned through voltage control, without leading to failure [Godaba et al., 2017]. In this perspective it would be interesting to show that the regularization provided by the term $S + B$ plays the role of an *interfacial energy* between different wrinkling phases.

4.2 Variational formulation of electroelasticity

The variational formulation of electroelastic equilibrium presented here is based on the approach proposed by Fosdick and Tang [Fosdick and Tang, 2007], which we briefly review. We denote by $\mathcal{R}$ the reference configuration of the elastic dielectric, by $\boldsymbol{f}$ the deformation that maps $\mathcal{R}$ into the current configuration $\mathcal{B}$, by $\mathbf{F} = \nabla \boldsymbol{f}$ the deformation gradient and by $\boldsymbol{d}$ the material description of the spatial electric displacement vector $\boldsymbol{d}_s$, in the sense that $\boldsymbol{d} = \boldsymbol{d}_s \circ \boldsymbol{f}$. Neglecting the electrostatic energy of the underlying vacuum, equilibrium configurations of a deformable dielectric in a system of N conductors are minimisers of the total potential energy

$$\mathcal{E}(\mathbf{F}, \boldsymbol{d}) = \int_{\mathcal{R}} \Psi(\mathbf{F}, \boldsymbol{d})\, dv_0 + \int_{\mathbb{R}^3 \setminus \mathcal{R}} \omega(\boldsymbol{d})\, dv_0 - \sum_{i=1}^{N} Q_i V_i - \mathcal{W}^m \tag{4.2}$$

where Ψ is the specific volumetric Helmholtz free energy stored in the dielectric, dv_0 is the Lagrangian volume measure, Q_i is the total charge on the i^{th} conductor and V_i is its voltage, and $\mathcal{W}^m$ is the mechanical work done by the electric field on the membrane boundary. The specific electrostatic energy ω of the free space surrounding the body can be expressed as $\omega = ||\boldsymbol{d}||^2/2\varepsilon_0$, where ε_0 is the vacuum permittivity. The terms $Q_i V_i$ may be identified with the electrostatic work done by an external battery in order to maintain a constant potential on the i^{th} conductor.

The total charge on each conductor can be written as

$$Q_i = \int_{\mathcal{C}_i} \sigma_i\, da_i, \tag{4.3}$$

where da_i is the current area measure and where the current surface charge density is

$$\sigma_i = [\![\boldsymbol{d}]\!] \cdot \widehat{\boldsymbol{n}}_i \tag{4.4}$$

with $\widehat{\boldsymbol{n}}_i$ the outward normal to the conductor surface $\mathcal{C}_i$, and where the notation $[\![\cdot]\!]$ denotes a jump discontinuity in the corresponding quantity. It has been shown [Fosdick and Tang, 2007] that the energy (4.2) is a non-increasing Lyapunov function for isolated thermomechanical-electromagnetic processes. Thus, the energy (4.2) can be used to determine static states of minimal energy within the setting of the calculus of variations.

For the free energy Ψ, we assume a linear *ideal dielectric* behaviour, in the sense that elastic and electric effects are constitutively uncoupled [Suo et al., 2008]. In this case, the additive decomposition $\Psi = W(\mathbf{F}) + ||\boldsymbol{d}||^2/2\varepsilon$ holds, where ε is the constant permittivity of the dielectric and where W describes the purely elastic response of the elastomer. At this point, classical identities [Kovetz, 2000] based on the requirement that the electrostatic potential at infinity decays to zero, that the jump conditions (4.4) hold, and that $\operatorname{div} \boldsymbol{d} = 0$ everywhere, permit the reformulation of the total free energy as

$$\int_{\mathcal{R}} \Psi(\mathbf{F}, \boldsymbol{d})\, dv_0 + \int_{\mathbb{R}^3 \setminus \mathcal{R}} \omega(\boldsymbol{d})\, dv_0 = \int_{\mathcal{R}} W(\mathbf{F})\, dv_0 + \frac{1}{2} \sum_{i=1}^{N} Q_i V_i. \tag{4.5}$$

While this reformulation simplifies the analysis, we remark that the *ideal dielectric* assumption should be regarded as valid at low stretches, since experiments suggests that the dielectric permittivity is generally stretch-dependent [Kollosche et al., 2015, Qiang et al., 2012]. For ideal dielectrics we thus seek minimisers of the total potential energy

$$\mathcal{E}(\mathbf{F}, \boldsymbol{d}) = \int_{\mathcal{R}} W(\mathbf{F})\, dv_0 - \frac{1}{2} \sum_{i=1}^{N} V_i \int_{\mathcal{C}_i} \sigma_i\, da_i - \mathcal{W}^m \tag{4.6}$$

where σ_i is given in terms of $\boldsymbol{d}$ and $\mathbf{F}$ by (4.4). In more general situations, the energy (4.2) should be considered instead. In the subsequent sections we make explicit the dependence of the total potential energy (4.6) on the reference thickness h.

4.3 Power series expansion of the energy

To gain insight into the physical mechanisms leading to wrinkling and pull-in, we confine the analysis to a specific class of deformations that permit both out-of-plane displacement, and inhomogeneous thinning, while keeping the theory analytically tractable.

The reference, stress-free configuration of the membrane is a right cylindrical domain

of uniform thickness h with flat mid-surface Σ,

$$\mathcal{R} = \left\{ \boldsymbol{x} = \mathbf{x} + z\boldsymbol{k} \,|\, \mathbf{x} = (x_1, x_2) \in \Sigma \subset \mathbb{R}^2,\, z \in \left(-\frac{h}{2}, \frac{h}{2}\right) \right\} \tag{4.7}$$

where the constant vector $\boldsymbol{k}$ is perpendicular to Σ. We thus assume that the reference plate $\mathcal{R}$ deforms according to the following *ansatz*

$$\boldsymbol{f}(\boldsymbol{x}) = \boldsymbol{g}(\mathbf{x}) + z\lambda_3(\mathbf{x})\boldsymbol{n}(\mathbf{x}) \tag{4.8}$$

where $\boldsymbol{g} : \mathbb{R}^2 \mapsto \mathbb{R}^3$ is the deformation of the mid-surface, $\lambda_3(\mathbf{x})$ is the thickness stretch, and where the vector $\boldsymbol{n}$ is the Lagrangian description of $\widehat{\boldsymbol{n}}$, in the sense that $\widehat{\boldsymbol{n}} \circ \boldsymbol{g} = \boldsymbol{n}$.

Before proceeding further, a comment is in order on the ansatz (4.8). In this precise form it was used to describe the cold drawing of polymer fibres and plates [Coleman and Newman, 1988], the stretching and bending of biological membranes [Deseri et al., 2008, Deseri and Zurlo, 2013] and, more pertinently to the current topic, the occurrence of thinning instabilities in flat dielectric membranes [Zurlo et al., 2017]. This linear approximation for the plate deformation is affected by known limitations: it imposes that straight fibers perpendicular to Σ remain straight during deformation and, for curved membranes, it secures that the incompressibility constraint is satisfied exactly only on the dielectric mid-surface. To overcome these limitations, more consistent approximations including higher order terms should be employed — see [Audoly and Hutchinson, 2016, Maleki et al., 2013] for example. However, besides the fact that such refinements lead to analytical complications, in conjunction with the incompressibility constraint they also introduce regularising effects that may suppress the thinning instability, see for example [Zurlo, 2013, De Tommasi et al., 2014] where this aspect was elucidated for dielectric elastomers; see also [Montes-Pizarro and Negrón-Marrero, 2007], for a more general discussion of this type of effect for surface instabilities in nonlinearly elastic solids. Despite the limitations of the simple linear ansatz (4.8), it was shown in [Zurlo et al., 2017] that it predicts pull-in for homogeneous planar systems for a variety of material behaviours and boundary conditions; remarkably, it precisely predicts also the electro-creasing instability [Wang et al., 2011], which is usually over-estimated by linear stability analysis. For all of these reasons, we here retain the linear ansatz (4.8), but we highlight that the improvement to more consistent approximations remains an open problem, possibly requiring much more sophisticated tools than the ones employed in this chapter — see for example [Rabinowitz, 1971], and also the more recent study

[Fu et al., 2018a]. Notwithstanding this, we will show that our theory correctly describes pull-in and wrinkling instabilities also for large, out-of-plane deformations.

In order to make explicit the dependence of the total potential energy on h, we first note that the gradient of the deformation (4.8) reads

$$\mathbf{F} = \nabla \boldsymbol{f} = \mathbf{G} + \lambda_3 \boldsymbol{n} \otimes \boldsymbol{k} + z(\boldsymbol{n} \otimes \nabla\lambda_3 - \lambda_3 \mathbf{L}\mathbf{G}). \tag{4.9}$$

Here we have $\mathbf{G} = \nabla \boldsymbol{g}$, and we have used the the chain rule to write $\nabla \boldsymbol{n} = -\mathbf{L}\mathbf{G}$, where $\mathbf{L} = -\mathrm{grad}\,\widehat{\boldsymbol{n}}$ is the material description of the curvature tensor of the current mid-surface of the dielectric. Note that $\mathbf{G}\boldsymbol{n} = \mathbf{G}^{\mathsf{T}}\boldsymbol{k} = \mathbf{0}$ and that $\mathbf{L}$ is a symmetric surface tensor that acts on the tangent plane of the current mid-surface of the dielectric. From the deformation gradient (4.9) we can now compute the right Cauchy-Green deformation tensor up to second order in z. Writing

$$\mathbf{C} = \mathbf{F}^{\mathsf{T}}\mathbf{F} = \mathbf{C}_0 + z\mathbf{C}_1 + z^2\mathbf{C}_2, \tag{4.10}$$

we obtain from (4.9) that

$$\mathbf{C}_0 = \mathbf{G}^{\mathsf{T}}\mathbf{G} + \lambda_3^2 \boldsymbol{k} \otimes \boldsymbol{k}, \tag{4.11}$$

$$\mathbf{C}_1 = \lambda_3 \boldsymbol{k} \otimes \nabla\lambda_3 + \lambda_3 \nabla\lambda_3 \otimes \boldsymbol{k} - 2\lambda_3 \mathbf{G}^{\mathsf{T}}\mathbf{L}\mathbf{G}, \tag{4.12}$$

and

$$\mathbf{C}_2 = \lambda_3^2 \mathbf{G}^{\mathsf{T}}\mathbf{L}^2\mathbf{G} + \nabla\lambda_3 \otimes \nabla\lambda_3. \tag{4.13}$$

It should be noted that the expansion of $\mathbf{C}$ here is given up to quadratic order in z, and so it may be more appropriate to expand $\mathbf{F}$ to quadratic order, rather than linear order in z [Fu et al., 2018b]. To further simplify the analysis, we impose bulk incompressibility of the membrane and assume that the elastic energy W depends on the deformation gradient through its first invariant $I = \mathrm{tr}\mathbf{C}$ which reads

$$I = I_0 + zI_1 + z^2 I_2, \tag{4.14}$$

where

$$I_0 = \mathrm{tr}(\mathbf{G}^{\mathsf{T}}\mathbf{G}) + \lambda_3^2, \quad I_1 = -2\lambda_3\,\mathrm{tr}(\mathbf{B}\mathbf{L}), \quad \text{and} \quad I_2 = \lambda_3^2\,\mathrm{tr}(\mathbf{B}\mathbf{L}^2) + |\nabla\lambda_3|^2. \tag{4.15}$$

In the foregoing, $\mathbf{B} = \mathbf{G}\mathbf{G}^{\mathsf{T}}$ is the left Cauchy-Green deformation tensor relative to the current mid-surface of the dielectric. To impose incompressibility, we first write $\det \mathbf{F} = \lambda_3 \alpha$, where α, a function of z, represents the lateral stretch in planes lying parallel to the midsurface, that is, perpendicular to the direction of the thickness stretch. For convenience we set

$$\alpha_0 = \sqrt{\det \mathbf{G}^{\mathsf{T}}\mathbf{G}}, \tag{4.16}$$

to be the areal stretch of the mid-surface. We next seek to calculate $\alpha(z)$ explicitly by noting that it is given by the square root of the determinant of $\mathbf{C}$, the right Cauchy-Green tensor of the surfaces lying parallel to the midsurface, where

$$\mathbf{C} = \mathbf{C}_0 + z\mathbf{C}_1 + z^2\mathbf{C}_2, \tag{4.17}$$

with

$$\mathbf{C}_0 = \mathbf{G}^{\mathsf{T}}\mathbf{G}, \quad \mathbf{C}_1 = -2\lambda_3 \mathbf{G}^{\mathsf{T}}\mathbf{L}\mathbf{G}, \quad \text{and} \quad \mathbf{C}_2 = \lambda_3^2 \mathbf{G}^{\mathsf{T}}\mathbf{L}^2\mathbf{G} + \nabla\lambda_3 \otimes \nabla\lambda_3. \tag{4.18}$$

Using (4.17) and setting $\delta = \det \mathbf{C}$, we expand in powers of z to obtain

$$\delta(z) = \delta(0) + z\dot{\delta}(0) + \frac{1}{2}z^2\ddot{\delta}(0),$$

where a superposed dot denotes differentiation with respect to z. Differentiating and using Jacobi's formula (3.25) for the determinant derivative, we obtain

$$\begin{aligned}
\dot{\delta} &= \delta \mathrm{tr}(\mathbf{C}^{-1}\dot{\mathbf{C}}), \\
\ddot{\delta} &= \delta \left(\mathrm{tr}(\mathbf{C}^{-1}\dot{\mathbf{C}})^2 + \mathrm{tr}(\mathbf{C}^{-1}\ddot{\mathbf{C}}) - \mathrm{tr}(\mathbf{C}^{-1}\dot{\mathbf{C}}\mathbf{C}^{-1}\dot{\mathbf{C}}) \right),
\end{aligned}$$

where $\dot{\mathbf{C}} = \mathbf{C}_1 + 2z\mathbf{C}_2$ and $\ddot{\mathbf{C}} = 2\mathbf{C}_2$, which gives

$$\begin{aligned}
\delta(0) = \alpha_0^2, \quad \dot{\delta}(0) &= -4\lambda_3\alpha_0^2 H, \\
\ddot{\delta}(0) &= 8\lambda_3^2\alpha_0^2 H^2 + 4\lambda_3^2\alpha_0^2 K + 2\alpha_0^2 |\mathrm{grad}\hat{\lambda}_3|^2.
\end{aligned}$$

We can similarly expand α as

$$\alpha(z) = \alpha(0) + z\dot{\alpha}(0) + \frac{1}{2}z^2\ddot{\alpha}(0),$$

and since $\alpha = \delta^{1/2}$ we obtain

$$\alpha(0) = \alpha_0, \quad \dot{\alpha}(0) = -2\lambda_3\alpha_0 H,$$
$$\ddot{\alpha}(0) = \alpha_0(2\lambda_3^2 K + |\mathrm{grad}\,\hat{\lambda}_3|^2)$$

so that

$$\alpha(z) = \alpha_0 - 2\alpha_0\lambda_3 H z + z^2\alpha_0\left(\lambda_3^2 K + \frac{1}{2}|\mathrm{grad}\hat{\lambda}_3|^2\right).$$

Thus we have

$$\sqrt{\det(\mathbf{F}^{\mathsf{T}}\mathbf{F})} = \lambda_3\alpha_0\left(1 - 2z\lambda_3 H + z^2(\lambda_3^2 K + \frac{1}{2}|\mathrm{grad}\,\hat{\lambda}_3|^2)\right), \tag{4.19}$$

where $H = \frac{1}{2}\mathrm{tr}\mathbf{L}$ and $K = \det\mathbf{L}$ are the mean and Gaussian curvatures of the membrane mid-surface, respectively. The expression (4.19) shows that the incompressibility constraint $\sqrt{\det(\mathbf{F}^{\mathsf{T}}\mathbf{F})} = 1$ can only be satisfied exactly on two surfaces: the mid-surface $z = 0$, and a second surface which depends on the fields $\mathbf{G}, \mathbf{L}$, and λ_3. To avoid this pathological feature, one could assume that λ_3 is dependent on z [Maleki et al., 2013]; this, however, introduces analytical difficulties. To avoid these complications, we thus impose that the incompressibility is satisfied exactly only on the mid-surface Σ, so that

$$\lambda_3\alpha_0 = 1. \tag{4.20}$$

This is usually called the *quasi-incompressibility* condition [Deseri et al., 2008], and it will be assumed henceforth. Note that if $\kappa_1 = 1/\varrho_1$ and $\kappa_2 = 1/\varrho_2$ are the two principal curvatures corresponding to principal radii of curvature ϱ_1, ϱ_2 of the membrane mid-surface, the constraint (4.20) leads to small errors if $h/\min(\varrho_1, \varrho_2)$ is small with respect to unity. For this reason, the validity of our results is limited to thin and mildly curved dielectric membranes.

Writing the energy density W as a power series up to second order in z,

$$W = W(I)|_{z=0} + z\left[\frac{dW}{dI}\frac{dI}{dz}\right]_{z=0} + \frac{1}{2}z^2\left[\frac{d^2W}{dI^2}\left(\frac{dI}{dz}\right)^2 + \frac{dW}{dI}\frac{d^2I}{dz^2}\right]_{z=0},$$

we use the invariant (4.14) to obtain

$$W = W_0 + zI_1W_0' + \frac{1}{2}z^2\left(W_0''I_1^2 + 2W_0'I_2\right),$$

where we have set $W_0^{(n)} = \frac{d^n}{dI^n} W\big|_{I=I_0}$. Thus we obtain that the elastic energy density, up to the first order where non-local terms appear, can be written as

$$\int_\Sigma \int_{-h/2}^{h/2} W \, dz \, dA = \int_\Sigma \left(hW_0 + \frac{h^3}{24} \left(2I_2 W_0' + I_1^2 W_0'' \right) \right) dA, \tag{4.21}$$

where the terms I_i are given in (4.14). In order to perform a power series expansion of the electrostatic energy terms, we first note that dielectric elastomer devices are formed by attaching compliant electrodes with negligible bending and stretching stiffnesses to the upper and lower surfaces

$$\Sigma^\pm = \{ \mathbf{x} \pm (h/2)\boldsymbol{k}, \quad \mathbf{x} \in \Sigma \}$$

of the dielectric membrane, where voltages $V^\pm = \pm V/2$ are applied. These electrodes deform into the surfaces $\mathcal{C}^\pm = \boldsymbol{f}(\Sigma^\pm)$ of the current configuration. By neglecting curvature effects on charge localisation [Puglisi and Zurlo, 2012], we assume that the electric field in the proximity of the conductors is perpendicular to their surface, so that $\boldsymbol{e} = e\boldsymbol{n}$, and that its magnitude is

$$e(\boldsymbol{x}) = \frac{V}{h_c(\mathbf{x})} \tag{4.22}$$

where

$$h_c(\mathbf{x}) = \lambda_3(\mathbf{x}) h$$

is the current thickness of the membrane. If the dielectric permittivity ε is constant and if we neglect the electric field outside the plate, the surface charge density per unit current area on the upper and lower electrodes can be recast as $\sigma^\pm = \boldsymbol{d} \cdot \boldsymbol{n}^\pm = \varepsilon \boldsymbol{e} \cdot \boldsymbol{n}^\pm = \pm \varepsilon e$. Then using (4.3) we obtain that

$$\sum_{i=1}^{2} Q_i V_i = \frac{V}{2} \left(\int_{\mathcal{C}^+} \sigma^+ \, da^+ - \int_{\mathcal{C}^-} \sigma^- \, da^- \right) = \int_\Sigma \frac{\varepsilon V^2}{h_c} \frac{\alpha^+ + \alpha^-}{2} \, dA \tag{4.23}$$

where $\alpha^\pm$ are the surface stretches of the upper and lower electrodes, which are defined through the cofactor $\mathbf{F}^* = (\det \mathbf{F}) \mathbf{F}^{-\mathsf{T}}$ of the deformation gradient as

$$\alpha^\pm(\mathbf{x}) = |\mathbf{F}^*(\boldsymbol{x}) \boldsymbol{k}|_{z=\pm h/2}. \tag{4.24}$$

We next calculate $\alpha^\pm$ explicitly, as follows. With $\det \mathbf{F} = \alpha \lambda_3$ given by (4.19) with

the constraint (4.20), we obtain, for an arbitrary z,

$$\alpha(z) = \alpha_0 - 2Hz + z^2 \left(\alpha_0^{-1} K + \frac{\alpha_0}{2} |\mathrm{grad}\hat{\lambda}_3|^2 \right). \tag{4.25}$$

Thus, by computing the average surface stretch $\widetilde{\alpha} = (\alpha^+ + \alpha^-)/2$ of the electrodes, we obtain

$$\tilde{\alpha} = \frac{1}{2}\left(\alpha\left(\frac{h}{2}\right) + \alpha\left(-\frac{h}{2}\right)\right) = \alpha_0 \left(1 + \frac{h^2}{8}\left(2K\alpha_0^{-2} + |\mathrm{grad}\hat{\lambda}_3|^2 \right)\right). \tag{4.26}$$

In general, this does not coincide with the surface areal stretch α_0 of the midsurface Σ. Thus we have that

$$\frac{1}{2}\sum_{i=1}^{2} Q_i V_i = h \int_{\boldsymbol{g}(\Sigma)} p\, \widetilde{\alpha}\, da, \tag{4.27}$$

where $p = \frac{\varepsilon V^2}{2h^2}$ may be interpreted physically as an electrostatic surface stress acting among equal charges on the surface of the conductors, performing positive work by increasing their area. It is precisely the competition between this work term, which lowers the total potential energy by increasing the area of the electrodes, and the elastic energy term, which is lowered by decreasing the amount of deformation of the dielectric, which is at the root of the thinning *pull-in* instability.

The expression (4.26) for the average stretch of the electrodes clearly shows that the surface areal stretch of the electrodes is influenced, at order $\mathcal{O}(h^2)$, both by the Gaussian curvature of the dielectric mid-surface, and by the presence of thinning inhomogeneities. Note that here $\hat{\lambda}_3 \circ \boldsymbol{g} = \lambda_3$, so by the chain rule we have $\mathbf{G}^{\mathsf{T}} \nabla \lambda_3 = \mathrm{grad}\hat{\lambda}_3$, where grad is the gradient with respect to spatial coordinates. Thus we have

$$\frac{1}{2}\sum_{i=1}^{2} Q_i V_i = h \int_{\Sigma} \frac{\varepsilon V^2}{2h^2} \alpha_0^2 \left(1 + \frac{h^2}{8}\left(2\alpha_0^{-2} K + |\mathrm{grad}\hat{\lambda}_3|^2 \right)\right) dA. \tag{4.28}$$

We can now collect the expansions of the elastic and electrostatic terms to derive a complete expansion of the total potential energy. Defining the dimensionless electric field [Zhao and Suo, 2007] as

$$E = \sqrt{\frac{\varepsilon}{\mu}} \frac{V}{h}, \tag{4.29}$$

where $\mu = 2W'(3)$ is the initial shear modulus in the absence of the electric field, and by neglecting higher-order terms, the total potential energy can be expressed in the

form

$$\mathcal{E} = \int_\Sigma \psi \, dA - \mathcal{W}^m \tag{4.30}$$

where we have introduced the surface electroelastic energy

$$\psi = hM + h^3(S + B) \tag{4.31}$$

where the three terms

$$\begin{aligned} M &= W_0 - \frac{\mu E^2}{2\lambda_3^2}, \\ S &= \frac{1}{12}\left(W_0'|\nabla\lambda_3|^2 - \frac{3}{4}\mu E^2\lambda_3^{-2}|\mathrm{grad}\,\hat{\lambda}_3|^2\right), \\ B &= \frac{1}{12}\left(\lambda_3^2 W_0'\,\mathrm{tr}(\mathbf{BL}^2) + 2W_0''\lambda_3^2\mathrm{tr}(\mathbf{BL})^2 - \frac{3}{2}\mu E^2 K\right), \end{aligned} \tag{4.32}$$

represent the *membranal*, *stretch-gradient*, and *bending* contributions, respectively. The representation (4.32), inspired by Hilgers and Pipkin [Hilgers and Pipkin, 1996] in their study of large deformations of elastic membranes, includes an explicit dependence on the electric field. As we now show, the parametric dependence on this controlled parameter plays a pivotal role in assessing the stability of elastic dielectric membranes with compliant electrodes.

4.4 Energy relaxation and voltage-induced wrinkles

The *relaxation approach* to dielectric membranes with compliant electrodes, first proposed in [De Tommasi et al., 2011, De Tommasi et al., 2012] within the context of planar systems, consists of neglecting the higher order term $Q = S + B$ and retaining the purely membranal term M. Here we show how this approach may be used to describe the onset of wrinkles on out-of-plane systems undergoing inhomogeneous deformations. We also establish a connection between the limit threshold of wrinkling instabilities and the so-called *Hessian criterion* for electromechanical instabilities [Zhao and Suo, 2007].

4.4.1 Construction of the relaxed membranal energy

The underlying idea of the relaxation approach is to replace the electroelastic membranal energy density $M(\lambda_1, \lambda_2; E)$ by a *relaxed* energy density $M^*(\lambda_1, \lambda_2; E)$, which

sets compressive stresses to zero whenever they would be present in the original energy. The relaxed energy represents the average energy that can be locally assigned to a region containing many wrinkles [Steigmann, 1990]; while relaxation does not provide a fine description of the wavelength of wrinkled regions, it effectively describes their onset and their orientation. A fundamental feature of the relaxed energy M^* is that, for a fixed voltage, it satisfies the *rank-one convexity* condition, which is fundamental in assessing the stability of wrinkled states [Pipkin, 1986].

We begin by illustrating the construction of the relaxed energy. Suppose that $s_1 = \partial_{\lambda_1} M$ and $s_2 = \partial_{\lambda_2} M$ are the Piola-Kirchhoff stress components, calculated from the original energy density M. Following [Steigmann, 1990], we introduce a *natural width in simple tension*, defined as the value of the stretch λ_1 (or λ_2) for which the stress s_1 (or s_2) becomes zero, that is, $\lambda_1^* = \nu(\lambda_2; E)$ is such that

$$s_1(\lambda_1^*, \lambda_2; E) = 0,$$

and likewise λ_2^* is such that

$$s_2(\lambda_1, \lambda_2^*; E) = 0.$$

Physically, the natural width is the point at which transition from compressed to tensile states occurs.

Thus, if $\lambda_1 < \lambda_1^*$, the stress s_1 will be compressive, and likewise for λ_2 and s_2. We thus replace the energy M by the *relaxed energy*

$$M^*(\lambda_1, \lambda_2; E) = \begin{cases} M(\lambda_1, \lambda_2; E) & \lambda_1 > \lambda_1^* \quad \lambda_2 > \lambda_2^* \\ M(\lambda_1, \nu(\lambda_1; E)) & \lambda_1 > 1 \quad 0 \le \lambda_2 \le \lambda_2^* \\ M(\nu(\lambda_2; E), \lambda_2) & \lambda_2 > 1 \quad 0 \le \lambda_1 \le \lambda_1^* \\ 0 & 0 \le (\lambda_1, \lambda_2) \le 1. \end{cases} \tag{4.33}$$

It can be easily verified that the relaxed energy is such that the relaxed stresses $s_{1/2}^* = \partial_{\lambda_{1/2}} M^*$ can not be negative. Taking the expression for M deduced in (4.32), imposing incompressibility as $\lambda_3 = (\lambda_1 \lambda_2)^{-1}$ and confining our attention to a neo-Hookean elastic behaviour, for which $W = \mu(I-3)/2$, we have

$$M = \frac{\mu}{2}\left(\lambda_1^2 + \lambda_2^2 + \lambda_1^{-2}\lambda_2^{-2} - 3 - E^2\lambda_1^2\lambda_2^2\right),$$

so that

$$s_1 = \frac{\partial M}{\partial \lambda_1} = \mu\lambda_1(1 - \lambda_1^{-4}\lambda_2^{-2} - E^2\lambda_2^2).$$

Thus the critical value of λ_1 for which $s_1 = 0$ is

$$\lambda_1^* = (\lambda_2^2 - E^2\lambda_2^4)^{-1/4},$$

so that the function ν is given by

$$\nu(a, E) = (a^2 - E^2 a^4)^{-1/4} \tag{4.34}$$

for neo-Hookean materials. The contrast between the original and relaxed energy densities is illustrated in Figure 4.3 for a neo-Hookean material. It is straightforward to show that the relaxed energy M^* is an increasing function of (λ_1, λ_2), see Figure 4.3.

It can be seen that for any given value of E there exists a region $\mathcal{D}_E$ in the plane of principal stretches (λ_1, λ_2) whose points are completely taut, in the sense that $s_{1/2}^* \geq 0$ [De Tommasi et al., 2011, De Tommasi et al., 2012]. As the voltage is increased, this region shrinks down until it collapses to a critical point. Since the region $\mathcal{D}_E$ is symmetric about the line $\lambda_1 = \lambda_2$, the critical point represents an equibiaxial state of deformation $(\lambda_1, \lambda_2) = (\lambda^*, \lambda^*)$. Thus, by finding the maximum value of E that solves $\nu(\lambda^*, E) = \lambda^*$, that is, the maximum of the function

$$E = \frac{\sqrt{\lambda^6 - 1}}{\lambda^4},$$

we obtain

$$E = E_{cr}^w = \frac{\sqrt{3}}{2^{4/3}} = 0.687. \tag{4.35}$$

It is interesting to compare this result with the outcomes of the *Hessian criterion*, proposed in [Zhao and Suo, 2007]. The latter identifies electromechanical instability with the loss of positive definiteness of the Hessian matrix of the free energy

$$\Omega^*(\lambda_1, \lambda_2, D_\ell) = \frac{\mu}{2}(\lambda_1^2 + \lambda_2^2 + \lambda_1^{-2}\lambda_2^{-2} - 3) + \frac{1}{2\varepsilon}\left(\frac{D_\ell}{\lambda_1\lambda_2}\right)^2 \tag{4.36}$$

where D_ℓ, the Lagrangian electric displacement, is related to E via

$$E = \frac{1}{\sqrt{\varepsilon\mu}}\frac{D_\ell}{\lambda_1^2\lambda_2^2}. \tag{4.37}$$

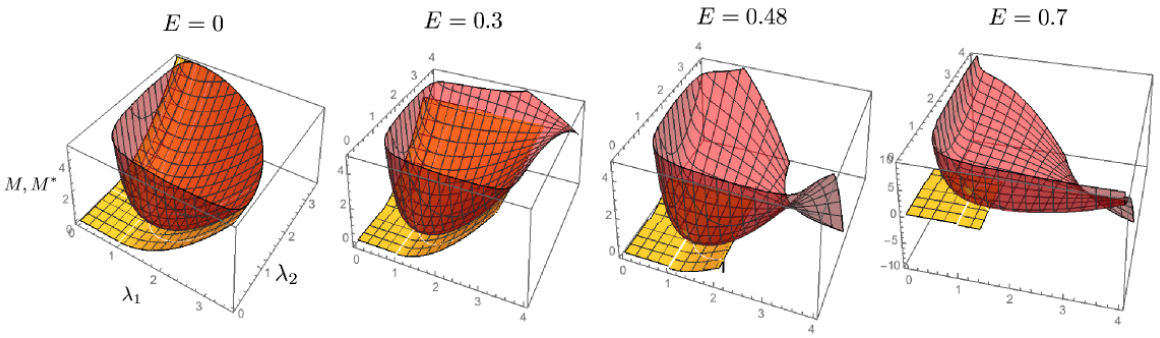

Figure 4.3: The membranal energy M given by $(4.32)_1$ for a dielectric membrane whose elastic part is neo-Hookean (red) and its relaxed energy M^* (yellow), for various values of the dimensionless applied electric field E. Above the critical value $E^w_{cr} = 0.687$, where the membrane ceases to be completely taut ($s^*_{1/2} \geq 0$), the energy M does not possess minimisers.

For equibiaxial deformations, where $\lambda_1 = \lambda_2 = \lambda$, the Hessian matrix of (4.36) reads

$$\mathcal{H} = \begin{pmatrix} \dfrac{2\mu\varepsilon(\lambda^6+5)+10D_\ell^2}{\lambda^6\varepsilon} & \dfrac{-4D_\ell}{\lambda^5\varepsilon} \\ \dfrac{-4D_\ell}{\lambda^5\varepsilon} & \dfrac{1}{\lambda^4\varepsilon} \end{pmatrix}. \tag{4.38}$$

Upon substitution for D_ℓ in terms of E using (4.37), this matrix has determinant

$$\det(\mathcal{H}) = -\frac{2\mu}{\lambda^{10}\varepsilon}(3E^2\lambda^8 - \lambda^6 - 5)$$

and thus becomes singular for

$$E^H_{cr} = \frac{\sqrt{5+\lambda^6}}{\sqrt{3}\lambda^4}. \tag{4.39}$$

This critical curve intersects the homogenous loading curve for equibiaxial deformations $E_{hom}(\lambda) = \sqrt{\lambda^{-2} - \lambda^{-8}}$ at the electric field

$$E^H_{cr,equib} = \frac{\sqrt{3}}{2^{4/3}} = 0.687, \tag{4.40}$$

which coincides precisely with (4.35): this highlights the fact that the Hessian criterion is strongly related to the onset of wrinkling, a finding already obtained in [De Tommasi et al., 2011, De Tommasi et al., 2012] by using similar arguments to the one adopted here, and recently confirmed by an incremental approach to electroelasticity in [Su et al., 2018].

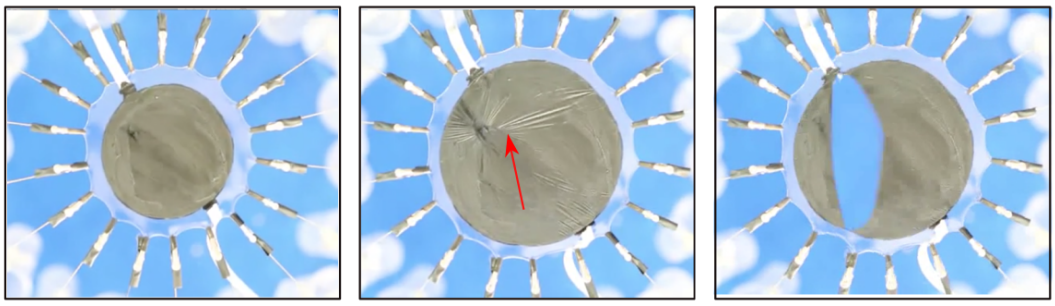

Figure 4.4: Electrically actuated VHB4905 membrane under equibiaxial dead loads; the grey areas represent the conductive carbon electrodes. Left: the deformed membrane at a voltage where no instability has yet occurred. Centre: the appearance of wrinkles, which is almost immediately followed by the pull-in instability (right). Although the proximity of the pull-in and wrinkling voltages evaluated through (4.35)-(4.41) refers to the case where dead loads are absent, this sequence confirms that the same behaviour holds in the presence of dead loads. Picture courtesy of Prof. T. Lu, Xi'an Jiaotong University, P. R. China.

It is interesting to anticipate that the pull-in instability — which we will discuss in the following section — is attained, for equibiaxially deformed states, when the electric field reaches the value

$$E^S_{cr,equib} = \frac{\sqrt{2}}{3^{2/3}} = 0.679. \tag{4.41}$$

The proximity of the voltages $E^S_{cr,equib}$ and $E^w_{cr,equib}$ suggests that in equibiaxial deformations the wrinkling and pull-in instabilities should be very close. This proximity, here deduced for unloaded membranes, is confirmed by experiments on dielectric membranes equibiaxially stretched under the action of dead load tractions, where the appearance of radial wrinkles is almost immediately followed by the onset of pull-in; see Figure 4.4. It should however be noted that while the proximity of wrinkling and pull-in is in agreement with experiments, the hierarchy of instabilities is reversed with respect to the experimental observations, since $E^S_{cr,equib} < E^H_{cr,equib}$.

4.4.2 Comparison with experiments

We now apply the relaxed energy approach to study the wrinkling of an annular dielectric membrane with compliant electrodes undergoing out-of-plane deformations. The onset of wrinkling in the same geometry, but without electric fields, was studied in [Roxburgh et al., 1995] by exploiting the relaxation approach.

The interesting aspect of this application is that we can compare the theoretical

outcomes with recent experimental results on the onset and progression of wrinkles on a voltage controlled annular membrane [Mao et al., 2018a]. For the same geometry, but referring to a different set of boundary conditions, we will later study the onset of pull-in instability.

We assume that the reference configuration of the dielectric membrane is a 2D annular region of internal radius A and external radius B. In axial symmetry, points $\boldsymbol{x} = R\boldsymbol{e}_R$ in the reference configuration — where $\boldsymbol{e}_R$ is the unit radial vector — are mapped to points $\boldsymbol{f}(\boldsymbol{x}) = r(R)\boldsymbol{e}_R + z(R)\boldsymbol{k}$ in the current configuration. If the membrane is equibiaxially prestretched before actuation by an amount λ_p, the principal stretches in the radial and hoop directions are

$$\lambda_1 = \lambda_p\sqrt{r'^2 + z'^2}, \qquad \lambda_2 = \lambda_p r/R \tag{4.42}$$

where a prime denotes differentiation with respect to R. Equilibrium equations can be obtained by perturbing the energy functional

$$\mathcal{E} = \int_A^B 2\pi R h M(\lambda_1, \lambda_2)\, dR - \mathcal{W}^m \tag{4.43}$$

where the work term is absent in the present setting of hard-device control, in which both boundaries of the device are fixed.

To obtain the Euler-Lagrange equations from the energy (4.43), we perturb $r(R)$ and $z(R)$ by introducing perturbations in each, so that, for example, $r(R)$ is perturbed to $r(R) + \varepsilon\eta(R)$, where $\varepsilon \ll 1$ and $\delta r(R) = \eta(R)$ is an arbitrary perturbation in $r(R)$. Setting $\bar{M} = RM$ for simplicity, the corresponding perturbation induced in $\bar{M}$ is

$$\begin{aligned}\delta\bar{M}(R, r + \varepsilon\eta, r' + \varepsilon\eta', z, z') &= \frac{\partial\bar{M}}{\partial r}\delta r + \frac{\partial\bar{M}}{\partial r'}\delta r' \\ &= \eta\frac{\partial\bar{M}}{\partial r} + \eta'\frac{\partial\bar{M}}{\partial r'}.\end{aligned}$$

This induces a perturbation in the energy, which reads

$$\delta\int_A^B 2\pi h\bar{M}dR = 2\pi h\int_A^B \left(\eta\frac{\partial\bar{M}}{\partial r} + \eta'\frac{\partial\bar{M}}{\partial r'}\right) dR.$$

Integrating the second term by parts yields

$$\int_A^B \eta' \frac{\partial \bar{M}}{\partial r'} dR = \left[\frac{\partial \bar{M}}{\partial r'} \eta \right]_A^B - \int_A^B \eta \frac{d}{dR} \left(\frac{\partial \bar{M}}{\partial r'} \right) dR.$$

Combining the integral terms gives

$$\delta \int_A^B 2\pi h \bar{M} dR = 2\pi h \int_A^B \eta \left(\frac{\partial \bar{M}}{\partial r} - \frac{d}{dR} \left(\frac{\partial \bar{M}}{\partial r'} \right) \right) dR + 2\pi h \left[\frac{\partial \bar{M}}{\partial r'} \eta \right]_A^B.$$

Then imposing stationarity of the energy, $\delta \mathcal{E} = 0$, we have

$$\frac{\partial \bar{M}}{\partial r} - \frac{d}{dR} \left(\frac{\partial \bar{M}}{\partial r'} \right) = 0, \tag{4.44}$$

the usual Euler-Lagrange equation, together with

$$2\pi h \left[\frac{\partial \bar{M}}{\partial r'} \eta \right]_A^B - \delta W^m = 0. \tag{4.45}$$

In the current setting of hard-device control, the boundaries are fixed such that $\eta(A) = \eta(B) = 0$, and so with the work term absent the latter equation is trivial; in such cases the boundary conditions are given by imposing values for $r(A)$ and $r(B)$ explicitly. For the alternative case of soft-device control considered later, one of the boundaries is not fixed, and the second equation yields a non-trivial relation for the work required for the perturbation.

An identical calculation for z gives a second set of equations, and thus the Euler-Lagrange equations of (4.43) are

$$\frac{\partial \bar{M}}{\partial r} - \frac{d}{dR} \left(\frac{\partial \bar{M}}{\partial r'} \right) = 0, \quad \frac{\partial \bar{M}}{\partial z} - \frac{d}{dR} \left(\frac{\partial \bar{M}}{\partial z'} \right) = 0. \tag{4.46}$$

It is useful at this point to recast the Euler-Lagrange equations into a more useful form in terms of the Piola-Kirchhoff stresses

$$s_1 = \frac{\partial \bar{M}}{\partial \lambda_1}, \quad s_2 = \frac{\partial \bar{M}}{\partial \lambda_2},$$

in the radial and hoop directions, respectively, for the non-wrinkled region and

$$s_1^* = \frac{\partial \bar{M}^*}{\partial \lambda_1}, \quad s_2^* = \frac{\partial \bar{M}^*}{\partial \lambda_2},$$

for the wrinkled region. Guided by experience, we know that in this problem the wrinkles appear in the hoop direction, so that $s_2^* = 0$, and furthermore that such wrinkles will start from the internal rim $R = A$, as observed in the experiments shown in Figure 4.5. For this reason, we denote by R^* the phase boundary between the wrinkled and non-wrinkled regions, so that the region (A, R^*) is wrinkled whereas the region (R^*, B) is not. Writing

$$\bar{M} = RM(R, r, r', z') = R\tilde{M}(\lambda_1, \lambda_2)$$

we have

$$\frac{\partial M}{\partial r} = R\left(\frac{\partial \tilde{M}}{\partial \lambda_1}\frac{\partial \lambda_1}{\partial r} + \frac{\partial \tilde{M}}{\partial \lambda_2}\frac{\partial \lambda_2}{\partial r}\right) = \lambda_p s_2$$

and

$$\frac{\partial M}{\partial r'} = R\left(\frac{\partial \tilde{M}}{\partial \lambda_1}\frac{\partial \lambda_1}{\partial r'} + \frac{\partial \tilde{M}}{\partial \lambda_2}\frac{\partial \lambda_2}{\partial r'}\right) = \lambda_p^2 R s_1 \frac{r'}{\lambda_1}.$$

Then the Euler-Lagrange equation in r for the non-wrinkled region becomes

$$\frac{d}{dR}\left(\frac{\lambda_p s_1 R r'}{\lambda_1}\right) = s_2, \quad R \in (R^*, B), \tag{4.47}$$

while for the wrinkled region, where $s_2^* = 0$, we have

$$\frac{d}{dR}\left(\frac{s_1^* R r'^*}{\lambda_1}\right) = 0, \quad R \in (A, R^*). \tag{4.48}$$

The corresponding equations in z are obtained similarly, and read

$$\frac{d}{dR}\left(\frac{s_1 R z'}{\lambda_1}\right) = 0, \quad R \in (R^*, B) \tag{4.49}$$

for the non-wrinkled region, and

$$\frac{d}{dR}\left(\frac{s_1^* R z'^*}{\lambda_1}\right) = 0, \quad R \in (A, R^*) \tag{4.50}$$

for the wrinkled region.

The equations (4.47)-(4.50) are a set of coupled ordinary differential equations for the unknown fields (r, z) and (r^*, z^*) in the non-wrinkled and wrinkled regions, respectively. Further simplification is possible in the wrinkled region by integrating equations (4.48) and (4.50) with respect to R and taking their quotient. This gives

$$z^{*\prime} = k r^{*\prime} \tag{4.51}$$

where k is an unknown constant. This confirms the well-known fact that in the absence of internal pressure, the meridians of the wrinkled membrane are straight lines [Roxburgh et al., 1995], and it is consistent with the analysis of [Mao et al., 2018a] for electrically active membranes, as can be seen in Figure 4.5. Boundary conditions for the coupled problem (4.47)-(4.50) are, at the outer and inner rims,

$$r^*(A) = A, \quad r(B) = B, \quad z^*(A) = z_0, \quad z(B) = 0 \tag{4.52}$$

where z_0 is a prescribed displacement of the internal rim. To these we append continuity conditions at the phase boundary $R = R^*$,

$$[\![r]\!] = 0, \qquad [\![z]\!] = 0, \qquad \left[\!\!\left[\frac{z'}{r'}\right]\!\!\right] = 0, \qquad [\![s_1]\!] = 0, \tag{4.53}$$

where the notation $[\![\cdot]\!]$ denotes a discontinuity in the corresponding quantity. For each value of the voltage, the unknown value of $R^*(V)$ is determined by checking iteratively that $s_2(R^*) = 0$ on the side of the non-wrinkled region. The numerical simulations, carried out using the Matlab `bvp4c` routine, result in the profiles represented in Figure 4.6. Consistent with the experimental findings of [Mao et al., 2018a], our predictions show that wrinkles first appear at a specific value of voltage at the internal rim and then, as the voltage is increased, they progress towards the external one.

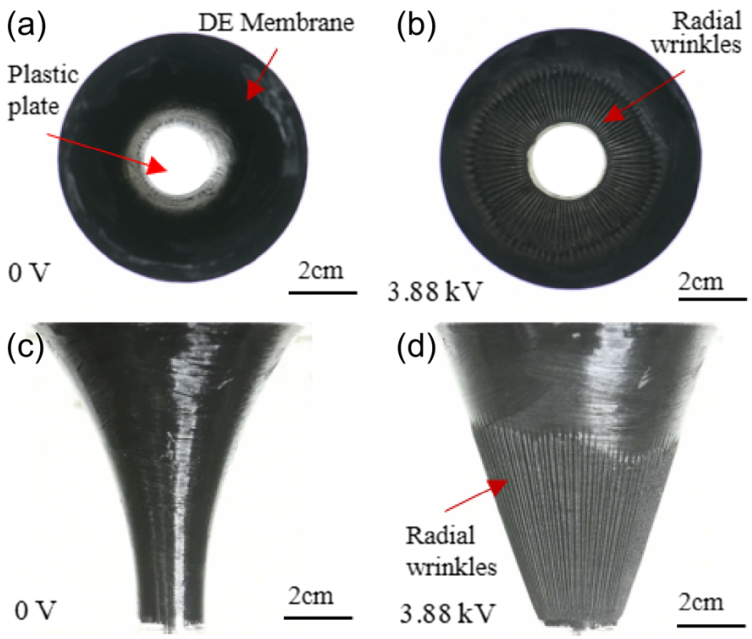

Figure 4.5: Experimental results of [Mao et al., 2018a], demonstrating the occurrence of wrinkling beginning from the lower rim at $R = A$, and moving upwards with increasing voltage towards the outer rim at $R = B$. The corresponding theoretical results are displayed in Figure 4.6.

4.5 Electroelastic stability

Formulations of the energy involving only the first derivative of the deformation describe membranes which have no bending stiffness, and this can lead to problems where the energy functional lacks minimisers [Hilgers and Pipkin, 1992]. This can be remedied by two approaches: either replacing the density by a relaxed energy density, as outlined in the previous section, or by using a strain energy function which depends both on the first and second derivatives of the deformation. In this case, energy minimisation problems will have solutions if the strain energy function is quasiconvex in its dependence on the second derivatives [Ball et al., 1981]. Thus the form of the energy given at the end of the previous section belongs in this category if the higher order terms are retained.

In the *regularization approach*, the question of existence of minimizers is dealt with by shifting the focus from the local term M to the non-local term $Q = S+B$, see [Hilgers and Pipkin, 1992, Hilgers and Pipkin, 1996]. If we note that the fields $\nabla\lambda_3$, $\operatorname{grad}\lambda_3$ and $\mathbf{L}$ are functions of the vectors $\boldsymbol{g}_a = \mathbf{G}\boldsymbol{e}_a$ and their gradients $\boldsymbol{g}_{a,b} = (\nabla\boldsymbol{g}_a)\boldsymbol{e}_b$, where $a, b = 1, 2$ and where $(\boldsymbol{e}_1, \boldsymbol{e}_2)$ are a couple of orthogonal unit vectors in Σ, by treating voltage as a controlled parameter the regularised electroelastic energy (4.30) can be

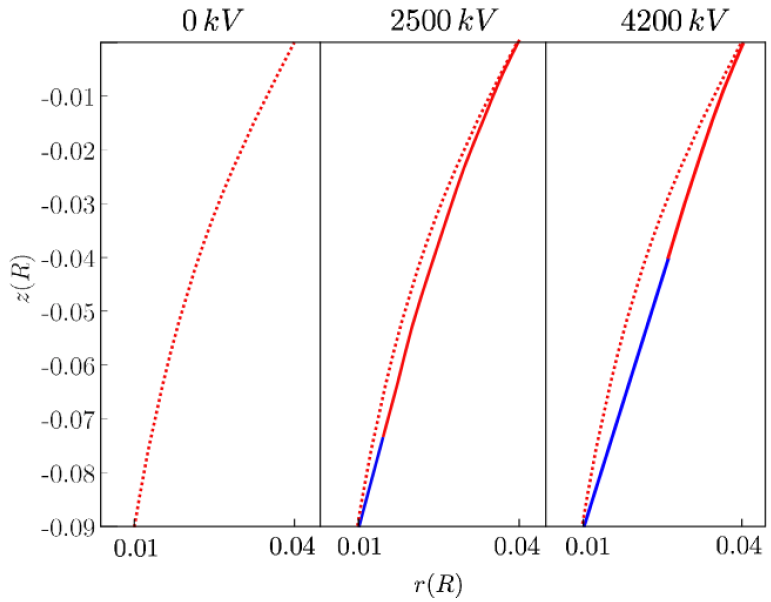

Figure 4.6: Theoretical profiles of the annular membrane under voltage control, obtained by using the relaxed energy M^*. The dotted curves in the three frames correspond to the non-wrinkled profile with $V = 0\,\text{kV}$. The red solid and blue solid curves describe the non wrinkled and wrinkled regions, respectively. Here the thickness is $h = 0.5\,\text{mm}$, the inner and outer radii are $A = 1\,\text{cm}$ and $B = 4\,\text{cm}$, respectively, the vertical displacement of the inner rim is $z_0 = 9\,\text{cm}$, the shear modulus is $\mu = 26.28\,\text{kPa}$, and the permittivity is $\varepsilon = 4.16 \times 10^{-11}\,\text{F/m}$, corresponding to the experiment shown in Figure 4.5.

recast as

$$\psi(\boldsymbol{g}_a, \boldsymbol{g}_{a,b}) = hM(\boldsymbol{g}_a) + h^3 Q(\boldsymbol{g}_a, \boldsymbol{g}_{a,b}). \tag{4.54}$$

where $Q = S + B$ is a quadratic form of $\boldsymbol{g}_{a,b}$.

Electroelastic stability of the regularised model is assessed by the requirement that the non-local term satisfies the *strong ellipticity* condition [Hilgers and Pipkin, 1996, Hilgers and Pipkin, 1992]

$$\frac{d^2}{dt^2} Q(\boldsymbol{g}_a, \boldsymbol{g}_{a,b} + t\boldsymbol{u}v_a v_b)\Big|_{t=0} > 0 \qquad \text{for all } \boldsymbol{u} \neq \boldsymbol{0} \text{ and } v_a \neq 0. \tag{4.55}$$

This is also known as the *Legendre-Hadamard material stability* condition.

4.5.1 Convexity and existence of minimisers

It is known that minimisers of Q exist when the function is convex in the second derivative term $\boldsymbol{g}_{a,b}$. We now show this explicitly for the energy given in (4.32), by considering the convexity of S and B separately, deriving conditions on the electric field E which ensure that S, B, and thus Q are convex in $\boldsymbol{g}_{a,b}$.

To discuss the implications of the stability requirement (4.55), we assume that $\mathbf{B}^{1/2}$ has eigenvalues (λ_1, λ_2) and that (κ_1, κ_2) are the eigenvalues of $\mathbf{L}$. We further assume that $\mathbf{B}$ and $\mathbf{L}$ are coaxial, which is satisfied in particular for axially symmetric membranes. In this case, the stretching and bending energies may be recast as

$$\begin{cases} S = \dfrac{1}{12}\left((W_0' - \dfrac{3}{4}\mu E^2\lambda_2^2)\lambda_{3,1}^2 + (W_0' - \dfrac{3}{4}\mu E^2\lambda_1^2)\lambda_{3,2}^2\right) \\ \\ B = \dfrac{1}{12}\left(\dfrac{\kappa_1^2}{\lambda_2^2}\left(W_0' + 2W_0''\lambda_1^2\right) + \dfrac{\kappa_2^2}{\lambda_1^2}\left(W_0' + 2W_0''\lambda_2^2\right) + \kappa_1\kappa_2\left(4W_0'' - \tfrac{3}{2}\mu E^2\right)\right) \end{cases} \tag{4.56}$$

where the $\lambda_{3,a}$ $(a = 1, 2)$ are derivatives of the function λ_3 in the direction of the principal directions of $\mathbf{G}^{\mathsf{T}}\mathbf{G}$. Next, we use the incompressibility condition $\lambda_3 = \alpha_0^{-1/2}$, with $\alpha_0 = |\boldsymbol{g}_1 \times \boldsymbol{g}_2|^2$, to obtain

$$\begin{aligned} \lambda_{3,1} &= -\alpha_0^{-1/2}\left((\boldsymbol{g}_{1,1} \times \boldsymbol{g}_2) + (\boldsymbol{g}_1 \times \boldsymbol{g}_{2,1})\right) \cdot \boldsymbol{n}, \\ \lambda_{3,2} &= -\alpha_0^{-1/2}\left((\boldsymbol{g}_{1,2} \times \boldsymbol{g}_2) + (\boldsymbol{g}_1 \times \boldsymbol{g}_{2,2})\right) \cdot \boldsymbol{n}, \end{aligned}$$

where we have used the definition of the normal vector, $\boldsymbol{n} = (\boldsymbol{g}_1 \times \boldsymbol{g}_2)/\alpha_0^{1/2}$. Thus we

can write the stretch-gradient term as

$$S = \frac{\alpha_0}{12}\left\{(W_0' - \frac{3}{4}\mu E^2\lambda_1^2)[(\boldsymbol{g}_{1,1}\times\boldsymbol{g}_2 + \boldsymbol{g}_1\times\boldsymbol{g}_{2,1})\cdot\boldsymbol{n}]^2 \right. \\ \left. +(W_0' - \frac{3}{4}\mu E^2\lambda_2^2)[(\boldsymbol{g}_{1,2}\times\boldsymbol{g}_2 + \boldsymbol{g}_1\times\boldsymbol{g}_{2,2})\cdot\boldsymbol{n}]^2\right\}$$

The Legendre-Hadamard material stability condition for convexity of S in $\boldsymbol{g}_{a,b}$ reads [Hilgers and Pipkin, 1992, Hilgers and Pipkin, 1996]

$$\frac{d^2}{dt^2}S(\boldsymbol{g}_{a,b} + t\boldsymbol{u}v_a v_b)\Big|_{t=0} \geq 0 \quad \text{for all} \quad \boldsymbol{u}\neq 0, \boldsymbol{v}\neq 0.$$

To obtain the critical value of E above which this condition is violated, we check each of the corresponding expressions for $a, b = \{1, 2\}$[1] with $\boldsymbol{g}_1$ and $\boldsymbol{g}_2$ fixed, and find that the condition is satisfied for values of E satisfying the inequalities

$$W_0' - \frac{3}{4}\mu E^2\lambda_1^2 \geq 0 \quad \text{and} \quad W_0' - \frac{3}{4}\mu E^2\lambda_2^2 \geq 0. \tag{4.57}$$

Thus we conclude that the stretch-gradient energy density S satisfies the Legendre-Hadamard condition provided that

$$E < E_{cr}^S = \frac{2}{\sqrt{3}}\sqrt{\frac{W_0'}{\mu}}\min\left(\frac{1}{\lambda_1}, \frac{1}{\lambda_2}\right). \tag{4.58}$$

If this condition is satisfied, the occurrence of thinning inhomogeneities in the membrane is energetically unfavoured.

We next consider the bending energy term B. Defining the bending moments as $M_a = \mathcal{K}_{ab}\kappa_b$, the tangential bending stiffness tensor $\mathcal{K}_{ab} = \partial^2 B/\partial\kappa_a\partial\kappa_b$ is given by

$$\mathcal{K}_{ab} = \frac{1}{12}\begin{pmatrix} 2(\lambda_2^{-2}(W_0' + 2W_0''\lambda_1^2)) & 4W_0'' - \frac{3}{2}\mu E^2 \\ 4W_0'' - \frac{3}{2}\mu E^2 & 2(\lambda_1^{-2}(W_0' + 2W_0''\lambda_2^2)) \end{pmatrix}, \tag{4.59}$$

Since a second-order tensor is always positive definite if its determinant is positive, we have that $\mathcal{K}_{ab}$ is positive definite if

$$\frac{4}{\lambda_1^2\lambda_2^2}(W_0' + 2W_0''\lambda_1^2)(W_0' + 2W_0''\lambda_2^2) - (4W_0'' - \frac{3}{2}\mu E^2) > 0, \tag{4.60}$$

[1]Since $\boldsymbol{g}_{1,2} = \boldsymbol{g}_{2,1}$, the inequalities for both are equivalent.

which is satisfied as long as

$$E < E_{cr}^{B} = \frac{2}{\sqrt{3\mu}}\sqrt{2W_0'' \pm \frac{\sqrt{(W_0' + 2\lambda_2^2 W_0'')(W_0' + 2\lambda_1^2 W_0'')}}{\lambda_1\lambda_2}}. \tag{4.61}$$

Since the Hessian of B may be interpreted as a tangential *bending stiffness* of the membrane, as long as (4.61) is satisfied the term B plays a beneficial stabilization effect relative to out-of-plane deformations of the membrane. This is particularly important during the onset of wrinkling instabilities.

It is now interesting to establish a comparison between the two critical voltages determined above. In order to do so, we assume that $W_0'' = 0$, which is possible if $W_0' = \mu/2$, as is the case for neo-Hookean elastic materials. Suppose, without loss of generality, that $\lambda_1 \leq \lambda_2$, so that $1/\lambda_1 \geq 1/\lambda_2$. Then we have that

$$\frac{1}{\lambda_1\lambda_2} \geq \frac{1}{\lambda_2^2}$$

so that the inequality

$$\frac{1}{\sqrt{\lambda_1\lambda_2}} \geq \frac{1}{\lambda_2} = \min\left(\frac{1}{\lambda_1}, \frac{1}{\lambda_2}\right)$$

holds, with equality if and only if $\lambda_1 = \lambda_2$. Thus we have

$$E_{cr}^{B} = \sqrt{\frac{2}{3}}\frac{1}{\sqrt{\lambda_1\lambda_2}} \geq E_{cr}^{S} = \sqrt{\frac{2}{3}}\min\left(\frac{1}{\lambda_1}, \frac{1}{\lambda_2}\right). \tag{4.62}$$

This expression shows that convexity of S in $\nabla\lambda_3$ implies convexity of B in $\mathbf{L}$. In particular, the two critical voltages coincide only for equibiaxial deformations, for which $\lambda_1 = \lambda_2$. Thus, as long as $E < E_{cr}^{S}$, the the whole term $Q = S + B$ is a *positive* quadratic form of $\boldsymbol{g}_{a,b}$, and for this reason below E_{cr}^{S} the membrane is always stable — regardless of whether or not it is wrinkled. This finding is consistent with the ubiquitous experimental observation that the occurrence of wrinkles does not, *per se*, induce instability. Rather, wrinkles are stable as long as the pull-in voltage is not reached.

If we instead consider the Legendre-Hadamard condition for B, neglecting the W_0'' term for simplicity, the Legendre-Hadamard condition reads

$$\frac{d^2}{dt^2}B(\boldsymbol{g}_{a,b} + t\boldsymbol{u}v_a v_b)\bigg|_{t=0} \geq 0 \quad \text{for all} \quad \boldsymbol{u} \neq 0, \boldsymbol{v} \neq 0.$$

To proceed, we first note that

$$\begin{aligned}\mathbf{B}\cdot\mathbf{L}^2 = \mathrm{tr}(\mathbf{B}\mathbf{L}^2) &= \mathrm{tr}((\nabla\boldsymbol{n})^{\mathsf{T}}\nabla\boldsymbol{n})\\ &= n_{1,1}^2 + n_{2,1}^2 + n_{3,1}^2 + n_{1,2}^2 + n_{2,2}^2 + n_{3,2}^2\\ &= \boldsymbol{n}_{,1}^2 + \boldsymbol{n}_{,2}^2,\end{aligned}$$

where the n_i are the components of $\boldsymbol{n}$. Then, writing the Gaussian curvature as

$$K = \frac{(\boldsymbol{n}_{,1}\times\boldsymbol{n}_{,2})\cdot\boldsymbol{n}}{\alpha_0},$$

where

$$\boldsymbol{n}_{,\beta} = \frac{\boldsymbol{g}_{1,\beta}\times\boldsymbol{g}_2 + \boldsymbol{g}_1\times\boldsymbol{g}_{2,\beta} - ([\boldsymbol{g}_{1,\beta}\times\boldsymbol{g}_2 + \boldsymbol{g}_1\times\boldsymbol{g}_{2,\beta}]\cdot\boldsymbol{n})\boldsymbol{n}}{\alpha_0},$$

we have

$$\frac{d^2}{dt^2}B\left(\boldsymbol{g}_{1,1} + t\boldsymbol{u}v_1^2\right)\Big|_{t=0} = \frac{1}{6}\lambda_3^2 W_0'\alpha_0^{-2}v_1^4(|\boldsymbol{u}\times\boldsymbol{g}_2|^2 - [(\boldsymbol{u}\times\boldsymbol{g}_2)\cdot\boldsymbol{n}]^2).$$

Now, decomposing $\boldsymbol{u}$ as

$$\boldsymbol{u} = \alpha_1\boldsymbol{g}_1 + \alpha_2\boldsymbol{g}_2 + (\boldsymbol{u}\cdot\boldsymbol{n})\boldsymbol{n}, \tag{4.63}$$

we have

$$\begin{aligned}[(\boldsymbol{u}\times\boldsymbol{g}_1)\cdot\boldsymbol{n}]^2 = \alpha_2^2\alpha^2, \quad |\boldsymbol{u}\times\boldsymbol{g}_1|^2 = \alpha_2^2\alpha^2 + (\boldsymbol{u}\cdot\boldsymbol{n})^2|\boldsymbol{g}_1|^2,\\ [(\boldsymbol{u}\times\boldsymbol{g}_2)\cdot\boldsymbol{n}]^2 = \alpha_1^2\alpha^2, \quad |\boldsymbol{u}\times\boldsymbol{g}_2|^2 = \alpha_1^2\alpha^2 + (\boldsymbol{u}\cdot\boldsymbol{n})^2|\boldsymbol{g}_2|^2,\end{aligned} \tag{4.64}$$

so that

$$\frac{d^2}{dt^2}B(\boldsymbol{g}_{1,1} + t\boldsymbol{u}v_1^2)\Big|_{t=0} = \frac{1}{6}\lambda_3^2 W_0'\alpha_0^{-2}v_1^4(\boldsymbol{u}\cdot\boldsymbol{n})^2|\boldsymbol{g}_2|^2,$$

which is always non-negative. By symmetry we obtain

$$\frac{d^2}{dt^2}B(\boldsymbol{g}_{2,2} + t\boldsymbol{u}v_2^2)\Big|_{t=0} = \frac{1}{6}\lambda_3^2 W_0'\alpha_0^{-2}v_2^4(\boldsymbol{u}\cdot\boldsymbol{n})^2|\boldsymbol{g}_1|^2,$$

which is similarly non-negative. Since $\boldsymbol{g}_{1,2} = \boldsymbol{g}_{2,1}$ it suffices to check the final condition,

$$\frac{d^2}{dt^2}B(\boldsymbol{g}_{1,2} + t\boldsymbol{u}v_1v_2)\Big|_{t=0} \geq 0 \quad \text{for all} \quad \boldsymbol{u}\neq 0, \boldsymbol{v}\neq 0.$$

Evaluating the left-hand side gives

$$\frac{d^2}{dt^2}B(\boldsymbol{g}_{1,2}+t\boldsymbol{u}v_1v_2)=\frac{1}{6}\alpha_0^{-2}v_1^2v_2^2\Big[W_0'\lambda_3^2\big\{(|\boldsymbol{u}\times\boldsymbol{g}_1|^2-[(\boldsymbol{u}\times\boldsymbol{g}_1)\cdot\boldsymbol{n}]^2) \\ +(|\boldsymbol{u}\times\boldsymbol{g}_2|^2-[(\boldsymbol{u}\times\boldsymbol{g}_2)\cdot\boldsymbol{n}]^2)\big\} \\ -\frac{3}{2}\mu E^2\alpha_0^{-1}[(\boldsymbol{u}\times\boldsymbol{g}_1)\times(\boldsymbol{u}\times\boldsymbol{g}_2)]\cdot\boldsymbol{n}\Big].$$

Using the relations (4.64), and noting that $[(\boldsymbol{u}\times\boldsymbol{g}_1)\times(\boldsymbol{u}\times\boldsymbol{g}_2)]\cdot\boldsymbol{n}=\alpha_0(\boldsymbol{u}\cdot\boldsymbol{n})^2$, we obtain

$$\frac{d^2}{dt^2}B(\boldsymbol{g}_{1,2}+t\boldsymbol{u}v_1v_2)=\frac{1}{6}\alpha_0^{-2}v_1^2v_2^2(\boldsymbol{u}\cdot\boldsymbol{n})^2\left[W_0'\lambda_3^2(|\boldsymbol{g}_1|^2+|\boldsymbol{g}_2|^2)-\frac{3}{2}\mu E^2\right].$$

Then noting that $|\boldsymbol{g}_i|=\lambda_i$ and using incompressibility, we obtain that B satisfies the Legendre-Hadamard condition provided that

$$W_0'\left(\frac{1}{\lambda_1^2}+\frac{1}{\lambda_2^2}\right)-\frac{3}{2}\mu E^2\geq 0,$$

from which we obtain that the expression for the critical electric field arising here is

$$E<E_{cr}^{BLH}=\sqrt{\frac{2W_0'}{3\mu}}\sqrt{\frac{1}{\lambda_1^2}+\frac{1}{\lambda_2^2}}. \tag{4.65}$$

Now, since

$$\min\left(\frac{1}{\lambda_1^2},\frac{1}{\lambda_2^2}\right)\leq\frac{1}{2}\left(\frac{1}{\lambda_1^2}+\frac{1}{\lambda_2^2}\right),$$

we have

$$E_{cr}^{S}=\frac{2}{\sqrt{3}}\sqrt{\frac{W_0'}{\mu}}\min\left(\frac{1}{\lambda_1},\frac{1}{\lambda_2}\right)\leq E_{cr}^{BLH}=\sqrt{\frac{2W_0'}{3\mu}}\sqrt{\frac{1}{\lambda_1^2}+\frac{1}{\lambda_2^2}}. \tag{4.66}$$

Thus, as long as $E\leq E_{cr}^{S}$, the term $Q=S+B$ satisfies the Legendre-Hadamard condition. Finally, we note that E_{cr}^{BLH} can be written

$$E_{cr}^{BLH}=\frac{2}{\sqrt{3}}\sqrt{\frac{W_0'}{\mu}}\sqrt{\frac{1}{2}\left(\frac{1}{\lambda_1}-\frac{1}{\lambda_2}\right)^2+\frac{1}{\lambda_1\lambda_2}},$$

from which it is immediately clear that

$$E_{cr}^{BLH} \geq E_{cr}^{B} = \frac{2}{\sqrt{3}}\sqrt{\frac{W_0'}{\mu}}\sqrt{\frac{1}{\lambda_1\lambda_2}}.$$

Thus we have established that

$$E_{cr}^{S} \leq E_{cr}^{B} \leq E_{cr}^{BLH},$$

which means that imposing convexity of $B(\kappa_1, \kappa_2)$ in the principal curvatures, given in general by (4.61), represents a stronger requirement than that arising from the Legendre-Hadamard condition for B.

4.6 Energy regularization and electroelastic stability

The onset of instabilities in the membrane can be detected by checking the loss of convexity of the regularization term Q. More specifically, when the stretch gradient term S becomes a non-convex function of $\nabla\lambda_3$, the term Q becomes a negative definite quadratic form, violating the stability requirement. This can be easily seen by noting that if $E > E_{cr}^{S}$ and if local values of $\mathbf{B}$ and $\mathbf{L}$ are fixed, so that the bending energy B in $(4.32)_3$ is fixed as well, then the stretching term S can be made negative by increasing the magnitude of $\nabla\lambda_3$. Thus, above the critical voltage, the regularization role of higher order terms is lost, and the onset of inhomogeneous deformations is not energetically penalised. We thus identify the *thinning instability* with the attainment of the critical electric field E_{cr}^{S}.

To assess the predictive power of our theoretical estimates for a system undergoing out-of-plane, inhomogeneous deformations, we consider another experiment, conducted on the same geometry discussed before. In particular, Zhang *et al.* [Zhang et al., 2016] have studied the state of deformation of an electrically actuated annular membrane with conductive hydrogels, and they have carefully measured the onset of thinning instabilities. This differs from the previously considered experiment in that the boundary condition at $z(A)$ is not operative and a work term is present, which here reads $\mathcal{W}^m = z(A)F$ where F is the resultant force. The corresponding perturbation is $\delta\mathcal{W}^m = F\xi(A)$, where $\xi(R)$ is the perturbation in $z(R)$, that is, $\delta z(R) = \xi(R)$. Since

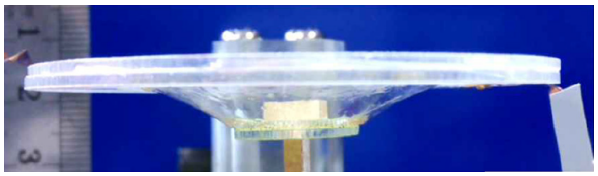

(a) unactuated state

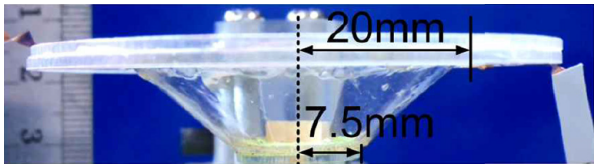

(b) actuated state before wrinkling

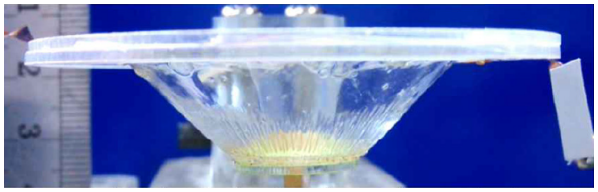

(c) actuated state before breakdown

Figure 4.7: Experimental setup of Zhang *et al.* [Zhang et al., 2016]; an annular dielectric membrane is laterally prestretched, the outer and inner radii fixed at 7.5 mm and 20 mm respectively, and the faces coated with hydrogel electrodes. A vertical downward force is applied at the inner rim, and the behaviour of the system upon application of a voltage is such that the inner rim moves vertically downwards.

Table 4.1: Comparison of experimental, theoretical and empirical (4.68) voltages.

λ_p	Experimental	Theoretical	% error	Empirical	% error
2	9795 V	10205 V	4.18	10319 V	5.3
3	6750 V	6378 V	5.51	6940 V	2.81
4	5164 V	4783 V	7.37	5291 V	2.46

the energy density does not depend on z'', we obtain from an equation analogous to (4.45) the boundary condition

$$\left.\frac{\partial \bar{M}}{\partial z'}\right|_{R=A} = \frac{F}{2h\pi}, \tag{4.67}$$

in addition to the conditions $r(A) = A$, $r(B) = B$, and $z(B) = 0$ given previously.

To describe the elastic behaviour of the membrane we again use a neo-Hookean model. For simplicity, in our calculations we neglect the stiffness of the hydrogel conductive electrodes, as this is an order of magnitude smaller than the stiffness of the dielectric elastomer, and we tune one single value, the shear modulus of the dielectric, to reproduce the loading curves at different prestretch values. Our results, given in Table 4.1 and represented in Figure 4.8, show that the our theoretical predictions are in very good agreement with the experimental data, with an error ranging from 4.18% at low prestretch to 7.37% at higher prestretch. The lower accuracy at higher prestretch may be attributed to the inadequacy of the neo-Hookean model to accurately describe the elastic response of the elastomer on a wide range of deformations.

Another interesting comparison is the one between our estimates for the thinning instability and the empirical formula for dielectric breakdown proposed by Huang *et al.* [Huang et al., 2012b]. For the type of VHB silicone used in the experiments on annular membranes considered above, in [Zhang et al., 2016] the expression

$$E_B = 21.5(\lambda_1\lambda_2/h)^{0.56} \tag{4.68}$$

is given for the electric breakdown field. This quantity, the breakdown voltage divided by the current thickness, is used to obtain the empirically predicted breakdown voltages given in Table 4.1, which compares the resulting predicted breakdown values with experimental values, and with our predicted breakdown values. The error in both cases is comparable, suggesting that our theoretical breakdown prediction offers a viable alternative to the empirical formula. As remarked previously, the error in our prediction increases with increasing prestretch, while the error in the empirical prediction appears not to depend on prestretch.

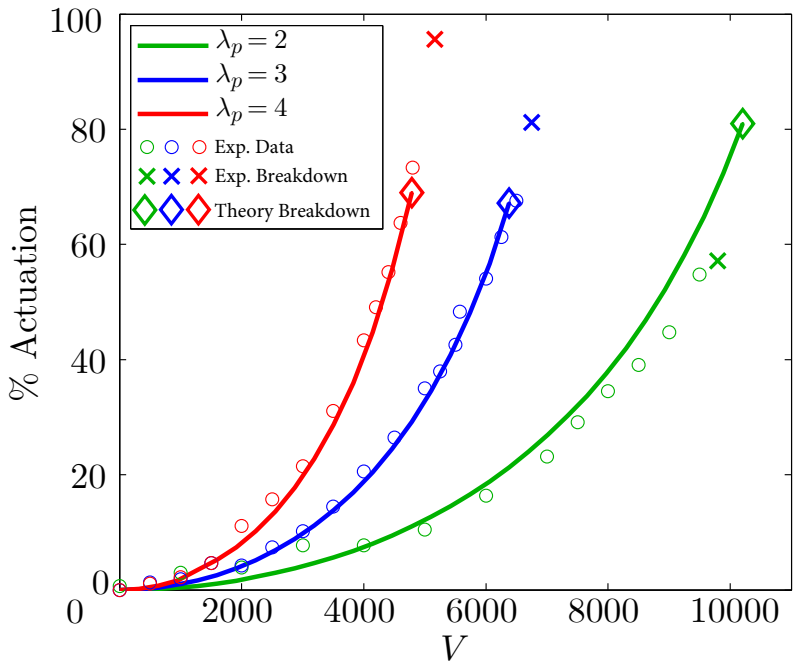

Figure 4.8: Actuation vs. voltage for the experiments reported in [Zhang et al., 2016] and shown in Figure 4.7, where the parameter values are $h = 1\,\text{mm}$, $F = 0.89\,\text{N}$, $\varepsilon = 3.54 \times 10^{-11}\,\text{F/m}$, $A = 7.5\,\text{mm}$, $B = 20\,\text{mm}$. The value of the shear modulus $\mu = 36\,\text{kPa}$ is chosen to match the experimental data.

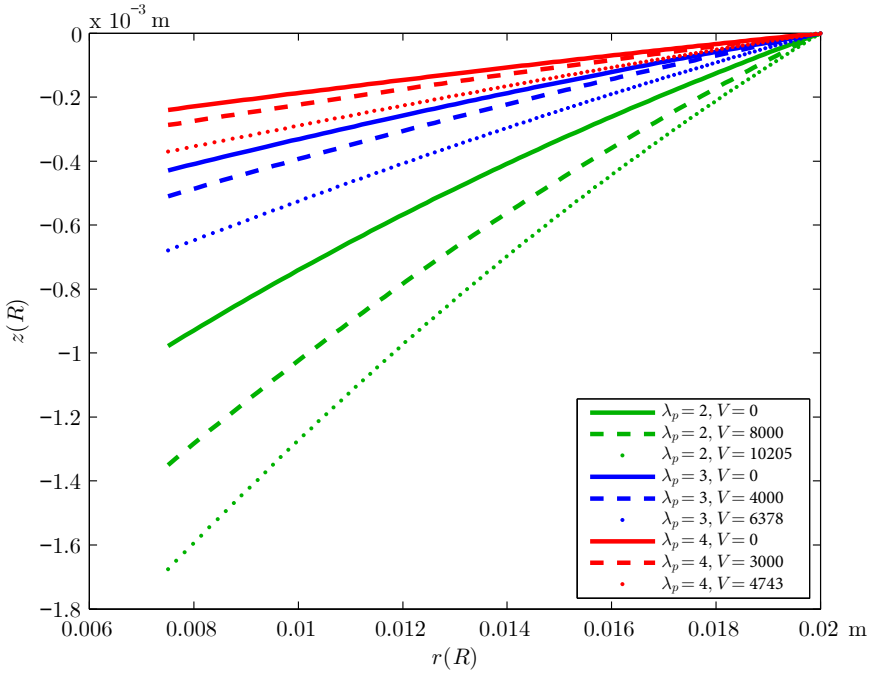

Figure 4.9: Membrane cross-section profiles at various voltages for $\lambda_p = 2, 3, 4$, with the same parameter values as those given in Figure 4.8.

4.7 Conclusion

We have shown in this chapter that the regularization and relaxation approaches to analysing equilibrium configurations offer a valid model for predicting the wrinkling and breakdown behaviour of thin dielectric elastomers. The onset and evolution of wrinkled regions can be accurately predicted using tension-field theory, and these predictions can be readily compared with experimental results for simple geometries. We have also demonstrated the role played by bending stiffness in regularizing wrinkled states and mitigating the occurrence of breakdown. Our prediction for the occurrence of the pull-in instability is valid at low stretches and shows good agreement with experimentally-measured breakdown voltages. For both wrinkling and thinning breakdown instabilities, we have shown that our theory is valid and accurate for axially symmetric configurations when compared with experiments.

We remark that our analysis should be confined to small stretches, where the assumption that the material can be described as an ideal neo-Hookean dielectric is valid. Furthermore, our results are valid upon restriction of the membrane deformation by the linear ansatz (4.8). While, as we have discussed in this chapter, we are aware of

the limitations of this assumption, we must acknowledge that a fully consistent and rigorous analysis of the pull-in instability by more rigorous means still remains a challenging open problem, which we leave for future studies. Further analysis, considering alternative constitutive behaviours, would also be a useful extension of the present work and may improve the predictive power of the model.

Our approach for the description of wrinkling may be fruitful in studying the coexistence of *phases* with multiple patterns of wrinkled states [Godaba et al., 2017], [Mao et al., 2018b] under voltage control. In problems where thick and thin regions may coexist [Zhao et al., 2007, An et al., 2015, Huang and Suo, 2011], we envisage that the stretch-gradient term S may be crucial to provide pattern regularisation below the pull-in voltage — see [Deseri and Zurlo, 2013], for example. Other interesting avenues for future studies include assessing if pull-in can be delayed by a judicious choice of boundary conditions, as proposed in [Yang et al., 2017] for example, or extending the analysis to the dynamical case, see [Lancioni and Tomassetti, 2002, Podio-Guidugli and Tomassetti, 2001], for example.

The theory outlined in this chapter, of membrane breakdown based on the loss of convexity of stretch-gradient and bending energy densities, will be futher developed and exploited in Chapter 5, where we extend these ideas to the domain of biological membranes. For biomembranes, the destabilising role of the electric field is replaced by a density of proteins binding to the membrane surface; a critical ratio of bound peptides to membrane lipids is shown to predict with reasonable accuracy the biological phenomenon of pore formation, a thinning instability in the language of our theory.

Chapter 5

Pore Formation in Lipid Membranes

5.1 Introduction

In this chapter, we briefly consider some ideas towards applying the theory developed in Chapter 4 to the modelling of biological membranes. Here, in place of the electric field, a density of peptide proteins binds to the outer leaflet of the lipid bilayer. Motivated by experimental evidence, we conjecture that the formation of pores in lipid membranes can be explained by the reaching of a critical density of peptides binding to the membrane, analogous to the critical electric field considered for dielectric membranes in the Chapter 4.

Cell membranes are typically described in the biophysics literature as a *fluid mosaic*, consisting principally of a biliayer of lipids, with various proteins embedded therein [Singer and Nicolson, 1972, Nicolson, 2014]. Whilst there are a myriad of different proteins performing distinct functions on the membrane at any time, a large class of these, known as host-defense antimicrobial peptides, perform a similar function in modulating cell defence [Brown and Hancock, 2006]. Of these, melittin has received significant attention as a representative model for pore-forming peptides. Depending on its concentration in the surrounding solution, it can induce transient or stable pores, with higher concentrations causing the membrane to disintegrate entirely, leading to cell lysis [Tosteson et al., 1985].

For low concentrations, melittin proteins bound to the lipid bilayer typically lie parallel to the membrane midsurface, within the region occupied by the head-group of lipids in the outer leaflet of the bilayer, as shown in Figure 5.1 (a). Thus an initially flat bilayer must develop a spontaneous curvature to maintain alignment with the undeformed inner leaflet of the bilayer. It has previously been shown that peptides such as

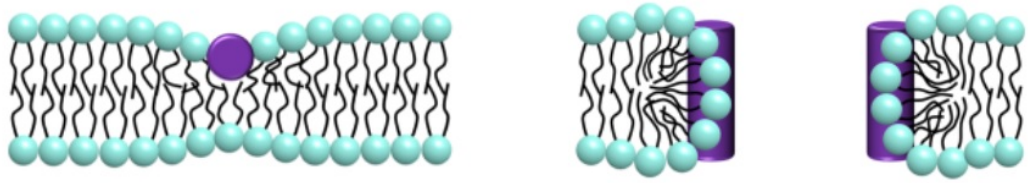

(a) Cross section of lipid membrane interacting with peptides: at low peptide concentrations (left), the peptide (purple) lies in the outer leaflet of the bilayer and may induce local thinning deformations of the membrane; at higher concentrations, peptides localise to form a transmembrane pore (right); adapted from [Lee et al., 2010].

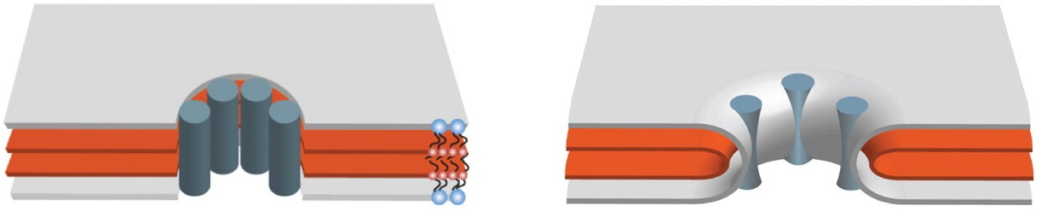

(b) Depending on the properties of the lipids and peptides, the pore may take two forms, referred to in the literature as the *barrel-stave* model (left) and the toroidal model (right); adapted from [Qian et al., 2008].

Figure 5.1: Schematic of pore formation in a lipid membrane interacting with peptides.

melittin may be stable at the edge of a lipid bilayer, and thus the creation of membrane edges may be facilitated by the presence of such proteins [Terwilliger et al., 1982]. It is the presence of these edges that allow formation of pores in the membrane. Depending on the properties of the specific peptide-lipid system under consideration, the type of pores formed are divided into two main categories, *barrel-stave* and *toroidal* pores; see Figure 5.1 (b).

It is generally agreed in the experimental literature that mellitin binds to the bilayer first, and then reorientates into a transmembrane configuration [Almeida and Pokorny, 2009]. At low concentrations, melittin adopts a parallel configuration, with the fraction of peptides in the transmembrane configuration increasing with increasing peptide concentration [Huang, 2006]. It has however been suggested that melittin binding parallel to membrane surface and direct perpendicular insertion may be competing processes [Van Den Bogaart et al., 2008]. Experimentally, the effect of melittin on the membrane may be observed by immersing lipid vesicles in a solution containing melittin, with the membrane area increase observed to be proportional to amount of melittin binding

[Lee et al., 2013].

Mechanically, it has been suggested based on experimental observations that peptide-bilayer binding creates an internal membrane stress, or internal membrane tension, which causes membrane thinning, with the induced tension being sufficiently large to cause pore formation for suitably high peptide concentrations [Huang et al., 2004]. Upon formation of a pore, a fraction of peptides are transferred from the outer bilayer leaflet to the pore rim, which causes a reduction in surface tension, stabilising the pore.

A simple mathematical justification for the stabilising role of peptides follows from considering the pore energy in a bilayer composed purely of lipids, given by [Lee et al., 2004] as

$$E = \gamma 2\pi R - \sigma \pi R^2,$$

where the first term represents the free energy cost of creating a rim on the edge of a pore of radius R with line tension γ, and the second represents the work done by a membrane tension σ in creating a pore of area πR^2. It follows from this that the energy has a maximum at $R = \gamma/\sigma$, so that a pore in a bilayer composed only of lipids is never stable: if $R < \gamma/\sigma$ the pore will close, while $R > \gamma/\sigma$ means the pore radius will continue to expand. Thus pore-inducing peptides must act so as to create a stress in the membrane which causes pores to open, and then act to stabilise these pores.

Lee *et al.* [Lee et al., 2004] have given an expression for the free energy change caused by peptide binding, which, normalised to per-lipid, reads

$$\Delta F = -\varepsilon_s \rho + \frac{1}{2} K_A (A_P^2/A_L)\rho^2, \tag{5.1}$$

where ε_s is the binding energy per peptide, $\rho = P/L$ is the peptide-to-lipid ratio, A_P and A_L are the cross-sectional area of a peptide and lipid, respectively, and K_A is the bilayer stretch modulus. The expression (5.1) for the free energy change is essentially the sum of binding energy and stretching energy terms. The values of the parameters K_A, A_L, A_P, as well as the thickness H of a purely lipid membrane, have been determined experimentally for various proteins; some typical values are given in Table 5.1 for the case of melittin interacting with DPhPC lipids.

Further analysis is possible based on considering the free energy change after pores have begun to form. When the critical concentration is reached and pore formation begins, a fraction $\phi\rho$ peptides are inserted in the bilayer perpindicular to the midsurface, so that $(1-\phi)\rho$ remain in the parallel state, with $0 \leq \phi \leq 1$. Consequently, the free

Parameter	Label	Value
Stretching rigidity	K_A	240 pN/nm
Membrane thickness	H	26.2 Å
Lipid cross section	A_L	91 Å^2
Peptide cross section	A_P	175Å^2
Critical peptide-lipid ratio	ρ^*	1/30

Table 5.1: Parameter Values for melittin and DPhPC, reported in [Lee et al., 2004]

energy change is modified to read

$$\Delta F = -\varepsilon_s(1-\phi)\rho - \varepsilon_I\phi\rho + \alpha[(1-\phi)\rho + \beta\phi\rho]^2 \tag{5.2}$$

where we have set $\alpha = K_A A_P^2/2A_L$, ε_I is the pore energy, and β accounts for the difference in the thinning effect between a peptide in the parallel and perpindicular state. The parameter β is required since less stretch is typically induced by a peptide lying perpindicular to the membrane midsurface than that induced by a peptide in the parallel state. Since the quantities ε_S, ε_I, α and β are fixed for a particular system, the free energy change can be considered as a function of ϕ, $\Delta F = \Delta F(\phi)$. Thus the system will behave so as to minimise the energy with respect to ϕ, that is, it must satisfy $\partial\Delta F/\partial\phi = 0$. This gives

$$\frac{\partial\Delta F}{\partial\phi} = (\varepsilon_S - \varepsilon_I)\rho + 2\alpha\left[(1-\phi)\rho + \beta\phi\rho\right](\beta-1)\rho = 0 \tag{5.3}$$

The *critical density* ρ^* at which pore formation begins corresponds to $\phi = 0$, when all of the peptides are still in the parallel state. Then setting $\phi = 0$ in (5.3) gives

$$\rho^* = \frac{\varepsilon_S - \varepsilon_I}{2\alpha(1-\beta)}. \tag{5.4}$$

In this framework, the instability occurs because the free energy change required when a peptide binds to form a pore, $-\varepsilon_I + \sigma\beta A_P$, is less than the free energy change when when the molecule binds to the surface, $-\varepsilon_S + \sigma A_P$. Thus at the critical density ρ^*, these two free energies will be the same, provided that the tension at pore formation σ^* satisfies $\sigma^* = (K_A A_P/A_L)\rho^*$, which follows from the linear relationship between membrane area expansion and tension [Lee et al., 2004]. The binding and pore energies must be negative here, since binding, if it is to occur, must be energetically favourable, so the free energy change must lower the overall free energy of the system.

If instead the number of peptides is written as the sum $P = P_S + P_I$ of the number of peptides P_S in the parallel state and the number P_I participating in the pore formation, and assuming that those participating in pore formation do not contribute to membrane thinning, then the free energy per lipid of the system reads [Huang et al., 2004]

$$F = -\underbrace{\varepsilon_S(P - P_I)/L}_{\text{binding energy}} - \underbrace{\varepsilon_I P_I/L}_{\text{pore energy}} + \underbrace{\frac{K_A A_P^2}{2A_L}\frac{(P - P_I)^2}{L^2}}_{\text{stretching energy}}.$$

If P is fixed, then minimising F with respect to P_I gives

$$P - P_I = P_S^* = \frac{(\varepsilon_S - \varepsilon_I)LA_L}{K_A A_P^2},$$

which is a constant – so P_S^* must be constant when peptides begin to participate in pore formation, that is, no peptides bind in the outer leaflet parallel to the membrane midsurface, so no further thinning occurs once pore formation commences.

5.2 Motivation

Whilst the foregoing theory gives a satisfactory explanation for the occurrence of pores, it does not offer insight into the relationship between membrane thickness and peptide binding. Moreover, there does not appear to be a comprehensive mechanical description of the instability available in the literature. Although we do not present a full analysis or theory for the mechanical instability here, the merits of this approach can be briefly demonstrated by a kinematic example which demonstrates the relationship between peptide binding and membrane thickness. Suppose we have a spherical lipid membrane of radius R and membrane thickness H. The volume of the membrane is

$$\frac{4}{3}\pi\left(R + \frac{H}{2}\right)^3 - \frac{4}{3}\pi\left(R - \frac{H}{2}\right)^3 = \frac{4}{3}\pi\left(\frac{H^3}{4} + 3HR^2\right). \tag{5.5}$$

If peptides bind to the outer leaflet of the membrane in a dispersed manner, so that the configuration remains spherical, this results in a membrane of radius r and thickness h, so the volume of the membrane is

$$\frac{4}{3}\pi\left(\frac{h^3}{4} + 3hr^2\right).$$

If the volume of the membrane is conserved, we obtain

$$r^2 = \frac{1}{3h}\left(\frac{H^3 - h^3}{4} + 3HR^2\right). \tag{5.6}$$

Supposing that the total number of lipids in the reference configuration is N_L and the areal cross section of a lipid is A_L, we have $A_L N_L = 4\pi R^2$. Similarly, defining A_P as the cross-sectional area of a peptide and N_P to be the number of peptides, we have

$$A_L N_L + A_P N_P = 4\pi r^2.$$

The total number of molecules in the system is $N = N_L + N_P$. This enables the definition of $\chi = N_P/N$, the fraction of peptide molecules in the system, so that $1 - \chi = N_L/N$ is the fraction of lipid molecules. Then we have that

$$\frac{A_L N_L + A_P N_P}{N} = A_L(1-\chi) + A_P\chi = \frac{4\pi r^2}{N}. \tag{5.7}$$

Rearranging this gives

$$\chi(A_P - A_L) + A_L = \frac{4\pi}{N} r^2, \tag{5.8}$$

and substituting for r^2 using (5.6) then yields

$$\chi = \chi(h) = \frac{4\pi}{3hN(A_P - A_L)}\left(\frac{H^3 - h^3}{4} + 3HR^2\right) - \frac{A_L}{A_P - A_L}. \tag{5.9}$$

Thus the functional dependence of χ on h takes the form

$$\chi(h) = c_1 h^{-1} + c_2 h^2 + c_3, \tag{5.10}$$

where the c_i are constants depending on the system. Furthermore, when there are no peptides present in the system, the thickness should remain at the thickness value for the purely lipid membrane, that is,

$$\chi(h = H) = 0.$$

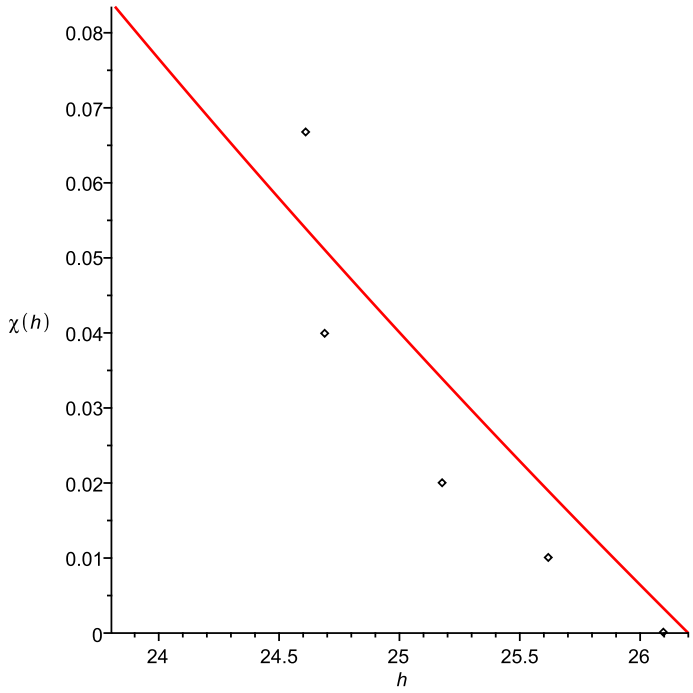

Figure 5.2: Plot of dimensionless molar fraction $\chi(h)$ vs. thickness h, using (5.11) and the parameter values given in Table 5.1, showing a satisfactory agreement with experimental data extracted from [Lee et al., 2004]

Imposing this, we obtain a relation between N and R,

$$R = \frac{1}{2}\sqrt{\frac{A_L N}{\pi}} \quad \text{or} \quad N = \frac{4\pi R^2}{A_L},$$

and substituting the latter in (5.9) gives

$$\chi(h) = \frac{A_L}{A_P - A_L}\left(\frac{1}{3h}\left(\frac{H^3 - h^3}{4R^2} + 3H\right) - 1\right). \tag{5.11}$$

The values of the peptide and lipid cross sections A_P and A_L, and the reference thickness H can be determined experimentally, and are given in Table 5.1 for the case of melittin peptides binding to DPhPC lipids. Then by fixing R, we plot χ as a function of h, with the result displayed in Figure 5.2. Whilst it can be seen that this fits to the experimental data in a reasonable manner, it fails to capture the saturation behaviour of the peptides, where the thinning reaches a plateau and pore formation commences [Huang et al., 2004].

A more realistic model for this process, in addition to being capable of predicting

the instability, should account for osmotic pressure within the membrane, and for the mechanical behaviour of the lipids and peptides, perhaps by considering each phase to have a neo-Hookean behaviour, or indeed by considering a more complex constitutive behaviour. The consideration of the peptide-lipid system as a more sophisticated mixture [Komura et al., 2004] might also yield useful insights. We envisage that the foregoing will be a fruitful avenue for future research in this area.

Chapter 6

Conclusion

This thesis has explored the mathematical modelling of membranes within a general framework. We now summarise the main conclusions of the thesis and discuss some potential avenues for future research.

6.1 Biological membranes

In Chapter 3, we derived equations describing the shape of biological membrane whose energy depends on its mean and Gaussian curvatures, the stretch of its midsurface, and the gradient of the stretch. These equations are derived in a fully general manner without making any assumption on geometry or parameterisation, and thus may be used in a wide range of applications. We have also shown how to specialise the equations to a specific geometry, and thus how they may be used to predict and model the behaviour of membranes, and possibly to then calibrate experimental results with the theory. As a possible avenue for future research, it would also be interesting to apply this theory to more complex geometries, requiring the use of more sophisticated methods such as finite element methods.

We also presented in Chapter 5 some considerations for a model for the prediction of peptide-induced pore formation in biological membranes. This phenomenon, which has been the subject of widespread attention in experimental studies, does not appear to have yet been studied comprehensively from a continuum mechanics perspective. An extension of the ideas presented in Chapter 5 may thus result in a realistic and useful model for the formation of pores in biological membranes. In particular, the consideration of the elastic behaviour of the lipids and peptides and the formulation of the problem as a more sophisticated mixture model might yield a more insightful expla-

nation for the thinning behaviour observed in peptide-lipid systems, and furthermore might assist in obtaining an explicit, mechanically-derived expression for the critical peptide-to-lipid density at which pore formation commences.

6.2 Electroactive devices

In Chapter 4, we showed that the approaches described by regularization and relaxation of the membrane energy density provide an accurate model for the prediction of wrinkling and breakdown phenomena exhibited by thin dielectric elastomers. The predictions for wrinkling of these devices compare quite favourably with experimental results for simple geometries, while the model predictions for the occurrence of thinning instabilities shows good agreement with experimentally-measured breakdown voltages at low stretches. In particular, we have demonstrated the validity and accuracy of our theory for the case of axially symmetric configurations when compared with experiments.

The analysis presented in Chapter 4, while valid at small stretches, is not appropriate for devices subjected to larger stretches. The assumption of a neo-Hookean behaviour is, perhaps, simplistic, and thus a comparison with a Gent or Mooney-Rivlin constitutive model might provide some further insights. The linear ansatz imposed on the deformation of the membrane may also limit the accuracy of the model predictions, and a more realistic description of the deformation might be useful in obtaining further results.

It would also be useful in validating the model to consider differing geometries, either on similarly symmetric geometries where the shape of the membrane is determined by ordinary differential equations, or by attempting to extend the model to more general geometries by using finite element methods, already an active research area within the field of dielectric elastomer modelling [Qu and Suo, 2012, Park et al., 2012].

Bibliography

[Agrawal and Steigmann, 2009] Agrawal, A. and Steigmann, D. J. (2009). Boundary-value problems in the theory of lipid membranes. *Continuum Mechanics and Thermodynamics*, 21(1):57–82.

[Agrawal and Steigmann, 2011] Agrawal, A. and Steigmann, D. J. (2011). A model for surface diffusion of trans-membrane proteins on lipid bilayers. *Zeitschrift für angewandte Mathematik und Physik*, 62(3):549.

[Alberts et al., 2015] Alberts, B., Johnson, A., Lewis, J., Morgan, D., Raff, M., Roberts, K., and Walter, P. (2015). *Molecular Biology of the Cell*. Garland Science, 6th edition.

[Almeida and Pokorny, 2009] Almeida, P. F. and Pokorny, A. (2009). Mechanisms of antimicrobial, cytolytic, and cell-penetrating peptides: From kinetics to thermodynamics. *Biochemistry*, 48(34):8083–8093.

[An et al., 2015] An, L., Wang, F., Cheng, S., Lu, T., and Wang, T. (2015). Experimental investigation of the electromechanical phase transition in a dielectric elastomer tube. *Smart Materials and Structures*, 24(3):035006.

[Andersen and Koeppe, 2007] Andersen, O. S. and Koeppe, R. E. (2007). Bilayer thickness and membrane protein function: An energetic perspective. *Annual Review of Biophysics and Biomolecular Structure*, 36:107–130.

[Atkin and Fox, 2005] Atkin, R. and Fox, N. (2005). *An Introduction to the Theory of Elasticity*. Dover.

[Audoly and Hutchinson, 2016] Audoly, B. and Hutchinson, J. W. (2016). Analysis of necking based on a one-dimensional model. *Journal of the Mechanics and Physics of Solids*, 97:68–91.

[Baesu et al., 2004] Baesu, E., Rudd, R., Belak, J., and McElfresh, M. (2004). Continuum modeling of cell membranes. *International Journal of Non-Linear Mechanics*, 39(3):369–377.

[Ball et al., 1981] Ball, J. M., Currie, J., and Olver, P. J. (1981). Null lagrangians, weak continuity, and variational problems of arbitrary order. *Journal of Functional Analysis*, 41(2):135–174.

[Bauer et al., 2014] Bauer, S., Bauer-Gogonea, S., Graz, I., Kaltenbrunner, M., Keplinger, C., and Schwödiauer, R. (2014). 25th anniversary article: A soft future: From robots and sensor skin to energy harvesters. *Advanced Materials*, 26(1):149–162.

[Bense et al., 2017] Bense, H., Trejo, M., Reyssat, E., Bico, J., and Roman, B. (2017). Buckling of elastomer sheets under non-uniform electro-actuation. *Soft Matter*, 13(15):2876–2885.

[Berndl et al., 1990] Berndl, K., Käs, J., Lipowsky, R., Sackmann, E., and Seifert, U. (1990). Shape transformations of giant vesicles: Extreme sensitivity to bilayer asymmetry. *Europhysics Letters*, 13(7):659.

[Berselli et al., 2011] Berselli, G., Vertechy, R., Vassura, G., and Parenti-Castelli, V. (2011). Optimal synthesis of conically shaped dielectric elastomer linear actuators: Design methodology and experimental validation. *IEEE/ASME Transactions on Mechatronics*, 16(1):67–79.

[Blok and LeGrand, 1969] Blok, J. and LeGrand, D. (1969). Dielectric breakdown of polymer films. *Journal of Applied Physics*, 40(1):288–293.

[Bortot and Gei, 2015] Bortot, E. and Gei, M. (2015). Harvesting energy with load-driven dielectric elastomer annular membranes deforming out-of-plane. *Extreme Mechanics Letters*, 5:62–73.

[Brown and Hancock, 2006] Brown, K. L. and Hancock, R. E. (2006). Cationic host defense (antimicrobial) peptides. *Current Opinion in Immunology*, 18(1):24–30.

[Canham, 1970] Canham, P. B. (1970). The minimum energy of bending as a possible explanation of the biconcave shape of the human red blood cell. *Journal of Theoretical Biology*, 26(1):61–81.

[Cao and Hutchinson, 2012] Cao, Y. and Hutchinson, J. (2012). Wrinkling phenomena in neo-Hookean film/substrate bilayers. *Journal of Applied Mechanics*, 79:031019.

[Chan et al., 2006] Chan, D. I., Prenner, E. J., and Vogel, H. J. (2006). Tryptophan-and arginine-rich antimicrobial peptides: Structures and mechanisms of action. *Biochimica et Biophysica Acta (BBA)-Biomembranes*, 1758(9):1184–1202.

[Coleman and Newman, 1988] Coleman, B. D. and Newman, D. C. (1988). On the rheology of cold drawing. I. elastic materials. *Journal of Polymer Science Part B: Polymer Physics*, 26(9):1801–1822.

[Danielli and Davson, 1935] Danielli, J. F. and Davson, H. (1935). A contribution to the theory of permeability of thin films. *Journal of Cellular and Comparative Physiology*, 5(4):495–508.

[De Tommasi et al., 2011] De Tommasi, D., Puglisi, G., and Zurlo, G. (2011). Compression-induced failure of electroactive polymeric thin films. *Applied Physics Letters*, 98(12):123507.

[De Tommasi et al., 2012] De Tommasi, D., Puglisi, G., and Zurlo, G. (2012). Taut states of dielectric elastomer membranes. *International Journal of Non-Linear Mechanics*, 47(2):355–361.

[De Tommasi et al., 2014] De Tommasi, D., Puglisi, G., and Zurlo, G. (2014). Failure modes in electroactive polymer thin films with elastic electrodes. *Journal of Physics D: Applied Physics*, 47(6):065502.

[Deseri et al., 2008] Deseri, L., Piccioni, M. D., and Zurlo, G. (2008). Derivation of a new free energy for biological membranes. *Continuum Mechanics and Thermodynamics*, 20(5):255–273.

[Deseri and Zurlo, 2013] Deseri, L. and Zurlo, G. (2013). The stretching elasticity of biomembranes determines their line tension and bending rigidity. *Biomechanics and Modeling in Mechanobiology*, 12(6):1233–1242.

[Deserno, 2004] Deserno, M. (2004). Elastic deformation of a fluid membrane upon colloid binding. *Physical Review E*, 69(3):031903.

[Deserno, 2015] Deserno, M. (2015). Fluid lipid membranes: From differential geometry to curvature stresses. *Chemistry and Physics of Lipids*, 185:11–45.

[Deuling and Helfrich, 1976] Deuling, H. and Helfrich, W. (1976). The curvature elasticity of fluid membranes: A catalogue of vesicle shapes. *Journal de Physique*, 37(11):1335–1345.

[Dharmavaram and Healey, 2015] Dharmavaram, S. and Healey, T. J. (2015). On the equivalence of local and global area-constraint formulations for lipid bilayer vesicles. *Zeitschrift für angewandte Mathematik und Physik*, 66(5):2843–2854.

[Do Carmo, 1976] Do Carmo, M. P. (1976). *Differential Geometry of Curves and Surfaces*. Prentice-Hall.

[Dos Remedios et al., 2003] Dos Remedios, C., Chhabra, D., Kekic, M., Dedova, I., Tsubakihara, M., Berry, D., and Nosworthy, N. (2003). Actin binding proteins: regulation of cytoskeletal microfilaments. *Physiological Reviews*, 83(2):433–473.

[Farago and Pincus, 2004] Farago, O. and Pincus, P. (2004). Statistical mechanics of bilayer membrane with a fixed projected area. *The Journal of Chemical Physics*, 120(6):2934–2950.

[Fosdick and Tang, 2007] Fosdick, R. and Tang, H. (2007). Electrodynamics and thermomechanics of material bodies. *Journal of Elasticity*, 88(3):255–297.

[Frye and Edidin, 1970] Frye, L. D. and Edidin, M. (1970). The rapid intermixing of cell surface antigens after formation of mouse-human heterokaryons. *Journal of Cell Science*, 7(2):319–335.

[Fu et al., 2018a] Fu, Y., Dorfmann, L., and Xie, Y. (2018a). Localized necking of a dielectric membrane. *Extreme Mechanics Letters*, 21:44–48.

[Fu et al., 2018b] Fu, Y., Xie, Y., and Dorfmann, L. (2018b). A reduced model for electrodes-coated dielectric plates. *International Journal of Non-Linear Mechanics*, 106:60–69.

[Godaba et al., 2017] Godaba, H., Zhang, Z.-Q., Gupta, U., Foo, C. C., and Zhu, J. (2017). Dynamic pattern of wrinkles in a dielectric elastomer. *Soft Matter*, 13(16):2942–2951.

[Gorter and Grendel, 1925] Gorter, E. and Grendel, F. (1925). On bimolecular layers of lipoids on the chromocytes of the blood. *Journal of Experimental Medicine*, 41(4):439–443.

[Greaney et al., 2019] Greaney, P., Meere, M., and Zurlo, G. (2019). The out-of-plane behaviour of dielectric membranes: Description of wrinkling and pull-in instabilities. *Journal of the Mechanics and Physics of Solids*, 122:84–97.

[Harris, 2000] Harris, H. (2000). *The Birth of the Cell*. Yale University Press.

[He et al., 2009] He, T., Zhao, X., and Suo, Z. (2009). Dielectric elastomer membranes undergoing inhomogeneous deformation. *Journal of Applied Physics*, 106(8):083522.

[Helfrich, 1973] Helfrich, W. (1973). Elastic properties of lipid bilayers: Theory and possible experiments. *Zeitschrift für Naturforschung C*, 28(11-12):693–703.

[Hilgers and Pipkin, 1992] Hilgers, M. and Pipkin, A. (1992). Bending energy of highly elastic membranes. *Quarterly of Applied Mathematics*, 50(2):389–400.

[Hilgers and Pipkin, 1996] Hilgers, M. and Pipkin, A. (1996). Bending energy of highly elastic membranes. II. *Quarterly of Applied Mathematics*, 54(2):307–316.

[Huang, 2006] Huang, H. W. (2006). Molecular mechanism of antimicrobial peptides: the origin of cooperativity. *Biochimica et Biophysica Acta - Biomembranes*, 1758(9):1292–1302.

[Huang et al., 2004] Huang, H. W., Chen, F.-Y., and Lee, M.-T. (2004). Molecular mechanism of peptide-induced pores in membranes. *Physical Review Letters*, 92(19):198304.

[Huang et al., 2012a] Huang, J., Li, T., Chiang Foo, C., Zhu, J., Clarke, D. R., and Suo, Z. (2012a). Giant, voltage-actuated deformation of a dielectric elastomer under dead load. *Applied Physics Letters*, 100(4):041911.

[Huang et al., 2012b] Huang, J., Shian, S., Diebold, R. M., Suo, Z., and Clarke, D. R. (2012b). The thickness and stretch dependence of the electrical breakdown strength of an acrylic dielectric elastomer. *Applied Physics Letters*, 101(12):122905.

[Huang and Suo, 2011] Huang, R. and Suo, Z. (2011). Electromechanical phase transition in dielectric elastomers. *Proceedings of the Royal Society A*, 468:1014–1040.

[Jenkins, 1977] Jenkins, J. (1977). Static equilibrium configurations of a model red blood cell. *Journal of Mathematical Biology*, 4(2):149–169.

[Kim and Steigmann, 2015] Kim, C.-I. and Steigmann, D. J. (2015). Distension-induced gradient capillarity in lipid membranes. *Continuum Mechanics and Thermodynamics*, 27(4-5):609.

[Kollosche et al., 2015] Kollosche, M., Kofod, G., Suo, Z., and Zhu, J. (2015). Temporal evolution and instability in a viscoelastic dielectric elastomer. *Journal of the Mechanics and Physics of Solids*, 76:47–64.

[Komura et al., 2004] Komura, S., Shirotori, H., Olmsted, P. D., and Andelman, D. (2004). Lateral phase separation in mixtures of lipids and cholesterol. *EPL (Europhysics Letters)*, 67(2):321.

[Kovetz, 2000] Kovetz, A. (2000). *Electromagnetic Theory*. Oxford University Press.

[Kreyszig, 1959] Kreyszig, E. (1959). *Introduction to Differential Geometry and Riemannian Geometry*. University of Toronto Press.

[Lancioni and Tomassetti, 2002] Lancioni, G. and Tomassetti, G. (2002). Flexure waves in electroelastic plates. *Wave Motion*, 35(3):257–269.

[Langmuir, 1917] Langmuir, I. (1917). The constitution and fundamental properties of solids and liquids. II. liquids. *Journal of the American Chemical Society*, 39(9):1848–1906.

[Lee et al., 2010] Lee, J.-H., Choi, S.-M., Doe, C., Faraone, A., Pincus, P. A., and Kline, S. R. (2010). Thermal fluctuation and elasticity of lipid vesicles interacting with pore-forming peptides. *Physical Review Letters*, 105(3):038101.

[Lee et al., 2004] Lee, M.-T., Chen, F.-Y., and Huang, H. W. (2004). Energetics of pore formation induced by membrane active peptides. *Biochemistry*, 43(12):3590–3599.

[Lee et al., 2013] Lee, M.-T., Sun, T.-L., Hung, W.-C., and Huang, H. W. (2013). Process of inducing pores in membranes by melittin. *Proceedings of the National Academy of Sciences*, 110(35):14243–14248.

[Liu et al., 2016] Liu, X., Li, B., Chen, H., Jia, S., and Zhou, J. (2016). Voltage-induced wrinkling behavior of dielectric elastomer. *Journal of Applied Polymer Science*, 133:43258.

[Magnus and Neudecker, 1988] Magnus, J. R. and Neudecker, H. (1988). *Matrix Differential Calculus with Applications in Statistics and Econometrics*. Wiley.

[Majidi, 2014] Majidi, C. (2014). Soft robotics: A perspective—current trends and prospects for the future. *Soft Robotics*, 1(1):5–11.

[Maleki et al., 2013] Maleki, M., Seguin, B., and Fried, E. (2013). Kinematics, material symmetry, and energy densities for lipid bilayers with spontaneous curvature. *Biomechanics and Modeling in Mechanobiology*, 12(5):997–1017.

[Mao et al., 2018a] Mao, G., Wu, L., Fu, Y., Liu, J., and Qu, S. (2018a). Voltage-controlled radial wrinkles of a trumpet-like dielectric elastomer structure. *AIP Advances*, 8:935314.

[Mao et al., 2017] Mao, G., Wu, L., Liang, X., and Qu, S. (2017). Morphology of voltage-triggered ordered wrinkles of a dielectric elastomer sheet. *Journal of Applied Mechanics*, 84:111005.

[Mao et al., 2018b] Mao, G., Xiang, Y., Huang, X., Hong, W., Lu, T., and Qu, S. (2018b). Viscoelastic effect on the wrinkling of an inflated dielectric-elastomer balloon. *Journal of Applied Mechanics*, 85(7):071003.

[Mateiu et al., 2017] Mateiu, R. V., Yu, L., and Skov, A. L. (2017). Electrical breakdown phenomena of dielectric elastomers. In *Electroactive Polymer Actuators and Devices (EAPAD) 2017*, volume 10163, page 1016328. SPIE Press.

[Mirvakili and Hunter, 2017] Mirvakili, S. M. and Hunter, I. W. (2017). Artificial muscles: Mechanisms, applications, and challenges. *Advanced Materials*, 30:1704407.

[Montes-Pizarro and Negrón-Marrero, 2007] Montes-Pizarro, E. L. and Negrón-Marrero, P. V. (2007). Local bifurcation analysis of a second gradient model for deformations of a rectangular slab. *Journal of Elasticity*, 86(2):173–204.

[Naghdi, 1973] Naghdi, P. M. (1973). The theory of shells and plates. In *Linear Theories of Elasticity and Thermoelasticity*, pages 425–640. Springer.

[Nicolson, 2014] Nicolson, G. L. (2014). The fluid–mosaic model of membrane structure: Still relevant to understanding the structure, function and dynamics of biological membranes after more than 40 years. *Biochimica et Biophysica Acta - Biomembranes*, 1838(6):1451–1466.

[Ogden, 1997] Ogden, R. W. (1997). *Nonlinear Elastic Deformations*. Dover.

[Park et al., 2012] Park, H. S., Suo, Z., Zhou, J., and Klein, P. A. (2012). A dynamic finite element method for inhomogeneous deformation and electromechanical instability of dielectric elastomer transducers. *International Journal of Solids and Structures*, 49(15-16):2187–2194.

[Pelrine et al., 2000] Pelrine, R., Kornbluh, R., Pei, Q., and Joseph, J. (2000). High-speed electrically actuated elastomers with strain greater than 100%. *Science*, 287(5454):836–839.

[Pelrine et al., 1998] Pelrine, R. E., Kornbluh, R. D., and Joseph, J. P. (1998). Electrostriction of polymer dielectrics with compliant electrodes as a means of actuation. *Sensors and Actuators A: Physical*, 64(1):77–85.

[Pipkin, 1986] Pipkin, A. C. (1986). The relaxed energy density for isotropic elastic membranes. *IMA Journal of Applied Mathematics*, 36(1):85–99.

[Plante and Dubowsky, 2006] Plante, J.-S. and Dubowsky, S. (2006). Large-scale failure modes of dielectric elastomer actuators. *International Journal of Solids and Structures*, 43(25-26):7727–7751.

[Podio-Guidugli and Tomassetti, 2001] Podio-Guidugli, P. and Tomassetti, G. (2001). Thickness waves in electroelastic plates. *Wave Motion*, 34(2):175–191.

[Podio-Guidugli and Vianello, 2010] Podio-Guidugli, P. and Vianello, M. (2010). Hypertractions and hyperstresses convey the same mechanical information. *Continuum Mechanics and Thermodynamics*, 22(3):163–176.

[Puglisi and Zurlo, 2012] Puglisi, G. and Zurlo, G. (2012). Electric field localizations in thin dielectric films with thickness non-uniformities. *Journal of Electrostatics*, 70(3):312–316.

[Qian et al., 2008] Qian, S., Wang, W., Yang, L., and Huang, H. W. (2008). Structure of transmembrane pore induced by bax-derived peptide: Evidence for lipidic pores. *Proceedings of the National Academy of Sciences*, 105(45):17379–17383.

[Qiang et al., 2012] Qiang, J., Chen, H., and Li, B. (2012). Experimental study on the dielectric properties of polyacrylate dielectric elastomer. *Smart Materials and Structures*, 21(2):025006.

[Qu and Suo, 2012] Qu, S. and Suo, Z. (2012). A finite element method for dielectric elastomer transducers. *Acta Mechanica Solida Sinica*, 25(5):459–466.

[Rabinowitz, 1971] Rabinowitz, P. H. (1971). Some global results for nonlinear eigenvalue problems. *Journal of Functional Analysis*, 7(3):487–513.

[Robertson, 1959] Robertson, J. D. (1959). The ultrastructure of cell membranes and their derivatives. In *Biochemical Society Symposium*, volume 16, pages 3–43.

[Roxburgh, 1995] Roxburgh, D. (1995). Inflation of nonlinearly deformed annular elastic membranes. *International journal of Solids and Structures*, 32(14):2041–2052.

[Roxburgh et al., 1995] Roxburgh, D., Steigmann, D., and Tait, R. (1995). Azimuthal shearing and transverse deflection of an annular elastic membrane. *International Journal of Engineering Science*, 33(1):27–43.

[Sahu et al., 2017] Sahu, A., Sauer, R. A., and Mandadapu, K. K. (2017). Irreversible thermodynamics of curved lipid membranes. *Physical Review E*, 96(4):042409.

[Sharp, 1934] Sharp, L. W. (1934). *Introduction to Cytology*. McGraw-Hill, 3rd edition.

[Singer and Nicolson, 1972] Singer, S. J. and Nicolson, G. L. (1972). The fluid mosaic model of the structure of cell membranes. *Science*, 175(4023):720–731.

[Stark and Garton, 1955] Stark, K. and Garton, C. (1955). Electric strength of irradiated polythene. *Nature*, 176(4495):1225.

[Steigmann, 1990] Steigmann, D. (1990). Tension-field theory. *Proceedings of the Royal Society A*, 429(1876):141–173.

[Steigmann, 1999] Steigmann, D. (1999). Fluid films with curvature elasticity. *Archive for Rational Mechanics and Analysis*, 150(2):127–152.

[Steigmann et al., 2003] Steigmann, D., Baesu, E., Rudd, R. E., Belak, J., and McElfresh, M. (2003). On the variational theory of cell-membrane equilibria. *Interfaces and Free Boundaries*, 5(4):357–366.

[Steigmann, 2018] Steigmann, D. J. (2018). Mechanics and physics of lipid bilayers. In *The Role of Mechanics in the Study of Lipid Bilayers*, pages 1–61. Springer.

[Su et al., 2018] Su, Y., Conroy Broderick, H., Chen, W., and Destrade, M. (2018). Wrinkles in soft dielectric plates. *Journal of the Mechanics and Physics of Solids*, 119:298–318.

[Suo, 2010] Suo, Z. (2010). Theory of dielectric elastomers. *Acta Mechanica Solida Sinica*, 23(6):549–578.

[Suo et al., 2008] Suo, Z., Zhao, X., and Greene, W. H. (2008). A nonlinear field theory of deformable dielectrics. *Journal of the Mechanics and Physics of Solids*, 56(2):467–486.

[Terwilliger et al., 1982] Terwilliger, T. C., Weissman, L., and Eisenberg, D. (1982). The structure of melittin in the form I crystals and its implication for melittin's lytic and surface activities. *Biophysical Journal*, 37(1):353–361.

[Terzi and Deserno, 2018] Terzi, M. M. and Deserno, M. (2018). Lipid membranes: From self-assembly to elasticity. In *The Role of Mechanics in the Study of Lipid Bilayers*, pages 105–166. Springer.

[Tosteson et al., 1985] Tosteson, M., Holmes, S., Razin, M., and Tosteson, D. (1985). Melittin lysis of red cells. *Journal of Membrane Biology*, 87(1):35–44.

[Van Den Bogaart et al., 2008] Van Den Bogaart, G., Guzmán, J. V., Mika, J. T., and Poolman, B. (2008). On the mechanism of pore formation by melittin. *Journal of Biological Chemistry*, 283(49):33854–33857.

[Venable et al., 2015] Venable, R. M., Brown, F. L., and Pastor, R. W. (2015). Mechanical properties of lipid bilayers from molecular dynamics simulation. *Chemistry and Physics of Lipids*, 192:60–74.

[Wang et al., 2014] Wang, Q., Gossweiler, G. R., Craig, S. L., and Zhao, X. (2014). Cephalopod-inspired design of electro-mechano-chemically responsive elastomers for on-demand fluorescent patterning. *Nature Communications*, 5:4899.

[Wang et al., 2011] Wang, Q., Zhang, L., and Zhao, X. (2011). Creasing to cratering instability in polymers under ultrahigh electric fields. *Physical Review Letters*, 106(11):118301.

[Yang et al., 2010] Yang, S., Khare, K., and Lin, P.-C. (2010). Harnessing surface wrinkle patterns in soft matter. *Advanced Functional Materials*, 20:2550.

[Yang et al., 2017] Yang, S., Zhao, X., and Sharma, P. (2017). Avoiding the pull-in instability of a dielectric elastomer film and the potential for increased actuation and energy harvesting. *Soft Matter*, 13(26):4552–4558.

[Zhang et al., 2016] Zhang, C., Sun, W., Chen, H., Liu, L., Li, B., and Li, D. (2016). Electromechanical deformation of conical dielectric elastomer actuator with hydrogel electrodes. *Journal of Applied Physics*, 119(9):094108.

[Zhao et al., 2007] Zhao, X., Hong, W., and Suo, Z. (2007). Electromechanical hysteresis and coexistent states in dielectric elastomers. *Physical Review B*, 76(13):134113.

[Zhao and Suo, 2007] Zhao, X. and Suo, Z. (2007). Method to analyze electromechanical stability of dielectric elastomers. *Applied Physics Letters*, 91(6):061921.

[Zhu et al., 2011] Zhu, Y., Wang, H., Zhao, D., and Zhao, J. (2011). Energy conversion analysis and performance research on a cone-type dielectric electroactive polymer generator. *Smart Materials and Structures*, 20(11):115022.

[Zurlo, 2013] Zurlo, G. (2013). Non-local elastic effects in electroactive polymers. *International Journal of Non-Linear Mechanics*, 56:115–122.

[Zurlo et al., 2017] Zurlo, G., Destrade, M., DeTommasi, D., and Puglisi, G. (2017). Catastrophic thinning of dielectric elastomers. *Physical Review Letters*, 118(7):078001.